

Zhang, P., Jiang, S.Y., Donelick, R.A., Li, R., Soares, C.J., and Mei, L., 2022, Frontal expansion of an accretionary wedge under highly oblique plate convergence: Southern Indo-Burman Ranges, Myanmar: GSA Bulletin, <https://doi.org/10.1130/B36560.1>.

Supplemental Material

Supplemental Material A. Field Investigation and Subsurface Data

Text S1. Summary of the criteria for folds and thrusts observed along the Pyay–Toungup Section

Fig. S1. Geological map of the Pyay-Kyaukpyu Section and field observations

Fig. S2. Summary of the paleontological data in the study area.

Fig. S3. Uninterpreted seismic reflection sections (offshore region, southern Indo-Burman Ranges)

Supplemental Material B. Analytical Methods

Text S2. Zircon U-Pb dating

Text S3. Apatite fission track analysis

Supplemental Material C. Full Results

Table S1. GPS coordinates and lithologies of surface samples from the study area

Table S2. Detrital zircon U-Pb ages

Table S3. Apatite fission track results

Supplemental Material D. Compiled Detrital Zircon U-Pb Data

Fig. S4. Extensive detrital zircon U-Pb data summary with MDS plot.

Table S4. Summarized detrital zircon U-Pb ages from western Myanmar and adjacent regions

Frontal expansion of an accretionary wedge under highly oblique plate convergence: Southern Indo-Burman Ranges, Myanmar

Peng Zhang^{1,2,*}, Shao-Yong Jiang¹, Raymond A. Donelick³, Renyuan Li⁴, Cleber J. Soares⁵, and Lianfu Mei²

¹State Key Laboratory of Geological Processes and Mineral Resources, Collaborative Innovation Center for Exploration of Strategic Mineral Resources, China University of Geosciences, Wuhan 430074, China

²Key Laboratory of Tectonics and Petroleum Resources (China University of Geosciences), Ministry of Education, Wuhan 430074, China

³Apatite.com Partners, LLC1075, Matson Road Viola, Idaho 83872-9709, United States

⁴International Limited, China National Offshore Oil Corporation, Beijing 10027, China

⁵ChronusCamp Research, São Paulo State 13974-160, Brazil

*Corresponding author at: State Key Laboratory of Geological Processes and Mineral Resources, Collaborative Innovation Center for Exploration of Strategic Mineral Resources, China University of Geosciences, Wuhan 430074, China

Email address: P. Zhang (p8.zhang@cug.edu.cn)

Supplemental Material A. Field Investigation and Subsurface Data

Text S1. Summary of the criteria for folds and thrusts observed along the Pyay–Toungup Section

Fig. S1. Geological map of the Pyay-Kyaukpyu Section and field observations

Fig. S2. Summary of the paleontological data in the study area.

Fig. S3. Uninterpreted seismic reflection sections (offshore region, southern Indo-Burman Ranges)

Supplemental Material B. Analytical Methods

Text S2. Zircon U-Pb dating

Text S3. Apatite fission track analysis

Supplemental Material C. Full Results

Table S1. GPS coordinates and lithologies of surface samples from the study area

Table S2. Detrital zircon U-Pb ages

Table S3. Apatite fission track results

Supplemental Material D. Compiled Detrital Zircon U-Pb Data

Fig. S4. Extensive detrital zircon U-Pb data summary with MDS plot.

Table S4. Summarized detrital zircon U-Pb ages from western Myanmar and adjacent regions

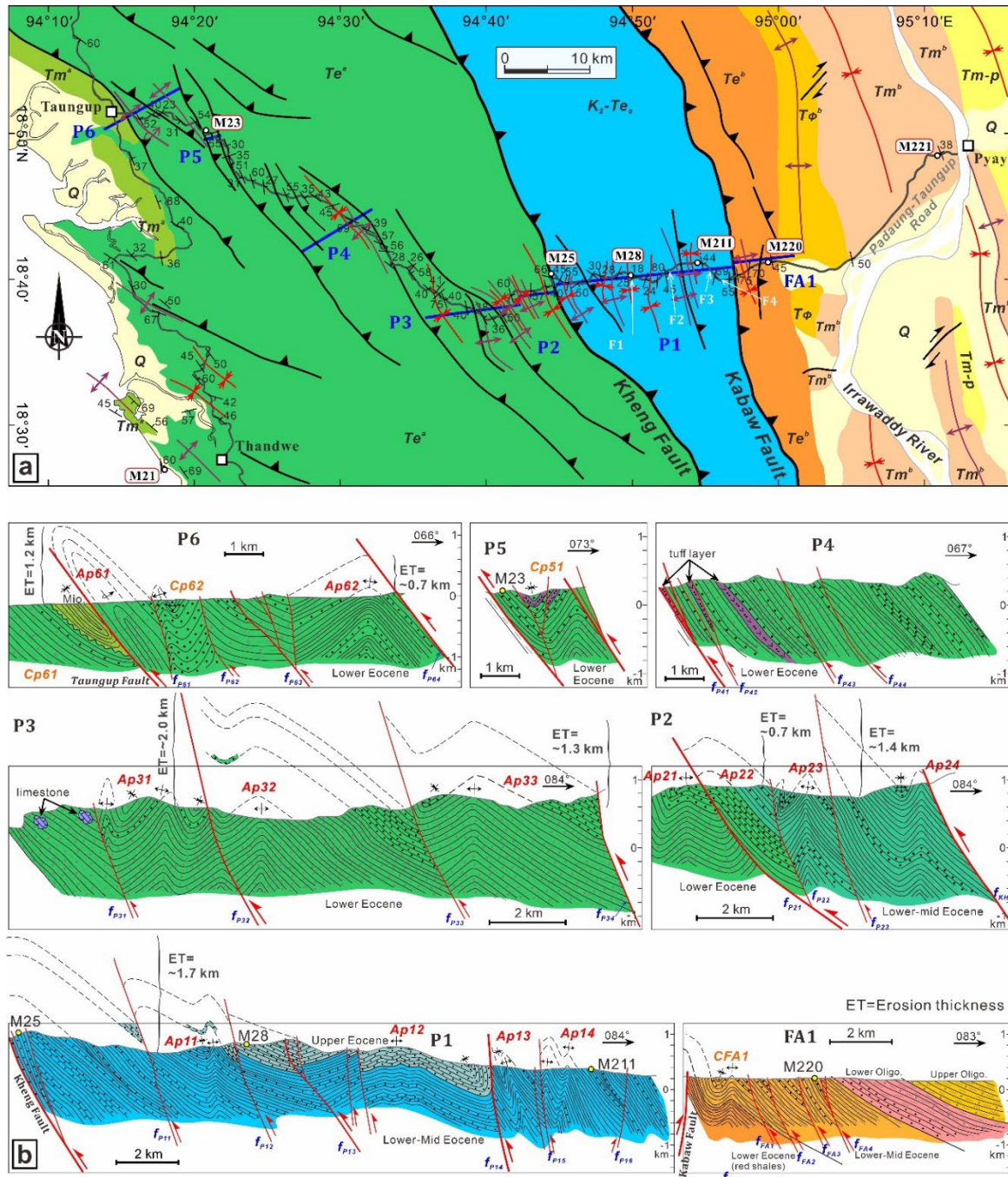
Supplemental Material A. Field Investigation and Subsurface Data

Text S1. Summary of the criteria for folds and thrusts observed and measured in the study area

Section	Description	Structure type	Horizontal offset of major thrust (km)						Amount of shortening of major folds (km)				Subtotal (km)
			f_{Kabaw}	f_{FA1}	f_{FA2}	f_{FA3}	f_{FA4}		A_{fa1}				
FA1	Western flank of the southern Minbu synclinorium, bounded on forelimb by the east-dipping Kabaw Fault. The westernmost part of the synclinorium was characterized by a small-scale anticlinorium with a width ca. 2 km; the lower Eocene red shales constituted its core. The overlying lower-mid Eocene shale and interbedded sandstone beds were cut through by the east-dipping thrusts (f_{FA1} - f_{FA4}).	Synclinal monocline	Undefined	0.13	0.27	0.27	0.27		1.20				2.14
P1	P1 cross section covers the ‘oldest’ part of the southern Indo-Burman Ranges that was originally interpreted as sediments of the Upper Cretaceous (BESRD, 1977). However, our new presented detrital zircon U-Pb ages provide a maximum depositional age of 50 Ma (Najman et al., 2020; this study), suggesting that these sediments were deposited in the early-middle Eocene. However, we cannot rule out the possibility that this may simply be the result of a data gap. The lower-middle Eocene shale beds and interbedded sandstone layers as well as the upper Eocene sandstone beds were west-vergent and cut through by the east-dipping thrusts. Overturned synclines were observed. It was estimated that at least 1.7 km sediments have been eroded from western flank of the anticline Ap11.	Ap11 —simple anticline; Ap12 —anticlinorium, the east limb was a syncline (1.5 km); Ap13 —fault-related anticlinorium, the forelimb was a syncline (1.0 km); Ap14 —faulted related anticlinorium, the forelimb was a syncline (1.0 km)	f_{P11} Undefined	f_{P12} 0.13	f_{P13} 0.27	f_{P14} 0.40	f_{P15} 0.27	f_{P16} 0.20	A_{p11} 0.26	A_{p12} 0.67	A_{p13} 1.33	A_{p14} 1.34	5.60 (This includes shortening values estimated for the tiled strata about 1.2 km)
P2	P2 section covers the region where the lower-middle Eocene sediments constitute the footwall of the Kheng Fault. This section is characterized by fault-related folds; forelimbs of these folds are often terminated against the east-dipping thrust. The crest parts of the anticlines were all eroded (with a thickness approximately 0.7-1.4 km).	Ap21 -fault-related fold (the forelimb is a syncline and the backlimb is cut by a thrust (f_{P21}), forming a faulted anticline- Ap22); Ap23 -fault-related fold and its forelimb is a syncline. Ap24 -faulted anticline and its backlimb is an anticline.	f_{P21} 0.20	f_{P22} 0.32	f_{P23} 0.26	f_{P24} 0.32			A_{p21} 0.84	A_{p22} 0.63	A_{p23} 0.53		3.10
P3	Sandstone and siltstone beds are often seen along the P3 cross section and could be correlated with westernmost part of the P2 section. Three fault-related anticlinoria were measured and these folds often showed shorter forelimbs and longer backlimbs. It was estimated that nearly 1.3-2.0 km sediments have been eroded from crest parts of the anticlines Ap32 and Ap33.	Ap31 —anticlinorium and both the forelimb and backlimb are marked by synclines; Ap32 and Ap33 —faulted anticlinorium;	f_{P31} 1.58	f_{P32} 0.53	f_{P33} 1.16	f_{P34} 0.74			A_{p31} 0.84	A_{p32} 0.53	A_{p33} 0.64		6.02

P4	Sedimentary rocks reveled by P4 section were all east-dipping and cut through by four east-dipping thrusts. These west-vergent strata may be backlimbs of the faulted anticlines and their crest parts of are inferred to be eroded during uplift of the wedge. In addition to the siltstones and interbedded sandstones, three tuff layers (each one was approximately 20 m) were observed.	Anticlinal monocline	f _{P41}	f _{P42}	f _{P43}	f _{P44}			folds				3.15
			Undefin ed	1.26	undefin ed	1.89			No data				
P5	Outcrops of the P5 section shows a classic syncline. Both its limbs are cut by east-dipping thrusts. Sandstones and tuff constitute the core of the syncline. The east limb was inferred to be shallow part of an anticline, which could harmonize with the strata observed on P4 section.	Simple syncline	fault						Cp51				0.42
			No data						0.42				
P6	Eastern part of the P6 section is a typical anticline with a vertical axis surface and approximately 3 km. It was estimated that nearly 0.8 km sedimentary rocks have been eroded from its crest. This anticline was separated from the synclinal monoclines to the west by an east-dipping thrust (f _{P63}). The synclinal monoclines consist primarily of sandstone and siltstone, which however, are not easy to correlate with rocks within the anticline. The western part of the P6 section includes three overturned folds (Ap61, Cp61 and Cp62). The crest part of the Ap61 and Ap62 anticlines were totally eroded—nearly 0.7-1.2 km sediments have been removed. The Cp61 syncline was cored by thin Miocene siltstones.	Ap61 —overturned anticline (faulted anticline); Cp61 —overturned syncline; Cp62 —synclinorium (its forelimb is a small-scale anticline	f _{Toungup}	f _{P61}	f _{P62}	f _{P63}	f _{P64}		Cp61	Cp62	Ap61	Ap62	12.37
			1.74	undefin ed	0.63	1.16	2.63		2.63	0.32	2.00	1.26	
P7	P7 section covers a region where mud volcano is often present. It was defined as circular syncline by Maurin and Rangin (2009) and thus its formation could be explained by mud activity followed by gravity tectonics. In the field however, both the core (Oligocene) and limbs (Eocene) of the syncline are sandstones—no mudstones are observed.	Syncline	Fault						Cp71				0.32
			No data						0.32				
P8	P8 section shows that the northwestern Ramree Island is composed of one syncline and two anticlines. The anticlines are only reveled their forelimbs in our section whereas the backlimbs are overthrust by the Eocene sedimentary rocks. These folds are often expressed as wide anticline or syncline.	Ap81 —faulted anticline Ap82 —simple anticline Cp81 —simple syncline	f _{Kaladan}	f _{P81}					Ap81	Ap82	Cp81		4.47
			3.06	Undefin ed					No data	0.23	1.18		

Figure S1. Geological map of the Pyay-Kyaukpyu Section and field observations



Field investigation. (a) Geologic map of the southern Indo-Burman Ranges showing locations of cross sections P1-P6 and analyzed samples (Burma Earth Sciences Research Division, 1977; Myint Swe, 2007; Tsung Aung, 1982); (b) Cross sections P1-P6; fault (f_x) and fold (Cp_x and Ap_x) numbers are referred to Table S1; (c) Geologic map of the Ramree Island showing cross sections P7-P8. Our new analyzed samples are marked on the geologic map with white circles. (d). Photos at F3, F4, F5, and F6 suggest that deposition of the Miocene turbiditic rocks were strongly affected by waves.

Figure S1 (continue)

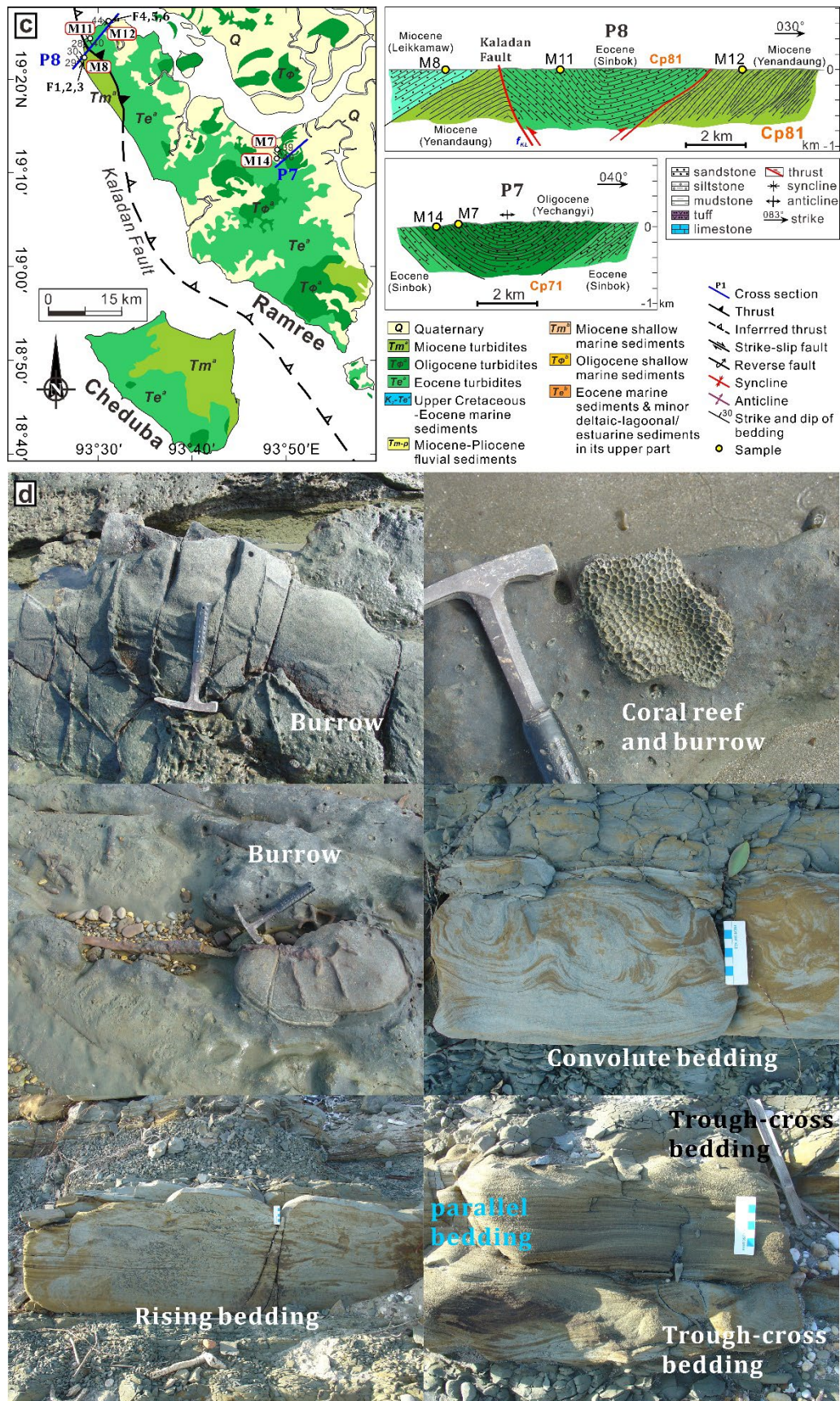


Figure S2. Summary of the paleontological data in the study area.

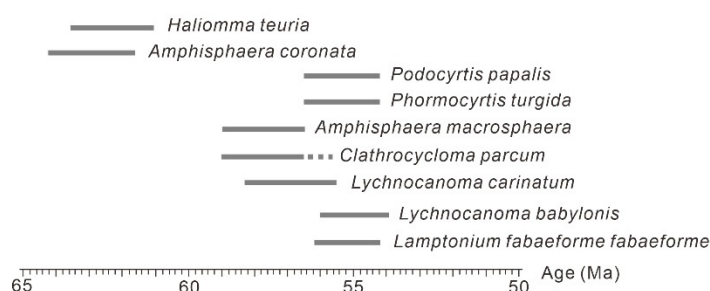
Pyay–Toungup Section

SHALE

1. *Amodiscus siliceus* (Terquem), *Glomospira irregularis* (Grzybowski), *Glomospira charoides* (Jones & Parker), *Glomospirella gaultina* (Berthelin) and *Haplophragmoides nonionoides* (Reuss); these were assigned as Upper Cretaceous to Paleogene by Gramann (1974).
2. Planktonic foraminiferal faunas (*Globotruncana* 2 and *Gumbelina* 7); these were assigned as Cretaceous by Fay Lain and Win Maw (1970).
3. (Samples collected from Cretaceous rocks) *Heterohelix globulosa* (Ehrenberg), *Hedbergella planispira* (Tappan), *Hedbergella delrioensis* (Carsey), *Prediscosphaera columnata* (Stover) and *Watznaueria* sp.; the age of planktonic foraminifera assemblage indicates the age range from Aptian to Maastrichtian and the nannofossils indicate Albian–Turonian (Naing, 2019).
4. (Samples collected from Paleogene rocks) *Chiloguembelina wilcoxensis* (Cushman & Ponton), *Chiloguembelina ototara* (Finlay), and *Globorotaloides carcoseleensis* (Toumarkine & Bolli), *Planorotalites chapmani* (Parr) and *Morozovella pseudobulloides* (Plummer); the age was assigned as Paleocene (Naing, 2019).

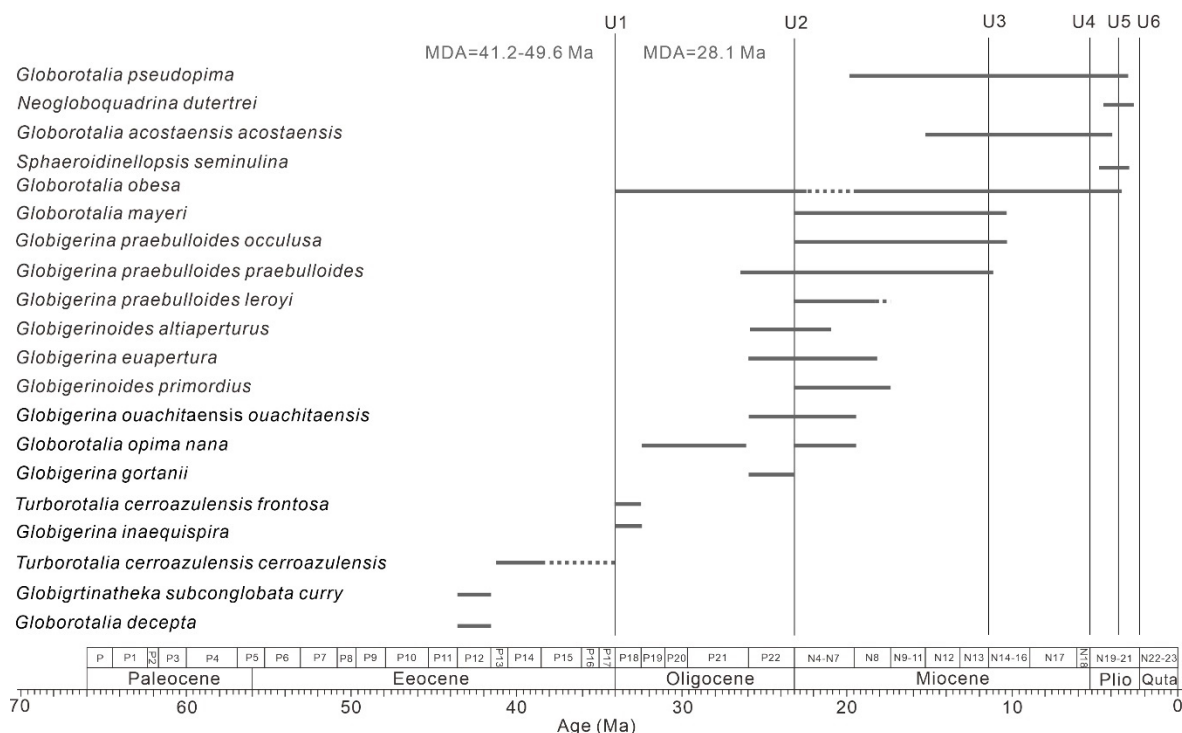
CHERT

1. Radiolarian fauna: *Amphisphaera macrosphaera* (Nishimura), *A. coronata* (Ehrenberg), *Actinommidae* gen. et sp. indet., *Phormocyrtis turgida* (Krasheninnikov), *Podocyrtis papalis* (Ehrenberg), *Lamptonium fabaeforme fabaeforme* (Krasheninnikov), *Lychnocanoma carinatum* (Ehrenberg), *L. babylonis* (Clark and Campbell), *Cryptamphorella macropora* (Dumitrica), *Clathrocycloma parcum* (Foreman), *Haliomma teuria* (Hollis), and *Spongodiscus* sp.; the radiolarian assemblage is assigned to a late Paleocene to early Eocene age (Naing, 2019).



Rakhine Coastal Region (well RM3-1 drilled on Ramree Island)

Data below are summarized from Lei et al. (2009)

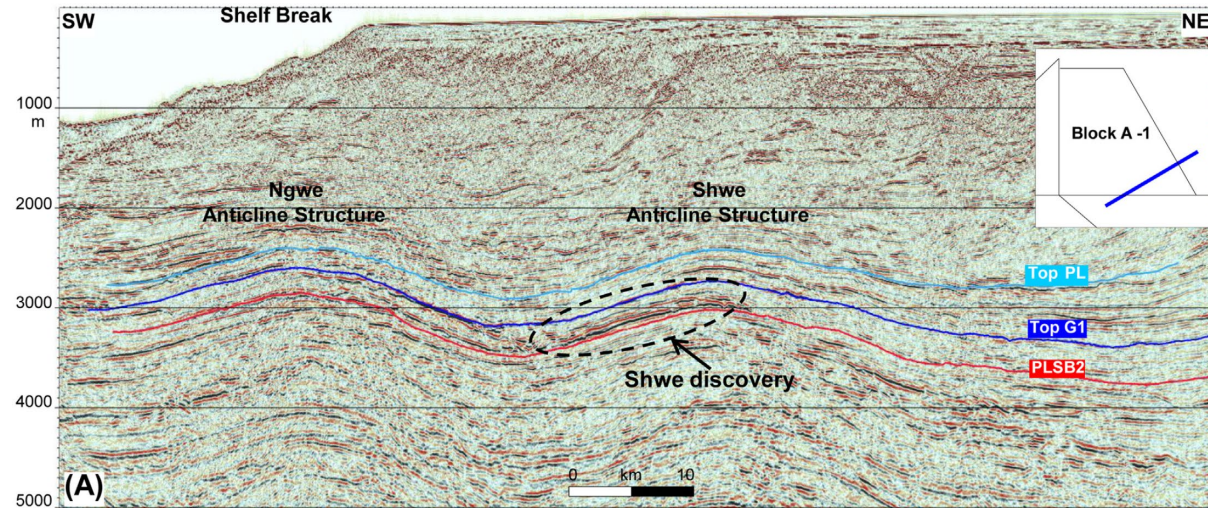


References

- Fay Lain and Win Maw, 1970. Geology of Arakan Coast and Offshore Islands; unpublished report MOGE.
- Gramann, F., 1974. Some palaeontological data on the Triassic and Cretaceous of the western part of Burma (Arakan Islands, Arakan Yoma, western outcrops of Central Basin). *Newsletters in Stratigraphy*, 3, 277–290
- Lei, Q. P., Wu, X., and Wan, X. Q., 2009. The Eocene–Pliocene planktonic foraminifera from Ramree Island, Burma: *Acta Micropalaeontologica Sinica*, v. 26, no. 4, p. 323–330. (In Chinese with English abstract)
- Naing, T. T., 2019. Age, depositional history, and tectonics of the Indo-Burman Ranges [Ph. D. thesis]: University of Oxford, 404 p.

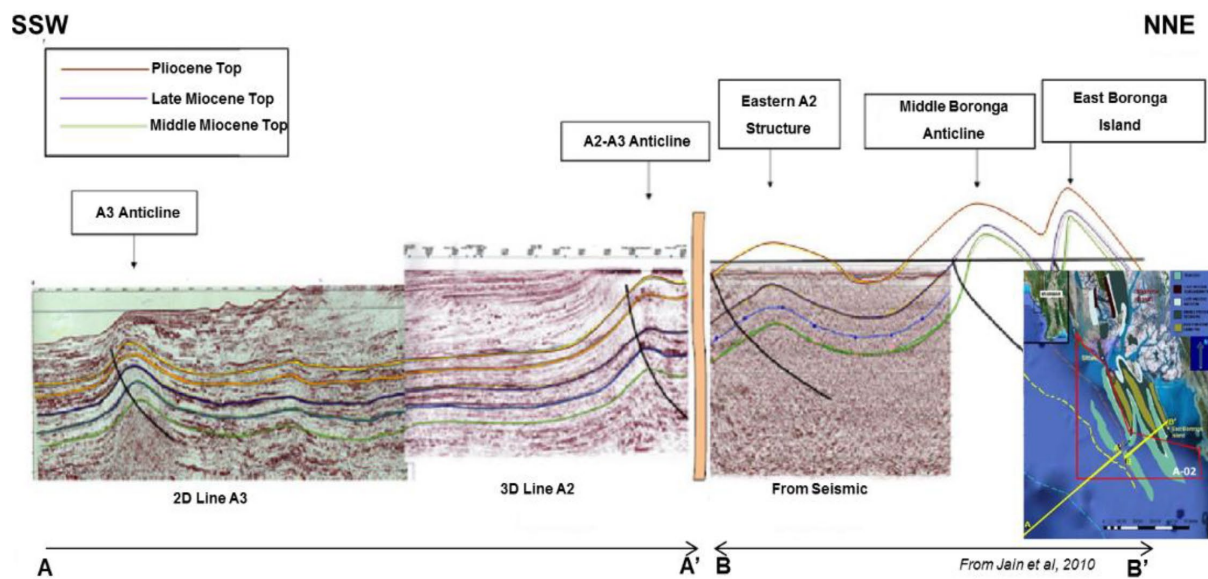
Figure S3. Uninterpreted seismic reflection sections (offshore region, southern Indo-Burman Ranges)

For Figure 5A



(From Yang S.Y. and Kim, J.W., 2014, *Marine and Petroleum Geology*, v.49, p.45-58)

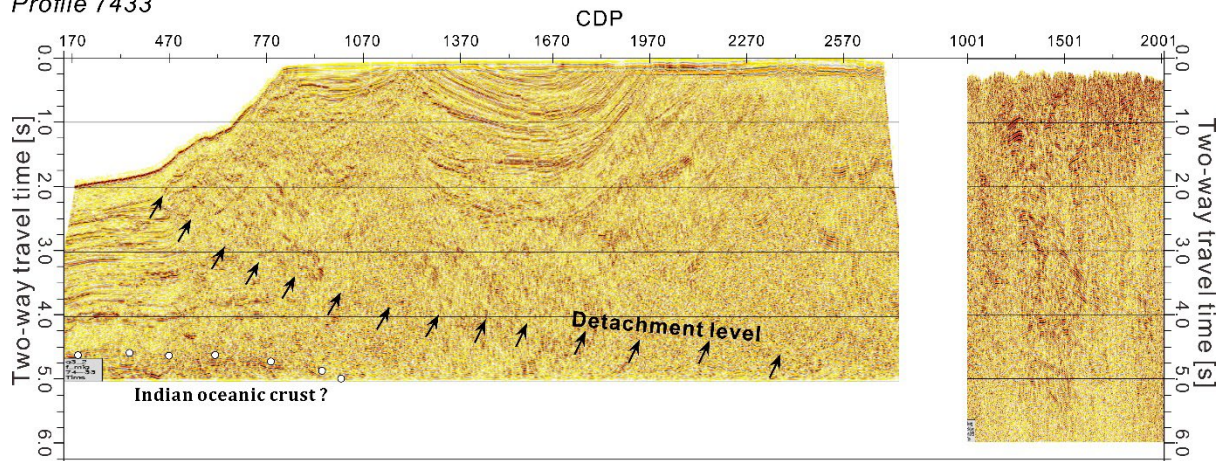
For Figure 5B



(From Jain, M., Das, P.S., Bandyopadhyay, B., 2010; 8th Biennial International Conference & Exposition on Petroleum Geophysics, P-58)

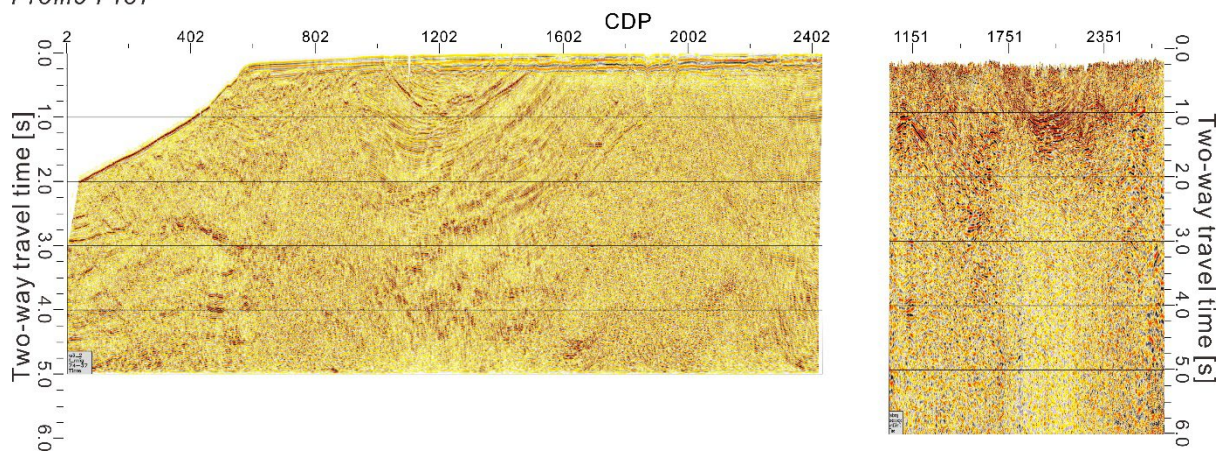
For Figure 5C

Profile 7433



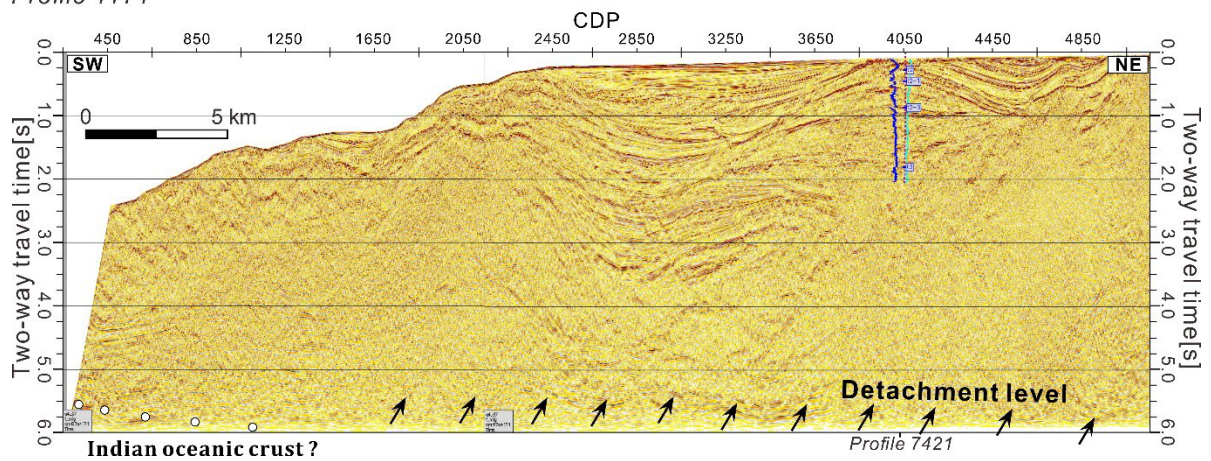
For Figure 5D

Profile 7437

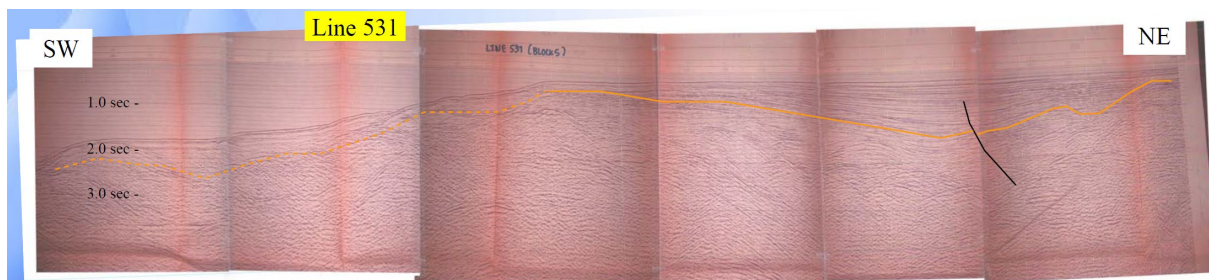


For Figure 5E

Profile 4171

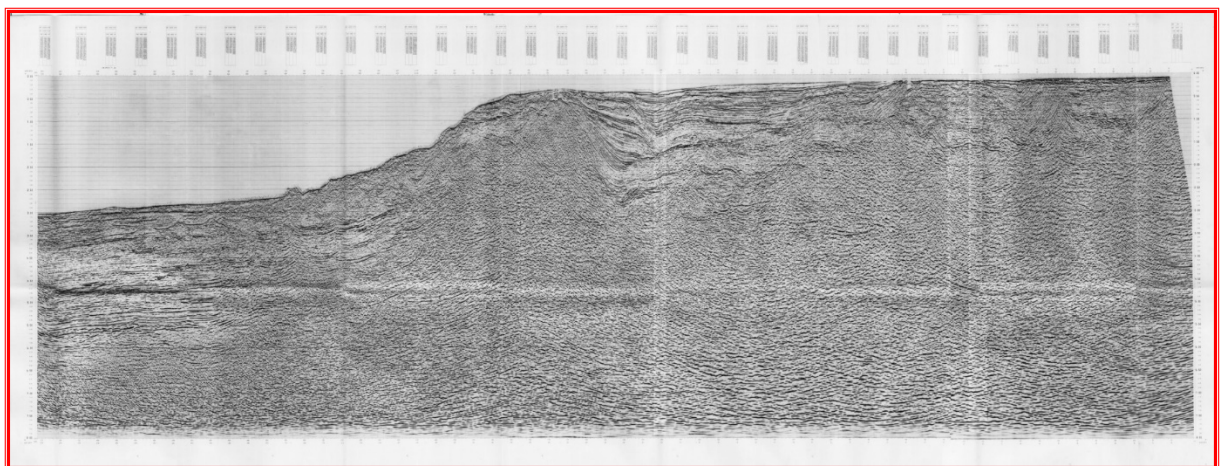


For Figure 5F



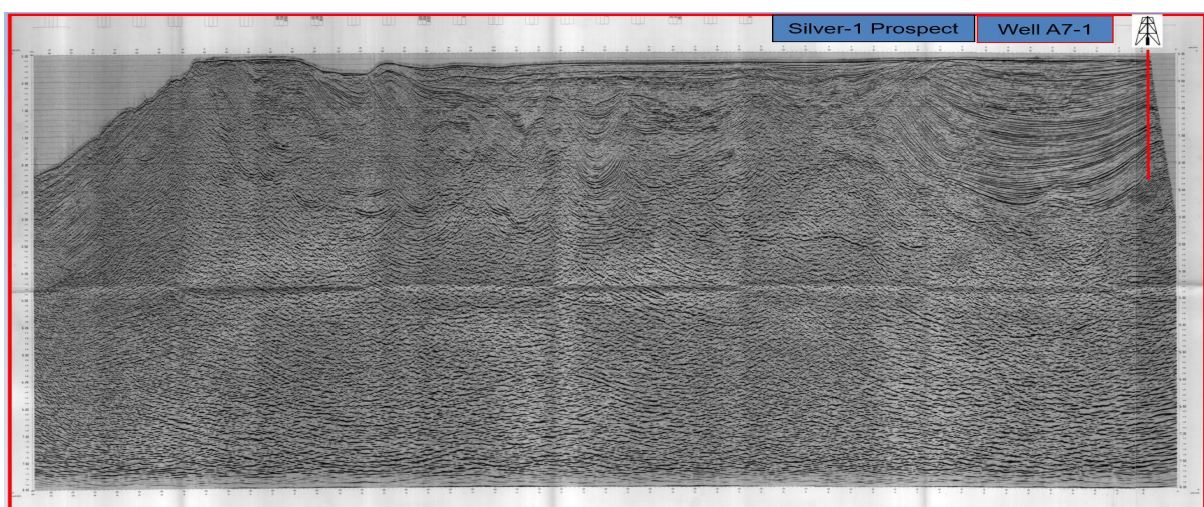
(From an internal report provided by CNOOC; Block A5 Seismic review and play type model)

For Figure 5G



(From Nyan Tun, Maung Maung Kyaw, Kyaw Myo Win, and Kyaw Hlaing, 2007; internal report of **SILVER WAVE ENERGY**)

For Figure 5H



(From Nyan Tun, Maung Maung Kyaw, Kyaw Myo Win, and Kyaw Hlaing, 2007; internal report of **SILVER WAVE ENERGY**)

Supplemental Material B. Analytical Methods

Text S2. Detrital zircon U-Pb dating

Detrital zircon and apatite separations were carried out at the Institute of Hebei Regional Geology and Mineral Survey, Langfang, Hebei Province. The sandstone samples were first crushed to pass a 60 mesh (250 μm) sieve. Manual washing with water and then alcohol was performed carefully for multiple aliquots of the crushed material to get denser components of various grain sizes. An eletro-magnetometer was used to remove magnetic minerals. Conventional heavy liquid separation method was then used to concentrate heavy minerals, and zircon and apatite grains were picked out by hand under a binocular.

Detrital zircon grains were mounted randomly in 24 mm epoxy resin and polished close to one-third of individual grain diameters. Cathodoluminescence (CL) images were obtained using a JEOL JXA-8100 electron microprobe operating at 10 kV at the State Key Laboratory of Geological Processes and Mineral Resources (SKLGPMR), China University of Geosciences, Wuhan, in order to examine the internal structures of individual zircon and to select suitable position for U-Pb analysis. U-Pb dating of detrital zircon was performed at the SKLGPMR by using LA-ICP-MS. Detailed operating conditions for the laser ablation system and the ICP-MS instrument data reduction are the same as description by Liu et al. (2008, 2010). Laser sampling was performed using an excimer laser ablation system (GeoLas, 2005). An Agilent 7500a ICP-MS instrument was used to acquire ion-signal intensities. Each analysis incorporated a background acquisition of approximately 20 s (gas blank) followed by 50 s of data acquisition from the sample. The Agilent Chemstation was utilized for the acquisition of each individual analysis. Off-line selection and integration of background and analytic signals, and time-drift correction and quantitative calibration for trace element analyses and U-Pb dating were performed by software ICPMSDataCal_8.4 (Liu et al., 2008, 2010). A beam of 24 μm was used. The NIST SRM 610 glass was used as an external standard to calculated U, Th and Pb concentrations of unknowns. Zircon 91500 was used as an external standard to normalize isotopic fractionation during analyses of unknowns, and was repeatedly analyzed every five analyses (i.e., 2 zircon 91500 + 5 samples +2 zircon 91500).

References

- Liu, Y.S., Hu, Z.C., Gao, S., Günther, D., Xu, J., Gao, C.G., and Chen, H.H., 2008. In situ analysis of major and trace elements of anhydrous minerals by LA-ICP-MS without applying an internal standard: *Chemical Geology*, v. 257, p. 34–43, <http://dx.doi.org/10.1016/j.chemgeo.2008.08.004>.
- Liu, Y.S., Gao, S., Hu, Z.C., Gao, C.G., Zong, K.Q., and Wang, D.B., 2010. Continental and oceanic crust recycling-induced melt-peridotite interactions in the Trans-North China orogen: U-Pb dating, Hf isotopes and trace elements in zircons from mantle xenoliths: *Journal of Petrology*, v. 51, p. 537–571, <http://dx.doi.org/10.1093/petrology/egp082>.

Text S3. Apatite fission track analysis

Part I: AFT Methods

AFT Sample Preparation

The apatite fission track (AFT) samples were prepared for analysis using the procedures described by Donelick et al. (2005). Detrital apatite grains were isolated from each sample using standard gravimetric and magnetic mineral separation techniques (see above).

Detrital apatite grains were mounted in epoxide resin and polished to a fine finish using 0.3 μm alumina slurry. AFTs were etched by stirring vigorously the grains mounts in reagent grade 5.5N HNO_3 solution for 20 seconds at 21°C, followed by rinsing with distilled water. This process also removes most common lead contamination on the grain and epoxy surfaces.

AFT Data Collection

AFT data were collected and compiled using the procedures described by Donelick et al. (2005). For samples M23, M25, M211, M220, M221, AFTs were viewed and measured by analyst Paul O'Sullivan in 2012 using a Zeiss optical microscope affixed with transmitted and reflected light, a manual digital XY stage (serial micrometers with 10 μm resolution in both X and Y directions), and a drawing tube. A serial digitizing tablet was positioned beneath the drawing tube and an LED light was affixed to the tablet's cursor. The drawing tube superimposed an image of the bright LED light onto the microscope field of view allowing points of geometrical significant to be digitized using the cursor and passed to the operating software. A magnification of 2000x was used (100x objective, 10x ocular, 2x drawing tube) to measure surface fission track (SFT) density, confined fission track (CFT) lengths and angle to c-axis, and etch figure diameters parallel and perpendicular to c-axis (D_{par} and D_{per} , respectively; Donelick, 1993; Donelick, 1995). The number of CFTs available for measurement was enhanced by irradiating the apatite grain mounts with ^{252}Cf -derived fission fragments (Donelick and Miller, 1991). For samples M02, M07, M08, M11, M12, M28 AFTs were viewed and measured by analyst Cleber Soares in 2012. The LA-ICP-MS was calibrated using NIST SRM 610 to obtain the low oxides, the ratio U/Th ~ 1 , and the maximum counts of the target elements. During the analyzes, the ^{238}U concentration was determined using uranium standard samples (Dur-2 and MT-7; Soares et al., 2015), which present $< 2\%$ U variation. The isotopes concentration is carried out with Agilent 7800 quadrupole ICP-MS coupled with 213 NewWave laser ablation system. The spot size is chosen to cover the maximum area which fission tracks were measured (30-40 μm). Finally, the NIST SRM 610 analyzed together with age and uranium standards in order to check the LA-ICP-MS performance during analysis. The fission-track age was determined following Donelick et al. (2005). AFT ages were calculated similar to those at Apatite to Zircon, Inc. DR is used as the AFT zeta age calibration standard. Ratios of primary zeta (original zeta LA-ICP-MS session) to secondary zeta (current LA-ICP-MS session) $^{238}\text{U}/^{43}\text{Ca}$ ratios for apatite were determined for each zeta calibration spot. The same ratios were used in unknown samples with the aim of normalizing the dataset.

LA-ICP-MS Data Collection

The laser ablation-inductively coupled plasma-mass spectrometry (LA-ICP-MS) sessions that were run in this study are summarized in Table A1. LA and ICP-MS settings for each session are detailed in Tables A2 and A3, respectively. Masses measured for each session are detailed in Table A4. Age and chemical composition standards used in this study are summarized in Table A5. Age ranges measured for selected age standards are detailed in Table A6.

LA-ICP-MS Data Modeling

The data for each spot are characterized by a series of data scans, each scan representing one measurement for each mass in order of increasing mass. The series of data scans may be divided into background and signal+background segments. Background represents data collected prior to firing the laser. Signal+background represents data collected during laser ablation of the spot. The following steps are taken to determine background-corrected signal intensities for each mass analyzed for each spot:

- The true time is calculated at which each measurement was collected for each mass for each scan.
- The time at which background ends and signal+background begins is determined using selected masses listed in Table A4 (for which Search Last Background? is TRUE).
- A line is fitted to all background values for each mass prior to the time at which background ends. For a negative slope, the background value for the current mass is set equal to the value of the line at the time at which background ends; the error is set equal to the standard deviation of the background values about the fitted line. For zero or positive slope, the background value for the current mass is set equal to the mean of the fitted background values; the error is set equal to the standard deviation of the background values about the mean.
- Signal+background values are smoothed (versus scan number) for each mass using a Savitzky and Golay (1964) filter based on the median of fitted polynomials; the error of each signal+background value is set equal to the standard deviation of the signal+background values about the smoothed curve.
- Signal+background values are corrected for background noise by subtracting background.

Fission track ages were calculated using the equations of Donelick et al. (2005), Soares et al. (2014), and Cogné et al. (2019). U-Pb ages were calculated for each spot using the general principles described in Donelick et al. (2009) for zircon and Chew and Donelick (2012) for apatite. Chemical composition values were calculated using the methods described in Donelick and Donelick (2014) and Chew et al. (2014).

References

- Barfod, G.H., Krogstad, E.J., Frei, R., and Albarede, F., 2005, Lu-Hf and PbSL geochronology of apatites from Proterozoic terranes: A first look at Lu-Hf isotopic closure in metamorphic apatite: *Geochimica et Cosmochimica Acta*, v. 69, n. 7, p. 1847-1859.
- Boyce, J.W. and Hodges, K.V., 2005. U and Th zoning in Cerro de Mercado (Durango, Mexico) fluorapatite: Insights regarding the impact of recoil redistribution of radiogenic ^4He on (U-Th)/He thermochronology: *Chemical Geology*, v. 219, p. 261-274.
- Carlson, W.D., Donelick, R.A., and Ketcham, R.A., 1999, Variability of apatite fission track annealing kinetics I: Experimental results: *American Mineralogist*, v. 84, p. 1213-1223.
- Chew, D.M., Babechuk, M.G., Cogné, N., Mark, C., O'Sullivan, G.J., Henrichs, I.A., Doepke, D., McKenna, C.A., 2016, (LA,Q)-ICPMS trace-element analyses of Durango and McClure Mountain apatite and implications for making natural LA-ICPMS mineral standards: *Chemical Geology*, v. 435, p. 35-48.
- Chew, D.M. and Donelick, R.A., 2012, Combined apatite fission track and U-Pb dating by LA-ICP-MS and its application in apatite provenance analysis: *Quantitative Mineralogy*

- and Microanalysis of Sediments and Sedimentary Rocks, Mineralogical Association of Canada, Short Course, v. 42, p. 219–247.
- Chew, D.M., Donelick, R.A., Donelick, M.B., Kamber, B.S. and Stock, M., 2014, Apatite Chlorine Concentration Measurements by LA-ICP-MS: Geostandards and Geoanalytical Research, v. 38, pp. 23-35.
- Cogné, N., Chew, D.M., Donelick, R.A., and Ansberque, C., 2019, LA-ICP-MS apatite fission track dating: A practical zeta-based approach: Chemical Geology, v. 531, no. 119302.
- Donelick, R.A., 1993, A method of fission track analysis utilizing bulk chemical etching of apatite. U.S. Patent Number 5, 267, 274.
- Donelick, R.A., 1995, A method of fission track analysis utilizing bulk chemical etching of apatite. Australian Patent Number 658,800.
- Donelick R.A., and Donelick M.B. (unpublished data).
- Donelick, R.A. and Donelick, M.B., 2014, Method of determining the concentration of an element in a solid using relative abundances of isotopes from the solid and a reference solid. U.S. Patent Number 8, 901, 485.
- Donelick, R.A. and Miller, D.S., 1991, Enhanced TINT fission track densities in low spontaneous track density apatites using ^{252}Cf -derived fission fragment tracks: A model and experimental observations: Nuclear Tracks and Radiation Measurements, v. 18, no. 3, pp. 301-307.
- Donelick, R.A., O’Sullivan, P.B., and Donelick, M.B., 2009, A discordia-based method of zircon U-Pb dating from LA-ICP-MS analysis of single spots. In P.J. Williams et al., Smart Science for Exploration and Mining. James Cook University, Townsville, Australia, pp. 276-278.
- Donelick, R.A., O’Sullivan, P.B., Ketcham, R.A., 2005. Apatite fission-track analysis: Reviews in Mineralogy and Geochemistry, Mineralogical Society of America, v. 58, p. 49-94.
- Kuiper, K.F., Deino, A., Hilgen, P.J., Krijgsman, W., Renne, P.R., and Wijbrans, J.R., 2008. Synchronizing rock clocks of Earth history: Science, 320, p. 500-504.
- Lanphere, M.A. and Baadsraard, H., 2001. Precise K-Ar, $^{40}\text{Ar}/^{39}\text{Ar}$, Rb-Sr and U-Pb mineral ages from the 27.5 Ma Fish Canyon Tuff reference standard: Chemical Geology, v. 175, p. 653-671.
- McDonough, W.F. and Sun, S.S., 1995, The Composition of the Earth: Chemical Geology, v. 120, p. 223-253.
- McDowell, F.W., McIntosh, W.C., and Farley, K.A., 2005, A precise $^{40}\text{Ar}/^{39}\text{Ar}$ reference age for the Durango apatite (U-Th)/He and fission-track dating standard: Chemical Geology, v.214, n.3-4, p. 249-263.
- Paces, J.B. and Miller, J.D., 1993, Precise U-Pb ages of Duluth Complex and related mafic intrusions, northeastern Minnesota: Geochronological insights to physical, petrogenic, paleomagnetic, and tectonomagmatic processes associated with the 1.1 Ga Midcontinent Rift System: Journal of Geophysical Research, v. 98, no. B8, p. 13997-14013.
- Roden, M.K., Parrish, R.R., Miller, D.S., 1990. The absolute age of the Eifelian Tioga ash bed: Journal of Geology, v. 98, p. 282-285.
- Savitzky, A. and Golay, M.J.E., 1964, Smoothing and differentiation of data by simplified least square procedure: Analytical Chemistry, v. 44, no. 11, p. 1906-1909.
- Schoene, B. and Bowring, S.A., 2006, U-Pb systematic of the McClure Mountain syenite: thermochronological constraints on the age of the $^{40}\text{Ar}/^{39}\text{Ar}$ standard MMhb: Contributions to Mineralogy and Petrology, v. 151, p. 615-630.
- Soares, C.J., Mertz-Kraus, R., Guedes, S., Stokli, D.F., Zack, T., 2015, Characterization of apatites as potential U reference materials for fission-track dating by LA-ICP-MS: Geostandards and Geoanalytical Research, v. 39, no. 3, p. 305-313, Doi: 10.1111/j.1751-

Table A1a. LA-ICP-MS session summary for samples M23, M25, M211, M220, M221.

Setting	Apatite AFT U-Th-Pb 20121029
Laboratory	Donelick Properties, Viola, ID, USA
Hardware	LA: Resonetics RESOlution M-50 ICP-MS: Agilent 7700x quadrapole
Laboratory Scientist	Dr. Margaret B. Donelick
Data Collected by	Dr. Margaret B. Donelick
Software	Apatite.com Partners LLC MSData
Data Processed by	Dr. Raymond A. Donelick

Table A1b. LA-ICP-MS session summary for samples M02, M07, M08, M11, M12, M28.

Setting	Apatite AFT U-Th-Pb 2004001-037
Laboratory	Chronuscamp Research, Brazil
Hardware	Agilent 7800x
Laboratory Scientist	Cleber J. Soares
Data Collected by	Cleber J. Soares
Software	Apatite.com Partners LLC MSData
Data Processed by	Cleber J. Soares

Table A2a. LA settings for samples M23, M25, M211, M220, M221.

Setting	Apatite AFT U-Th-Pb 20121029
Warmup Time	TTL 7.6 s
Dwell Time	48 s
Washout Time	28 s
Laser Repetition Rate	8 Hz
Ablation Type	26 micron diameter spot
Attenuation	50%
Stabilization Mode	constant energy 4.2 mJ
Carrier Gas 1	950 mL/min ultra high purity He
Carrier Gas 2	4.1 mL/min ultra high purity N2
Stage Position Correction	Donelick Properties proprietary correction

Table A2b. LA settings for samples M02, M07, M08, M11, M12, M28.

Setting	Apatite AFT U-Th-Pb 2004001-037
Warmup Time	15000 ms
Dwell Time	TTL 35000 ms
Washout Time	TTL 20000 ms
Laser Repetition Rate	5.0 Hz
Ablation Type	30-40 micron diameter spot
Stabilization Mode	constant energy 6.40-6.50 kV
Carrier Gas 1	680 mL/min ultra high purity He
Carrier Gas 2	3.15 mL/min ultra high purity H2

Table A3a. ICP-MS settings for samples M23, M25, M211, M220, M221.

Setting	Apatite AFT U-Th-Pb 20121029
Carrier Gas	5.10 kPa 1.0 L/min high purity Ar

Plasma RF Power	1400 V
Plasma RF Matching	1.80 V
Plasma Sample Depth	4.2 mm
Plasma Carrier Gas	0.85 L/min
Plasma Option Gas	disabled
Plasma Nebulizer Pump	0.00 rps
Plasma S/C Temperature	2 degC
Plasma Gas Switch	Makeup Gas
Plasma Makeup Gas	0.00 L/min
Lenses Extract 1	-11.2 V
Lenses Extract 2	-195 V
Lenses Omega Bias	-110 V
Lenses Omega Lens	8.9 V
Lenses Cell Entrance	-40 V
Lenses Cell Exit	-60 V
Lenses Deflect	14.2 V
Lenses Plate Bias	-50 V
Cell Use Gas	not checked
Cell He Flow	disabled
Cell H2 Flow	disabled
Cell 3rd Gas Flow	disabled
Cell Octapole Bias	-18 V
Cell Octapole RF	200 V
Cell Energy Discrimination	5.0 V
Quadrupole Mass Gain	134
Quadrupole Mass Offset	121
Quadrupole Axis Gain	1.0017
Quadrupole Axis Offset	0
Quadrupole QP Bias	-13 V
Torch Axis Torch H	0.0 mm
Torch Axis Torch V	0.0 mm
EM (Hardware Settings) Discriminator	4.0 mV
EM (Hardware Settings) Analog HV	1723 V
EM (Hardware Settings) Pulse HV	1030 V
Operator	Margaret B. Donelick
Technical Assistance	Raymond A. Donelick

Table A3b. ICP-MS settings for samples M02, M07, M08, M11, M12, M28.

Setting	Apatite AFT U-Th-Pb 2004001-037
Carrier Gas	5.00-5.40 kPa 0.87 L/min high purity Ar
Plasma RF Power	1550 W
Plasma RF Matching	1.80 V
Plasma Sample Depth	8.0 mm
Lenses Extract 1	0.0
Lenses Extract 2	-200 V
Lenses Omega Bias	-90 V
Lenses Omega Lens	9.4 V
Lenses Cell Entrance	-30 V

Lenses Cell Exit	-50 V
Lenses Deflect	10.2 V
Lenses Plate Bias	-35 V
Operator	Cleber J. Soares
Technical Assistance	Cleber J. Soares

Table A4a. Masses measured for samples M23, M25, M211, M220, M221.

Mass	Element	Sampling Time Apatite AFT U-Th-Pb 20121029	Search Last Background?
23	Na	0.0001	
24	Mg	0.0001	
27	Al	0.005	
29	Si	0.0005	
31	P	0.0005	TRUE
34	S	0.001	
35	Cl	0.1	
43	Ca	0.05	TRUE
48	Ca	0.05	TRUE
55	Mn	0.001	
56	Fe	0.001	
75	As	0.0005	
79	Br	0.1	
88	Sr	0.0005	
89	Y	0.0005	
139	La	0.003	TRUE
140	Ce	0.003	TRUE
141	Pr	0.003	TRUE
146	Nd	0.003	TRUE
147	Sm	0.003	
151	Eu	0.003	
157	Gd	0.003	
159	Tb	0.003	
163	Dy	0.003	
165	Ho	0.003	
166	Er	0.003	
169	Tm	0.003	
172	Yb	0.003	
175	Lu	0.003	
202	Hg	0.05	
204	Pb	0.15	
206	Pb	0.15	
207	Pb	0.15	
208	Pb	0.15	
232	Th	0.0125	TRUE
235	U	0.0125	
238	U	0.0125	TRUE

Table A5a. Apatite UPb and matrix-matched chemical composition standards.

Standard Name	Age Standard Type	Accepted Age	Reference
AZ = Arizona	secondary Ap	~440 Ma	Donelick and Donelick (unpublished data)
B3 = Bamble	secondary Ap	~1128 Ma	Carlson et al. (1999) Donelick and Donelick (unpublished data)
DR = Durango	secondary Ap	31.44 ± 0.18 Ma 33.15±0.98 Ma (Cleber' s lab)	McDowell et al. (2005) Boyce and Hodges (2005)
F5 = Duluth anorthosite	secondary Ap	1099.0±0.6 Ma	Paces et al. (1993)
FC = Duluth anorthosite	secondary Ap	1099.0±0.6 Ma	Paces et al. (1993)
IF = Fish Canyon Tuff	secondary Ap	28.201 ± 0.012 Ma	Lanphere and Baadsraard (2001) Kuiper et al. (2008)
MM = McClure Mtn.	primary Ap	523.98 ± 0.12 Ma	Schoene and Bowring (2006)
OL=Otter Lake	secondary Ap	913 ± 7 Ma	Barfod et al. (2005)
RA = Russian	secondary Ap	~410 Ma	Donelick and Donelick (unpublished data)
TI=Tioga Bed B	secondary Ap	390.5 ± 0.5 Ma	Roden et al. (1990)

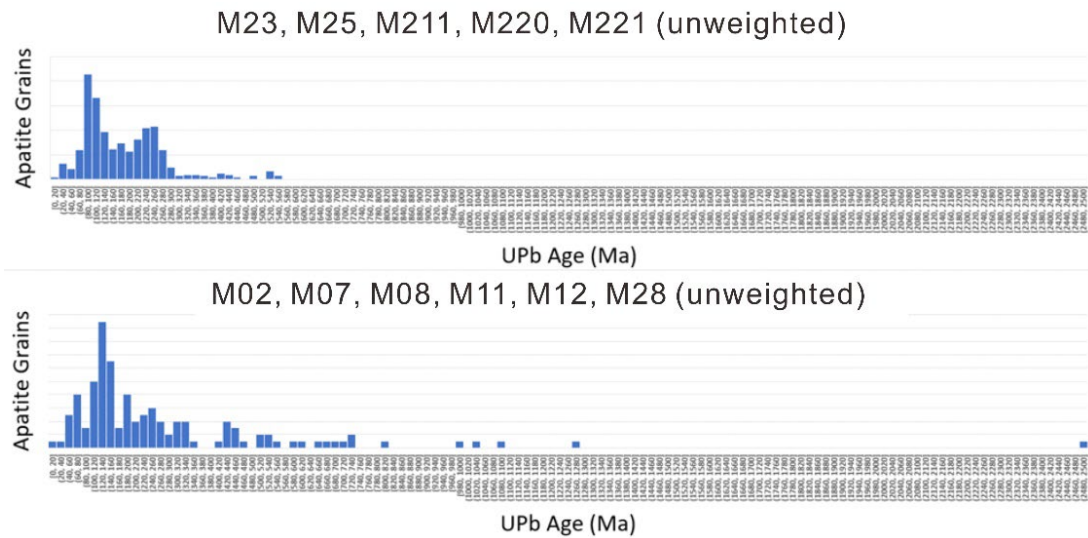
Table A5b. Reference and measured element concentrations of Durango (DRG) apatite (Chew et al., 2016) for LA-ICP-MS session for samples M23, M25, M211, M220, M221. Also listed are reference concentrations for of C1 chondrite (McDonough and Sun, 1995).

REE	Durango Reference Concentration (ppm)	Durango/Apatite AFT /UThPb 20121029 Measured Concentration (ppm)	C1/Chondrite Reference Concentration (ppm)
La	3786.00	3789.91	0.2370
Ce	5306.00	5308.46	0.6130
Pr	472.50	472.76	0.0928
Nd	1534.00	1536.09	0.4570
Sm	215.20	215.72	0.1480
Eu	18.90	19.02	0.0563
Gd	186.90	187.21	0.1990
Tb	24.25	24.32	0.0361
Dy	129.90	130.26	0.2460
Ho	26.35	26.41	0.0546
Er	68.69	68.89	0.1600
Tm	8.75	8.80	0.0247
Yb	45.10	45.33	0.1610
Lu	5.17	5.21	0.0246
Th	235.00	235.81	
U	13.00	13.06	

Table A6a. Pb-corrected apatite UPb ages measured for apatite UPb age standards for LA-ICP-MS session for samples M23, M25, M211, M220, M221. McClure Mountain (MM) was the primary standard.

Standard	Accepted Age	Measured Age	2 sigma	Spots	mswd	P(mswd)
Apatite AFT UThPb 20121029						
AZ	~440	422.54	6.92	39/43	1.37	0.454123
B3	~1128	1082.45	23.58	32/28	1.30	0.666090
DR + DRG	31.44	30.33	0.598	117/169	1.28	0.331916
F5	1099.0	1048.00	17.44	41/43	1.32	0.588628
FC	1099.0	1037.42	20.10	32/38	1.23	0.899578
IF	28.201	28.32	1.77	5/39	2.33	0.088135
MM primary	523.98	528.77	5.02	125/127	0.70	0.122757
OL	913	905.23	13.50	42/42	0.45	0.026769
RA	~410	400.54	6.87	37/43	1.17	1.000000
TI	390.5	429.57	7.41	37/40	1.00	1.000000

Figure A1. Distribution of apatite UPb ages for M23, M25, M211, M220, M221 (top plot; N = 514) and M02, M07, M08, M11, M12, M28 (bottom plot; N=127).



Part II: High Resolution – AFT using REEs and U-Pb Data

Background

In sedimentary rocks and modern sediments, mineral grains such as apatite and zircon from multiple provenance sources may be mixed together. A practical example of where this may be important is the interpretation of apatite fission track (AFT) data from a sandstone. To properly interpret AFT data from such a mixture of sources, it is necessary to bin apatite grains, and their associated AFT data, into discrete groups based on AFT-independent data such as chemical composition or isotopic age.

The Radial Plot uses the AFT ages and age errors to produce one or more vectors that point to an age or ages of presumed geological significance. Algorithm BinomFit deconvolves the AFT age probability density function into one or more age peaks, each peak yielding an age of presumed geological significance. Neither of these approaches requires any AFT-independent data. O'Sullivan et al. (2018) use laser ablation-inductively coupled plasma-mass spectrometry (LA-ICP-MS) to measure rare earth element (REE) concentrations and uranium-lead ($^{206}\text{Pb}^*/^{238}\text{U}$) ages for apatite grains and sort them into groups using principal component analysis.

For High Resolution-AFT (HR-AFT), we sort apatite grains into groups using the following steps: 1) for each of approximately 9 different apatite standard species analyzed during a LA-ICP-MS session, measure REE concentrations and $^{206}\text{Pb}^*/^{238}\text{U}$ ages and calculate the mean and standard deviation for each measured value for each standard, 2) derive a session-specific, best-fit line for each measured value that gives standard deviation as a function of mean among all standards, 3) for each unknown apatite grain (from an unknown group), use the derived best-fit lines to define an apatite grain group centered at the measured values for the unknown grain and bounded by 2 standard deviations about the measured values, and 4) search for and isolate other unknown apatite grains that exhibit measured values that fall within the bounds of the defined apatite grain group.

Using the color ramp for $^{206}\text{Pb}^*/^{238}\text{U}$ age shown in Figure A2, REE plots for all standard apatite grains are shown in Figure A3a; these data were calculated for the mean (Mean), standard deviation (Std Dev), skewness, and kurtosis for 29 FT-independent parameters (Table A7). Major standard apatite grain sub-groups produced by program *Sort by Spot* are shown in Figure A3b.

Using the color ramp for $^{206}\text{Pb}^*/^{238}\text{U}$ age shown in Figure A2, REE plots for all unknown apatite grains are shown in Figure A4a. These apatite grain sub-groups were sorted by program *Sort by Spot* and each sub-group for which the number of age grains is ≥ 2 is shown for each sample in Figure A4b. Pooled fission track ages for each sub-group are given in Table A8. Confined fission track length statistics for each sub-group are given in Table A9.

Sort by Spot Method

The *Sort by Spot* method depends on the assumption that each of the 10 standard groups studied here represent a typical group of apatite grains. We derive a linear function

$$Y = m \cdot X + b$$

where:

Y = Std Dev of the calibration parameter for a given standard group

X = Mean log(C1 normalized ppm by weight) value for a given standard group

m = fitted slope

b = fitted Y-intercept

for each FT-independent parameter in Table A7 to constrain the data range for that parameter for any apatite grain group. Figure A5 shows plots of the (X,Y) data from Table A1 and their respective regression lines fitted using the least-squares method. Table A11 lists the slope (m) and intercept (b) values for each fitted line. Table A11 also lists

$b_u = b + (\text{maximum}(Y \text{ measured} - Y \text{ fitted value}))$ for a given FT-independent parameter

Y_{\min} = minimum value of Y measured for a given FT-independent parameter

$Y_{\min} = Y_{\min} + (b_u - b)$.

The *Sort by Spot* method treats each spot as the center of an apatite grain population. At the current spot, data ranges for each FT-independent parameter are calculated as follows:

$Y_u = Y_c + n_{\text{StdDev}} \cdot (m \cdot X + b_u)$

$Y_l = Y_c - n_{\text{StdDev}} \cdot (m \cdot X + b_u)$; Y_l never set less than Y_{\min}

where:

Y_u = upper limit of current FT-independent parameter range

Y_l = lower limit of current FT-independent parameter range

Y_c = current value of FT-independent parameter

n_{StdDev} = number of Std Dev on each side of Y_c .

In this study, the following n_{StdDev} values were used:

$n_{\text{StdDev}} = 3.00$ for $^{206}\text{Pb}/^{238}\text{U}$ Age data range

$n_{\text{StdDev}} = 2.00$ for all other data ranges.

For a general population of spots, the *Sort by Spot* method searches for the spot that has the greatest number of other spots consistent with the hypothesis that they represent the same apatite grain group. Once found, the spot data for this apatite grain sub-group are processed and stored, the spots in this apatite sub-group are removed from the general population of spots, and the process is repeated on the diminished general population of spots until there remain zero spots in the general population.

Thermal History Reconstruction

FT^3 is Apatite.com Partners' software package for calculating thermal histories based on conventional AFT and HR-AFT data. The thermal history implications of the AFT data are summarized in Table A12. The time-temperature constraints used for modeling each sample are summarized in Table A13. Details of the model results for each sample are shown in Part III.

The philosophy of FT^3 is similar to that of AFTSolve (Ketcham et al., 2000) but allows provenance history to vary among modeled apatite grain populations. FT^3 uses the experimental data of Donelick (unpublished), Donelick (1988), Donelick et al. (1990), Donelick (1991), Vrolijk et al. (1992), Carlson et al. (1999), and the calibration of Rmr0 provided by Ketcham et al. (1999). All CFT data are projected onto the c-axis using the model of Donelick (1991) after Donelick et al. (1999).

FT^3 yields tT paths with corresponding AFT age goodness-of-fit (GOF; based on Gaussian probability) and CFT length GOF (based on Kuiper's statistic) values for each population. Models are deemed acceptable when all GOF values are ≥ 0.05 in this study.

References

- Burnham, A.K., Sweeney, J.J., 1989, A chemical kinetic model of vitrinite maturation and reflectance: *Geochimica Cosmochimica Acta*, v. 53, p. 2649–2657.
- Carlson, W.D., Donelick, R.A., and Ketcham, R.A., 1999, Variability of apatite fission track annealing kinetics I: Experimental results: *American Mineralogist*, v. 84, p. 1213-1223.
- Chew, D.M., Babechuk, M.G., Cogné, N., Mark, C., O'Sullivan, G.J., Henrichs, I.A., Doepke, D., and McKenna, C.A., 2016, (LA,Q)-ICPMS trace-element analyses of Durango and McClure Mountain apatite and implications for making natural LA-ICPMS mineral standards: *Chemical Geology*, v. 435, p. 35-48.
- Donelick, R.A., 1988, Etchable fission track length reduction in apatite: Experimental observations, theory, and geological applications. Ph.D. Dissertation, Rensselaer Polytechnic Institute, Troy, New York, 414 p.
- Donelick, R.A., 1991, Crystallographic orientation dependence of mean etchable fission track length in apatite: An empirical model and experimental observations: *American Mineralogist*, v. 76, nos. 1 and 2, p. 83-91.
- Donelick, R.A., Ketcham, R.A., and Carlson, W.D., 1999, Variability of apatite fission track annealing kinetics II: Crystallographic orientation effects: *American Mineralogist*, v. 84, p. 1224-1234.
- Donelick, R.A., Roden, M.K., Mooers, J.D., Carpenter, B.S. and Miller, D.S., 1990, Etchable length reduction of induced fission tracks in apatite at room temperature (23°C): Crystallographic orientation effects and "initial" mean lengths: *Nuclear Tracks and Radiation Measurements*, v. 17, no. 3, p. 261-265.
- Ketcham, R.A., Donelick, R.A., and Carlson, W.D., 1999, Variability of apatite fission track annealing kinetics III: Extrapolation to geological time scales: *American Mineralogist*, v. 84, p. 1235-1255.
- Ketcham, R.A., Donelick, R.A., and Donelick, M.B., 2000, AFTSolve: A program for multi-kinetic modeling of apatite fission-track data: *Geological Materials Research*, v.88, n.5-6, p. 929-929.
- Nielsen, S.B., Clausen, O.R., McGregor, E., 2017, Basin%Ro: A vitrinite reflectance model derived from basin and laboratory data: *Basin Research*, v. 29, suppl. 1, p. 515-536. doi:10.1111/bre.12160
- O'Sullivan, G., Chew, D.M., Morton, A.C., and Mark, C., 2018, An integrated apatite geochronology and geochemistry tool for sedimentary provenance analysis: *Geochemistry, Geophysics, Geosystems*, v. 19, no. 9, p. 1309-1326.
- Schenk, O., Peters, K.E., Burnham, A.K., 2017, Evaluation of alternatives to Easy%R0 for calibration of basin and petroleum system models. Extended abstract, EAGE, Paris, France.
- Vrolijk, P., Donelick, R.A., Queng, J., and Cloos, M., 1992, Testing models of fission track annealing in apatite in a simple thermal setting: Site 800, Leg 129. In: Larson, R.L. et al., *Proceedings of the Ocean Drilling Program, Scientific Results, Volume 129*, p. 169-176.

Figure A2. REE plots in this study are color-coded by $^{206}\text{Pb}^*/^{238}\text{U}$ age using this color ramp.

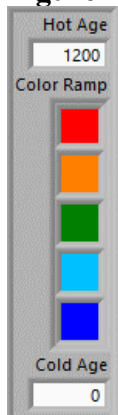
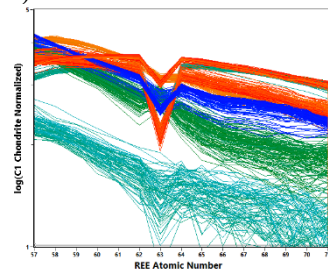


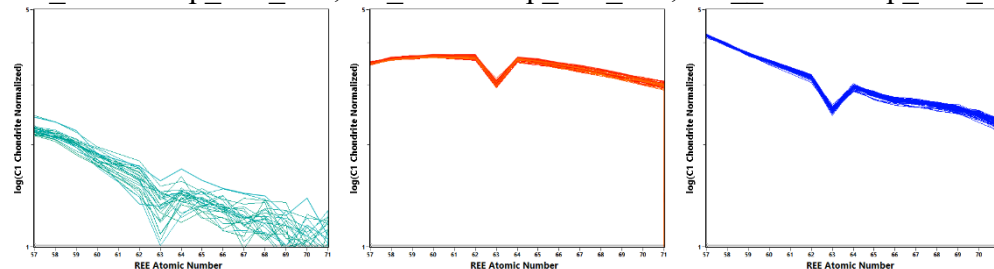
Figure A3. REE plots colored by U-Pb age (Figure A2) for apatite standards in this study.

a) All standards.

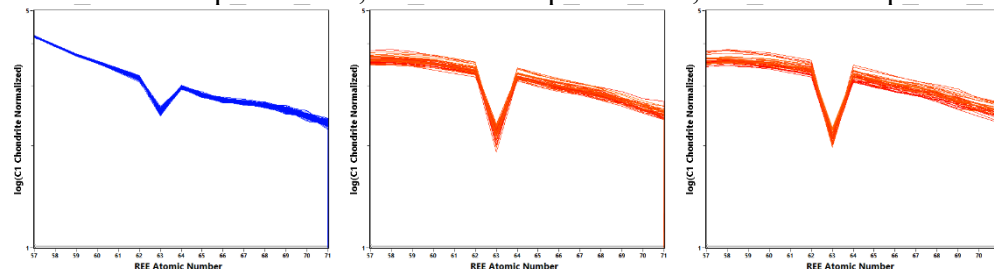


b) Major standard sub-groups from *Sort by Spot*. Based on 2.5σ general including REE values, 2.5σ U-Pb age, 2.5σ Eu anomaly, and 2.5σ REE difference values.

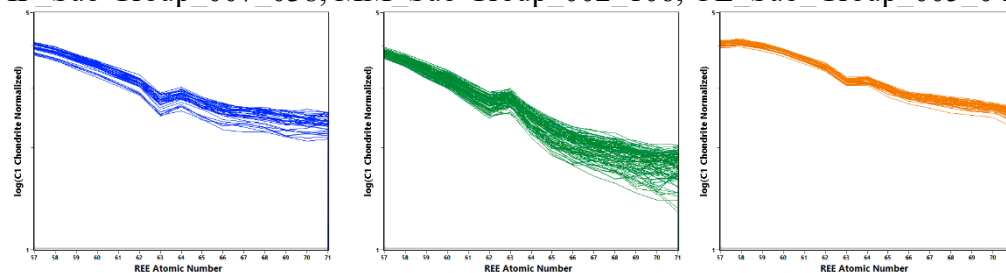
AZ_Sub Group_004_053, B3_Sub Group_006_038, DR_Sub Group_001_169



DRG_Sub Group_001_169, F5_Sub Group_003_077, FC_Sub Group_003_077



IF_Sub Group_007_038, MM_Sub Group_002_106, OL_Sub Group_005_042



RA Sub Group 004_053, TI Sub Group 008_038

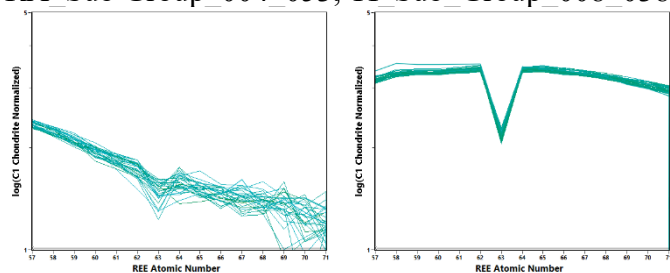
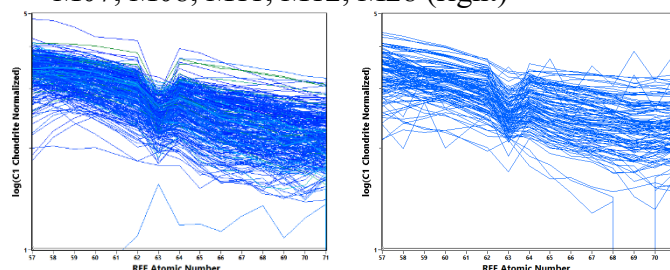


Figure A4. REE plots colored by U-Pb age (Figure A2) for apatite unknowns in this study.

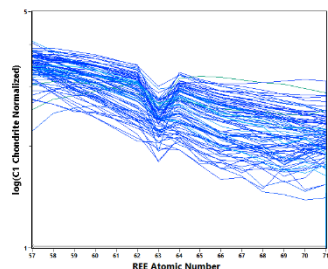
a) All apatite grains from samples M23, M25, M211, M220, M221 (left) and samples M02, M07, M08, M11, M12, M28 (right)



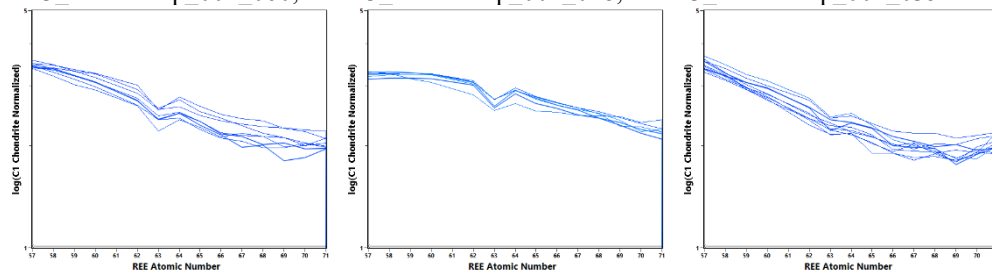
b) Unknown sub-groups having 2 or more AFT grain ages, from *Sort by Spot*. Based on 2.5σ general including REE values, 2.5σ U-Pb age, 2.5σ Eu anomaly, and 2.5σ REE difference values.

M23

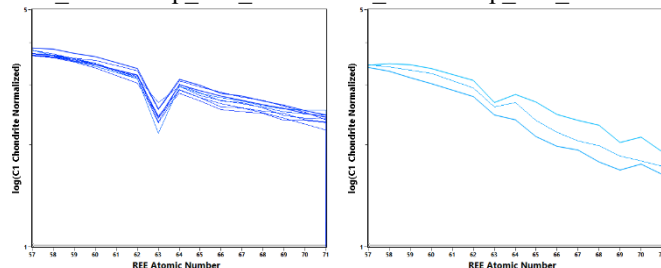
All



M23 Sub Group 001_060, MM23 Sub Group 002_048, MM23 Sub Group 004_035

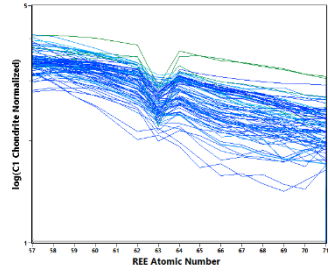


M23 Sub Group 005_033 MM23 Sub Group 010_015

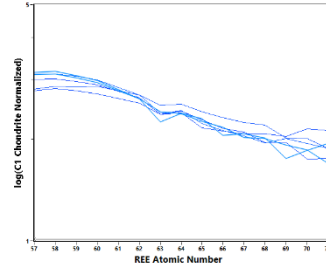
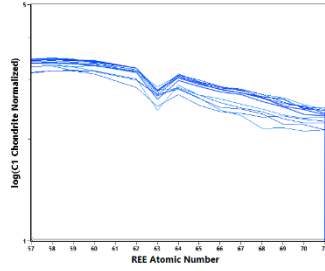
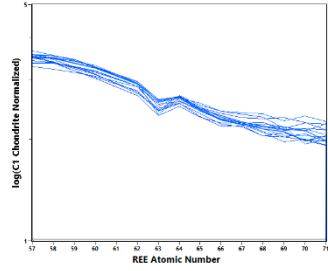


M25

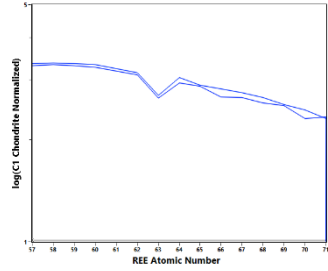
All



M25_Sub Group_001_060, MM25_Sub Group_002_048, MM25_Sub Group_006_033

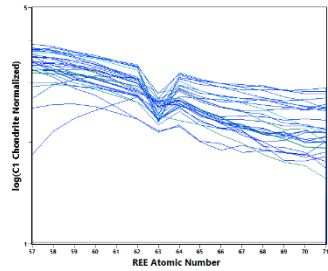


M25_Sub Group_009_018

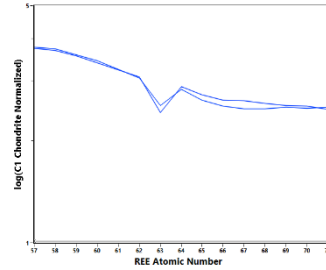
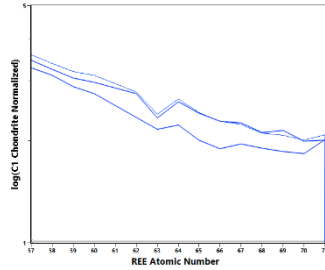
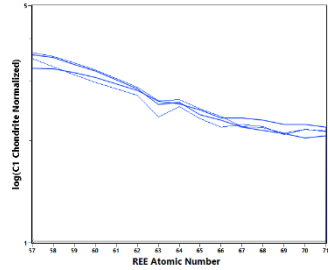


M211

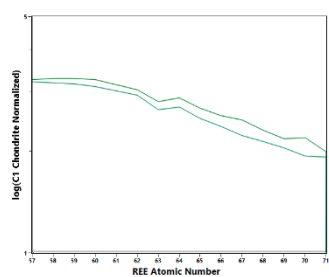
All



MM211_Sub Group_001_060, MM211_Sub Group_004_035, MM211_Sub Group_033_004

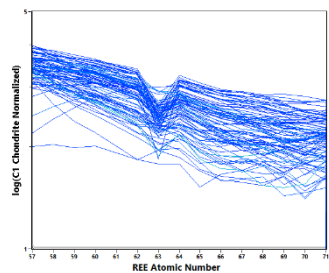


M211_Sub Group_037_003

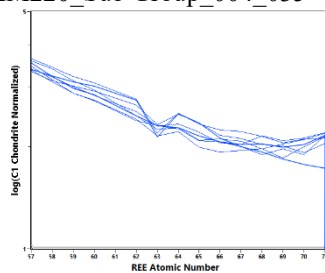
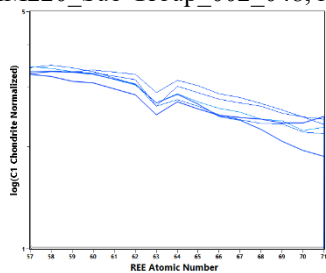
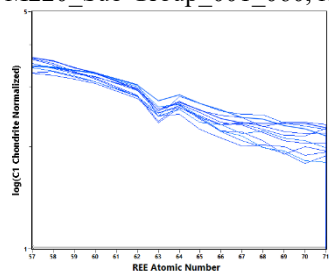


M220

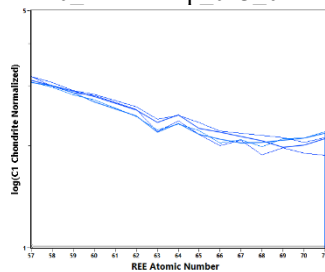
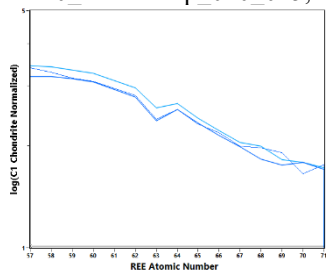
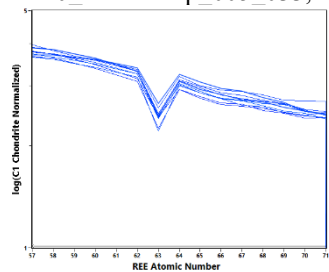
All



M220_Sub Group_001_060, MM220_Sub Group_002_048, MM220_Sub Group_004_035

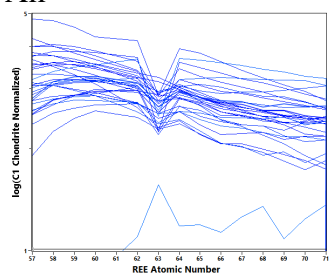


M220_Sub Group_005_033, MM220_Sub Group_010_015, MM220_Sub Group_013_011



M221

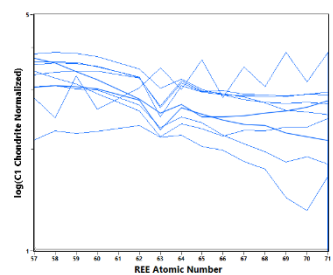
All



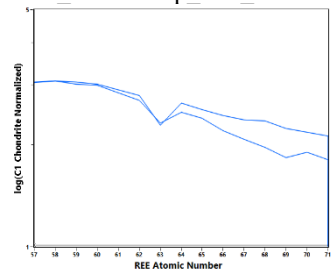
No sub-groups with 2 or more AFT grain ages.

M02

All

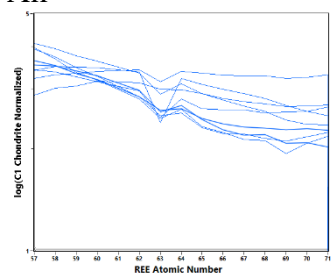


M02_Sub Group_006_033

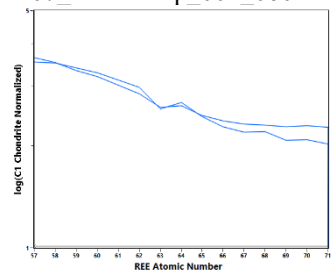


M07

All

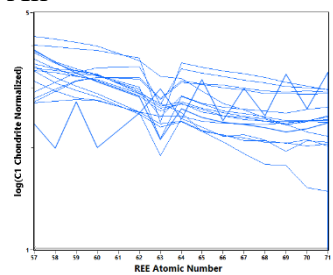


M07_Sub Group_001_060

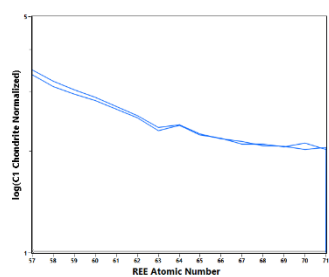


M08

All

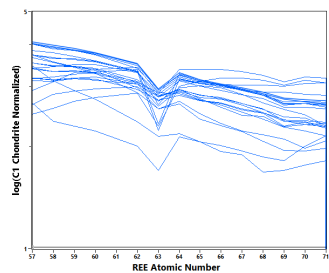


M08_Sub Group_004_035

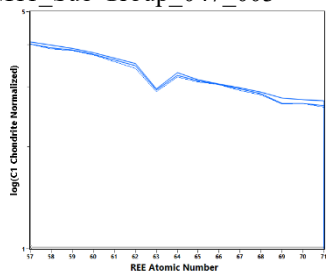
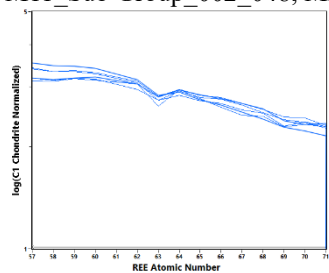


M11

All

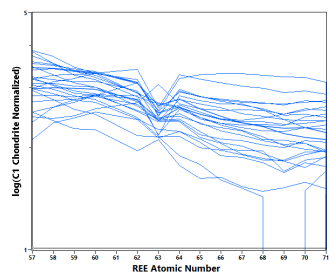


M11_Sub Group_002_048, MM11_Sub Group_047_003

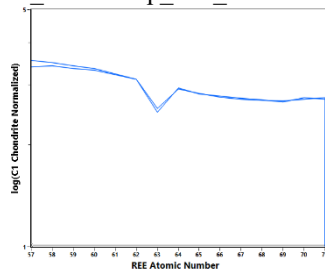
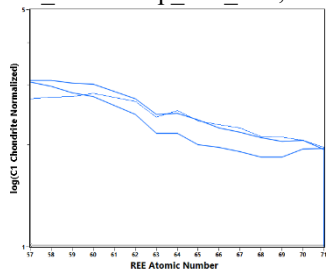
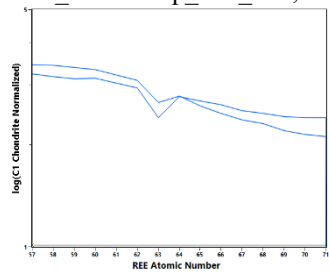


M12

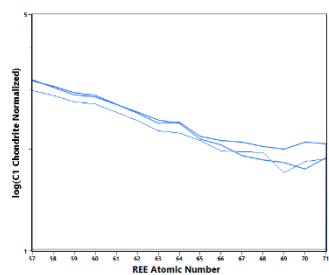
All



M12_Sub Group_002_048, MM12_Sub Group_006_033, MM12_Sub Group_009_018

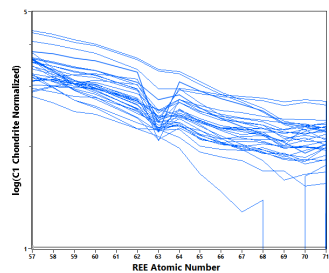


M12_Sub Group_013_011

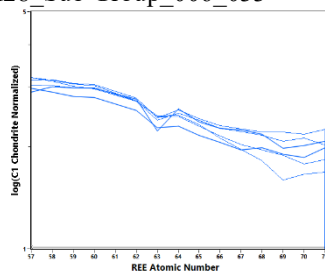
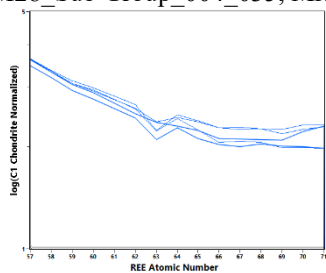
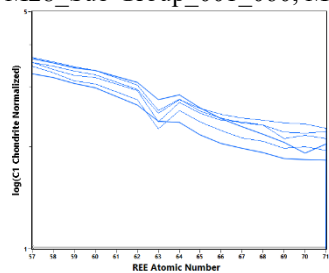


M28

All



M28_Sub Group_001_060, MM28_Sub Group_004_035, MM28_Sub Group_006_033



M28_Sub Group_019_008, MM28_Sub Group_078_002

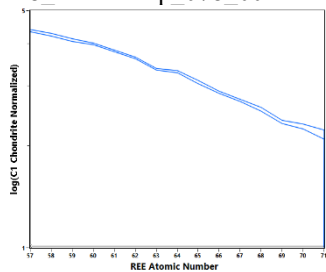
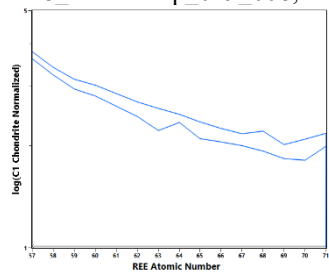


Figure A5a. Calibrations of log(C1 Normalized La ppm) Std Dev and log(C1 Normalized Ce ppm)-log(C1 Normalized La ppm) Std Dev versus Mean log(C1 Normalized La ppm).

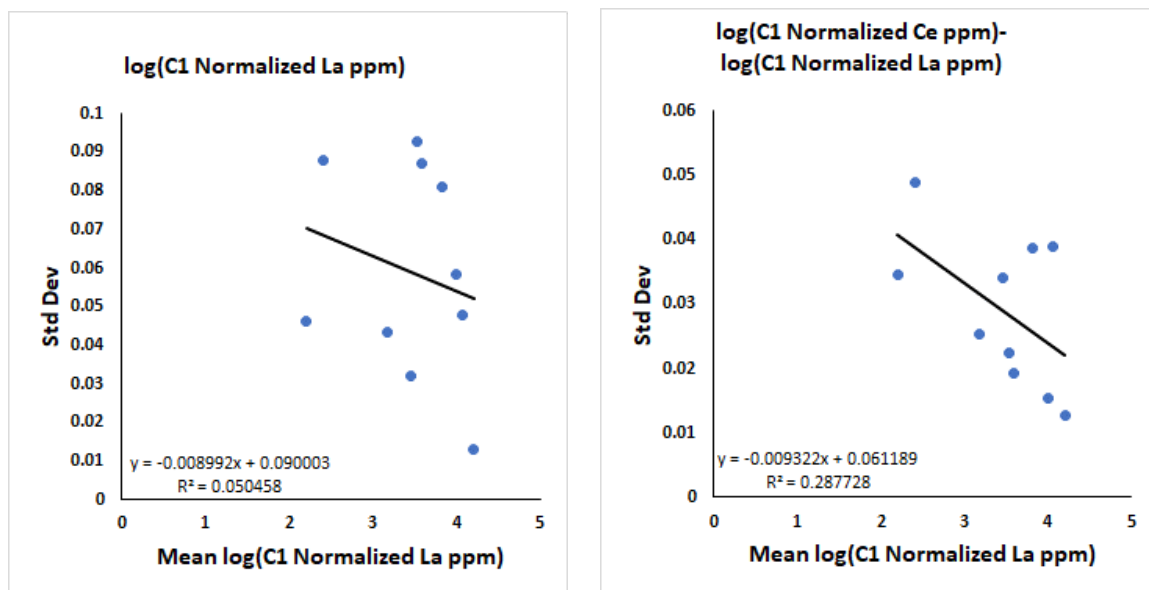


Figure A5b. Calibrations of log(C1 Normalized Ce ppm) Std Dev and log(C1 Normalized Pr ppm)-log(C1 Normalized Ce ppm) Std Dev versus Mean log(C1 Normalized Ce ppm).

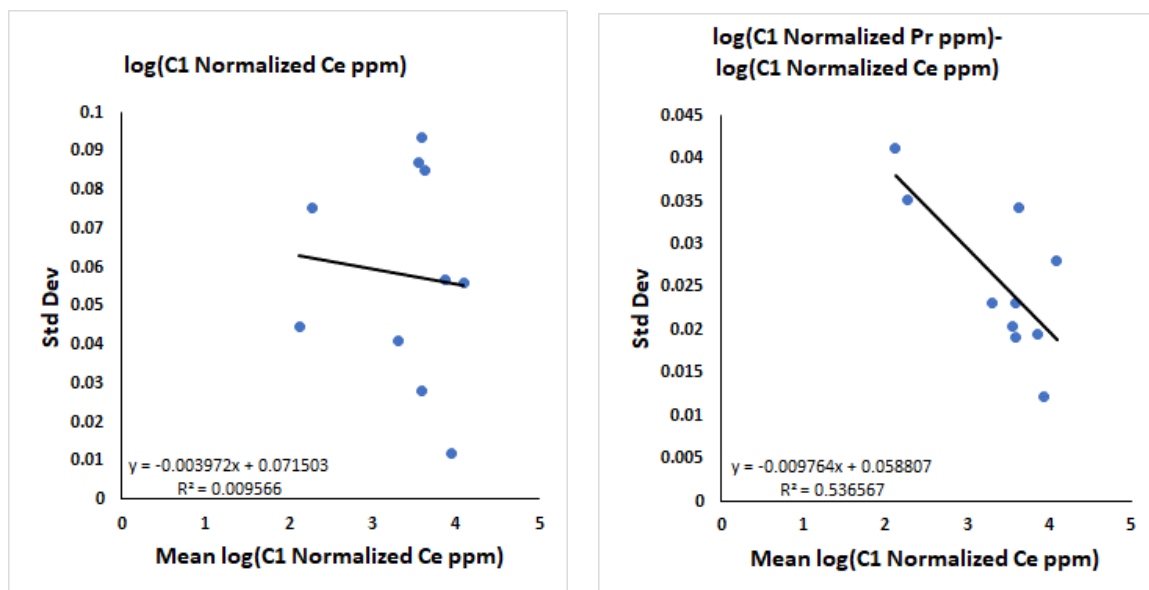


Figure A5c. Calibrations of $\log(\text{C1 Normalized Pr ppm})$ Std Dev and $\log(\text{C1 Normalized Nd ppm})$ - $\log(\text{C1 Normalized Pr ppm})$ Std Dev versus Mean $\log(\text{C1 Normalized Pr ppm})$.

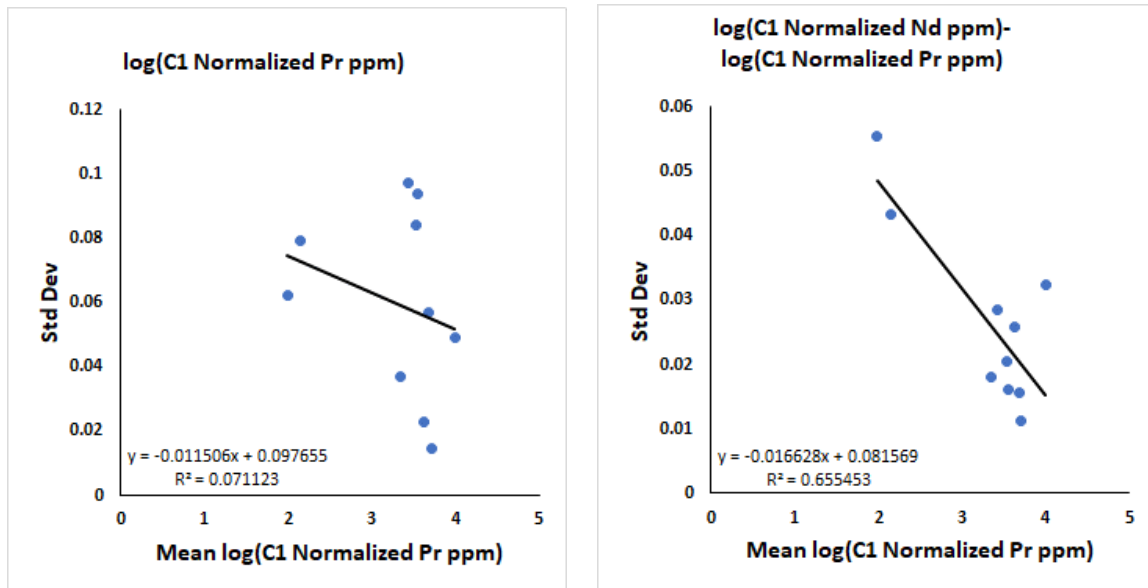


Figure A5d. Calibrations of $\log(\text{C1 Normalized Nd ppm})$ Std Dev and $\log(\text{C1 Normalized Sm ppm})$ - $\log(\text{C1 Normalized Nd ppm})$ Std Dev versus Mean $\log(\text{C1 Normalized Nd ppm})$.

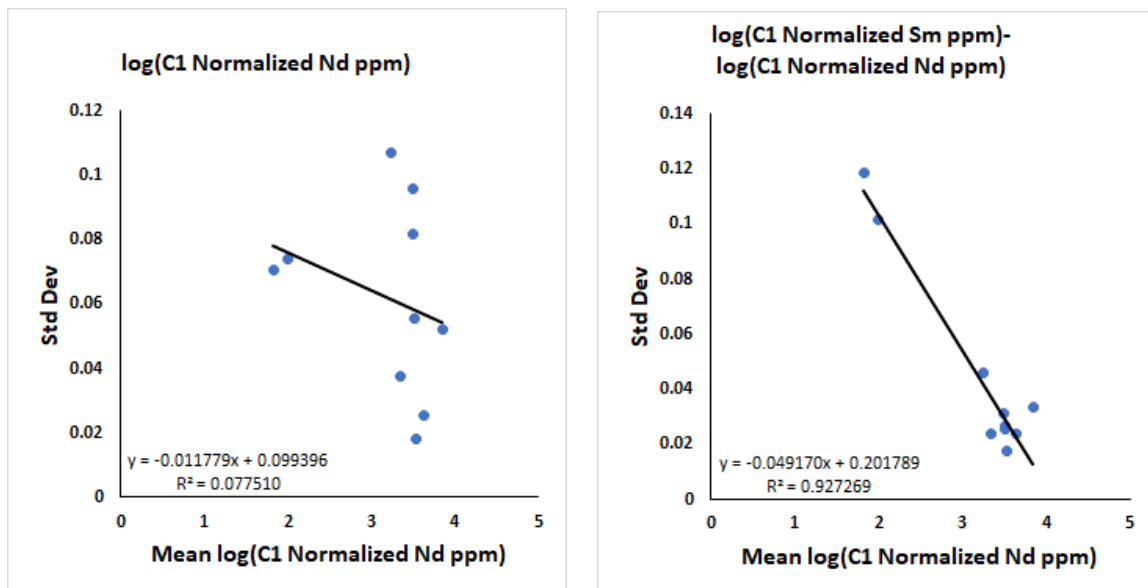


Figure A5e. Calibrations of $\log(\text{C1 Normalized Sm ppm})$ Std Dev and $\log(\text{C1 Normalized Eu ppm}) - \log(\text{C1 Normalized Sm ppm})$ Std Dev versus Mean $\log(\text{C1 Normalized Sm ppm})$.

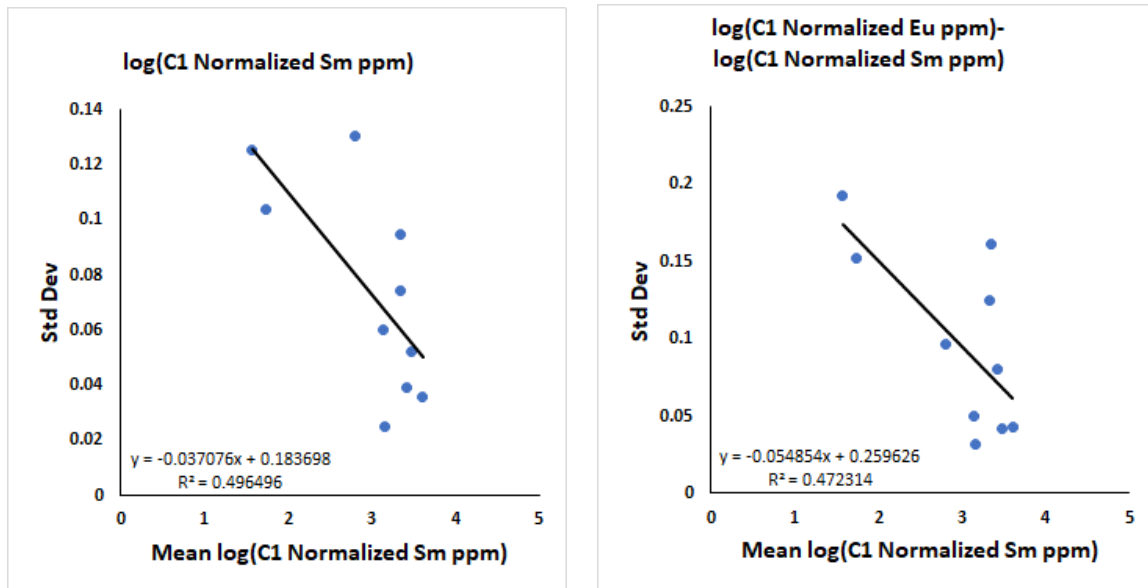


Figure A5f. Calibrations of $\log(\text{C1 Normalized Eu ppm})$ Std Dev and $\log(\text{C1 Normalized Gd ppm}) - \log(\text{C1 Normalized Eu ppm})$ Std Dev versus Mean $\log(\text{C1 Normalized Eu ppm})$.

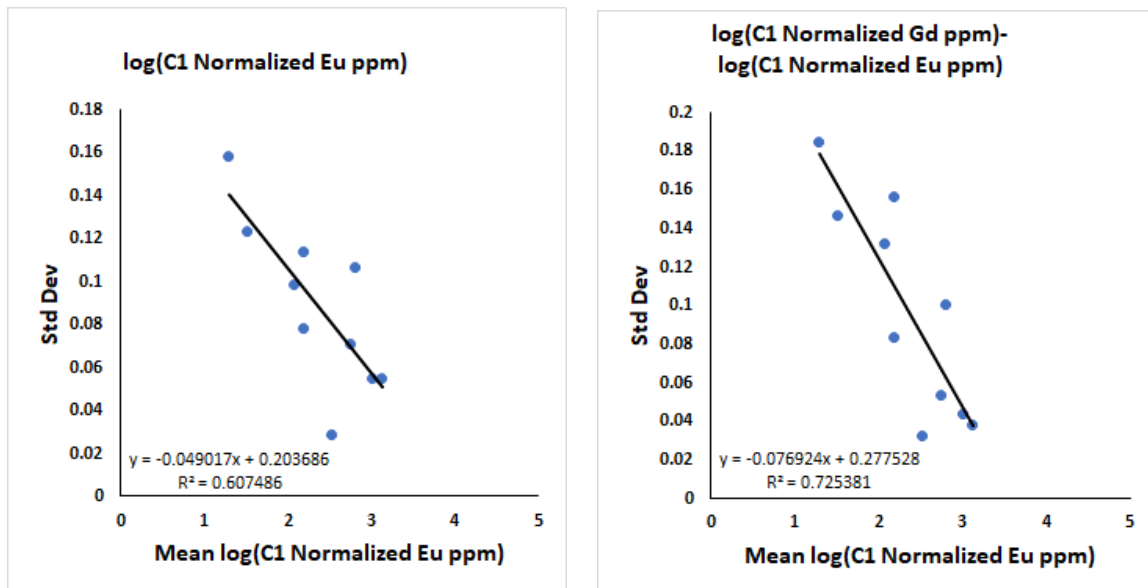


Figure A5g. Calibrations of log(C1 Normalized Gd ppm) Std Dev and log(C1 Normalized Tb ppm)-log(C1 Normalized Gd ppm) Std Dev versus Mean log(C1 Normalized Gd ppm).

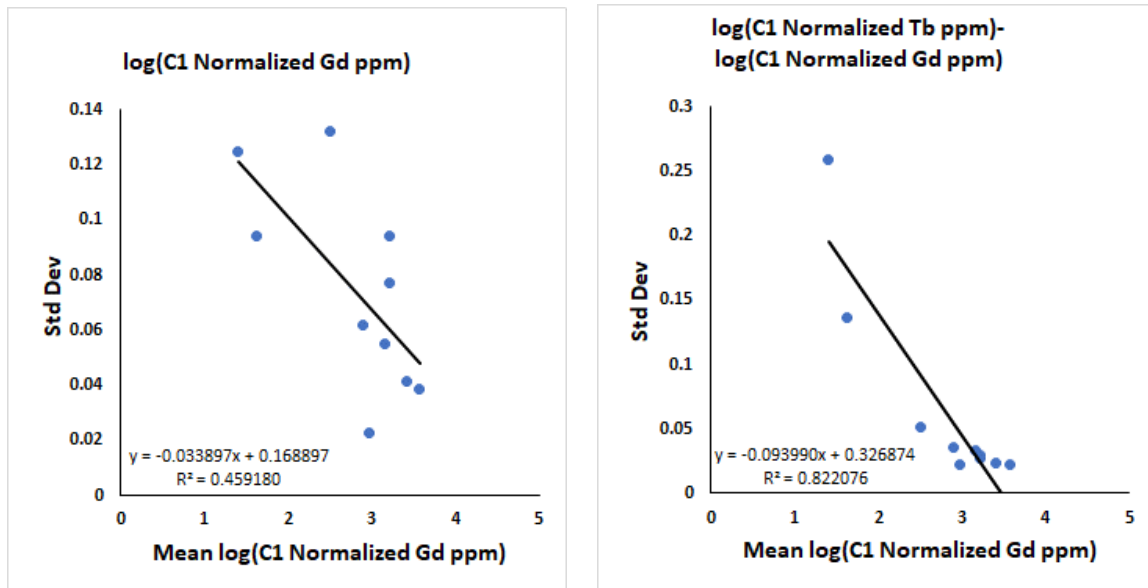


Figure A5h. Calibrations of log(C1 Normalized Tb ppm) Std Dev and log(C1 Normalized Dy ppm)-log(C1 Normalized Tb ppm) Std Dev versus Mean log(C1 Normalized Tb ppm).

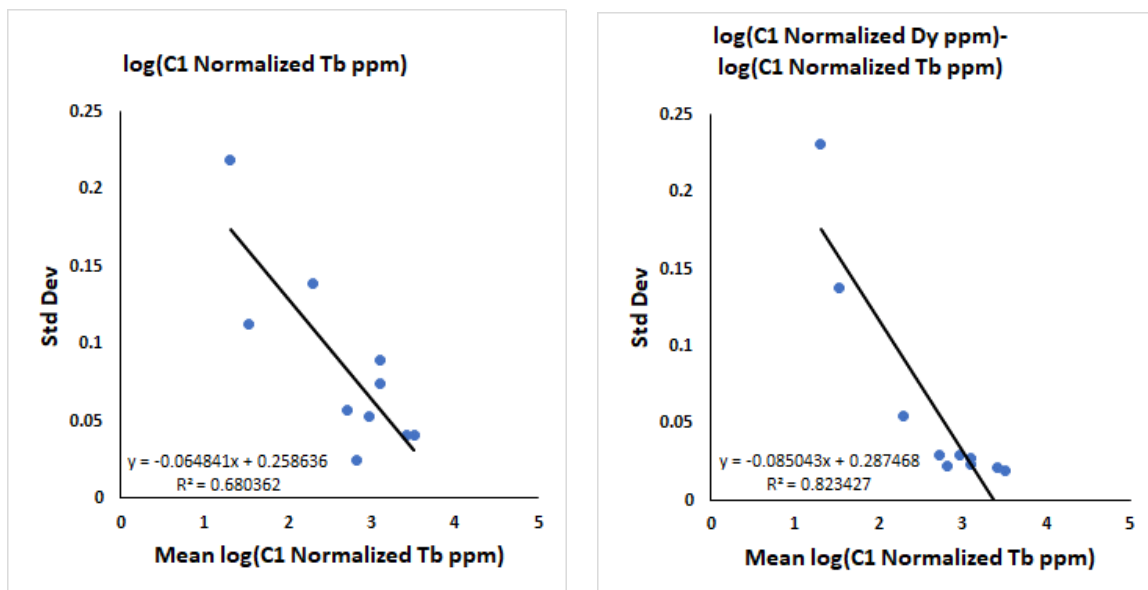


Figure A5i. Calibrations of $\log(\text{C1 Normalized Dy ppm})$ Std Dev and $\log(\text{C1 Normalized Ho ppm}) - \log(\text{C1 Normalized Dy ppm})$ Std Dev versus Mean $\log(\text{C1 Normalized Dy ppm})$.

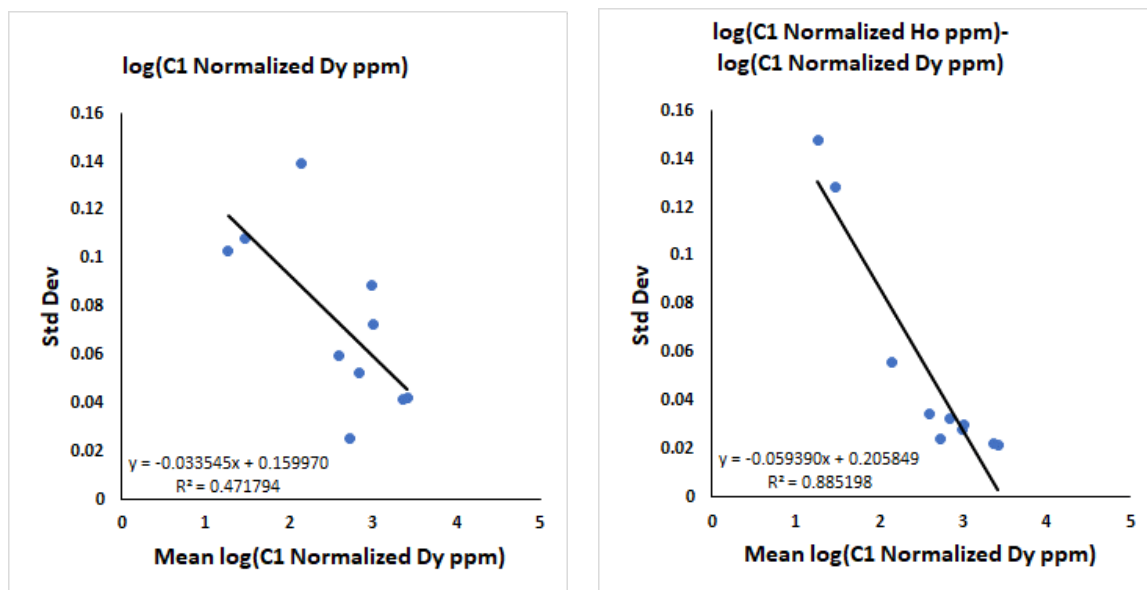


Figure A5j. Calibrations of $\log(\text{C1 Normalized Ho ppm})$ Std Dev and $\log(\text{C1 Normalized Er ppm}) - \log(\text{C1 Normalized Ho ppm})$ Std Dev versus Mean $\log(\text{C1 Normalized Ho ppm})$.

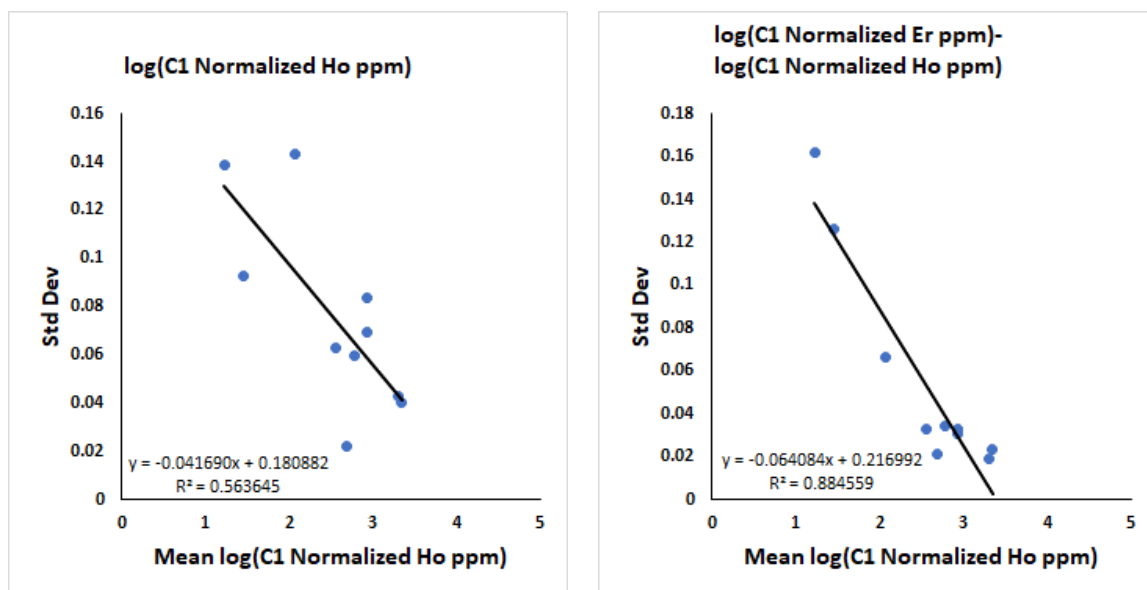


Figure A5k. Calibrations of log(C1 Normalized Er ppm) Std Dev and log(C1 Normalized Tm ppm)-log(C1 Normalized Er ppm) Std Dev versus Mean log(C1 Normalized Er ppm).

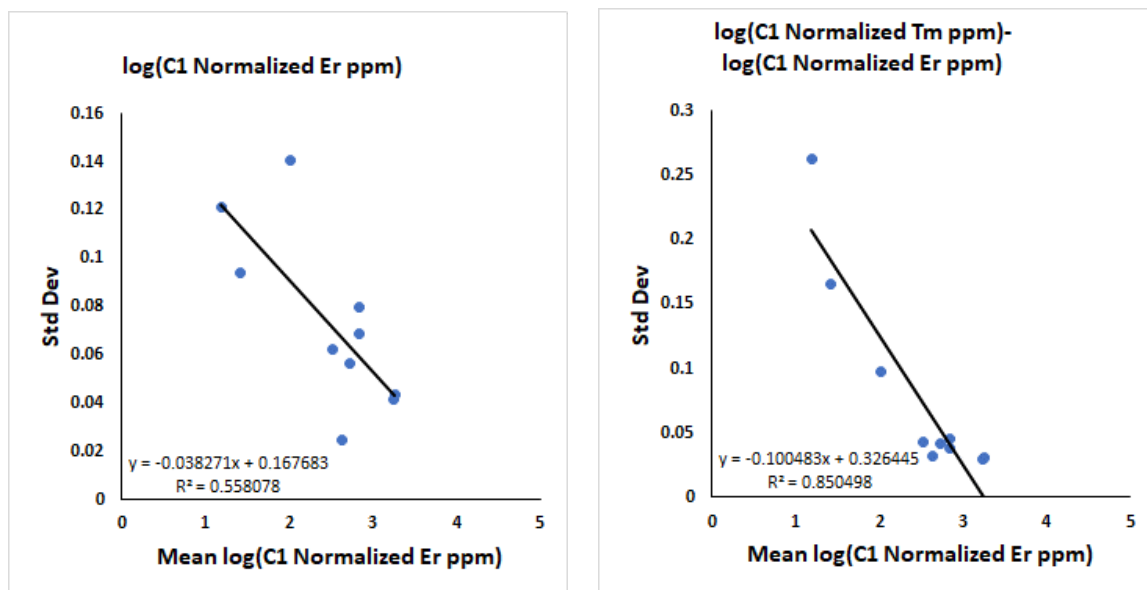


Figure A5l. Calibrations of log(C1 Normalized Tm ppm) Std Dev and log(C1 Normalized Yb ppm)-log(C1 Normalized Tm ppm) Std Dev versus Mean log(C1 Normalized Tm ppm).

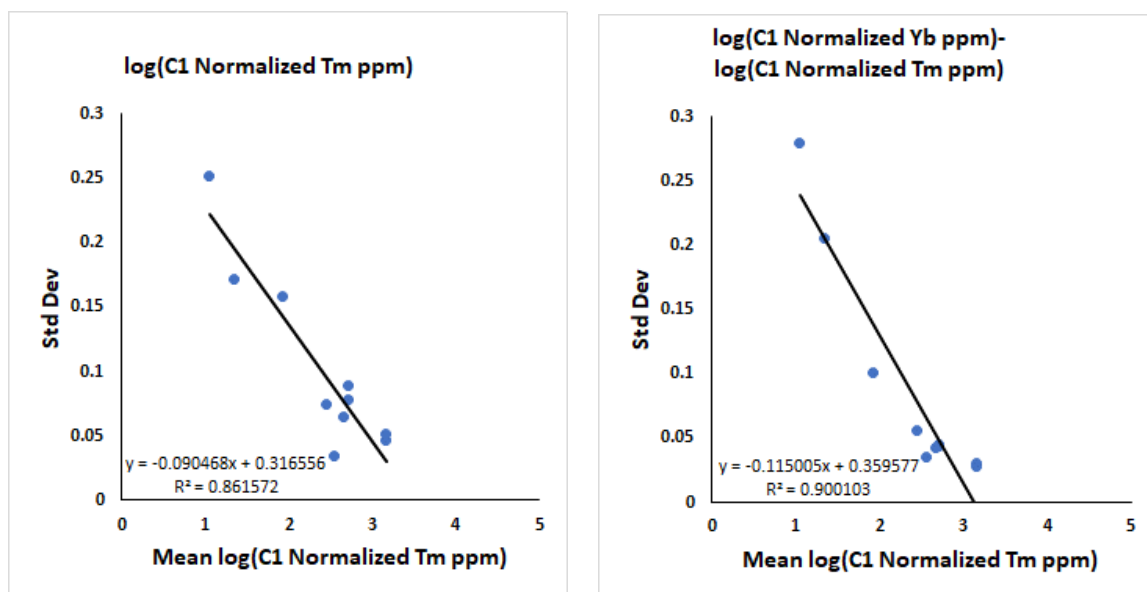


Figure A5m. Calibrations of $\log(\text{C1 Normalized Yb ppm})$ Std Dev and $\log(\text{C1 Normalized Lu ppm}) - \log(\text{C1 Normalized Yb ppm})$ Std Dev versus Mean $\log(\text{C1 Normalized Yb ppm})$.

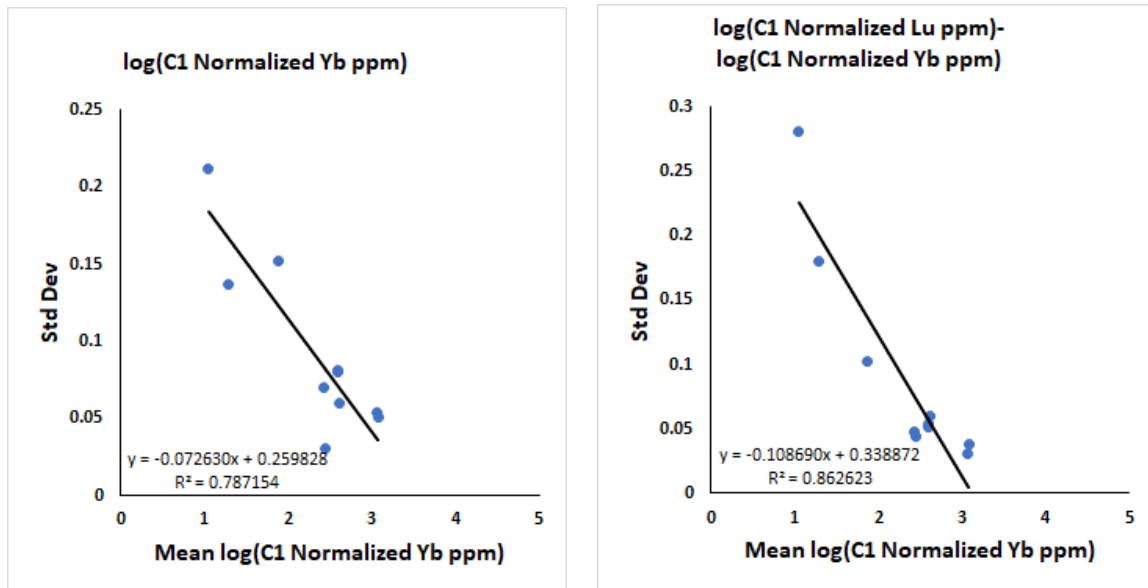


Figure A5n. Calibrations of $\log(\text{C1 Normalized Lu ppm})$ Std Dev and $\log(\text{C1 Normalized La ppm}) - \log(\text{C1 Normalized Lu ppm})$ Std Dev versus Mean $\log(\text{C1 Normalized Lu ppm})$.

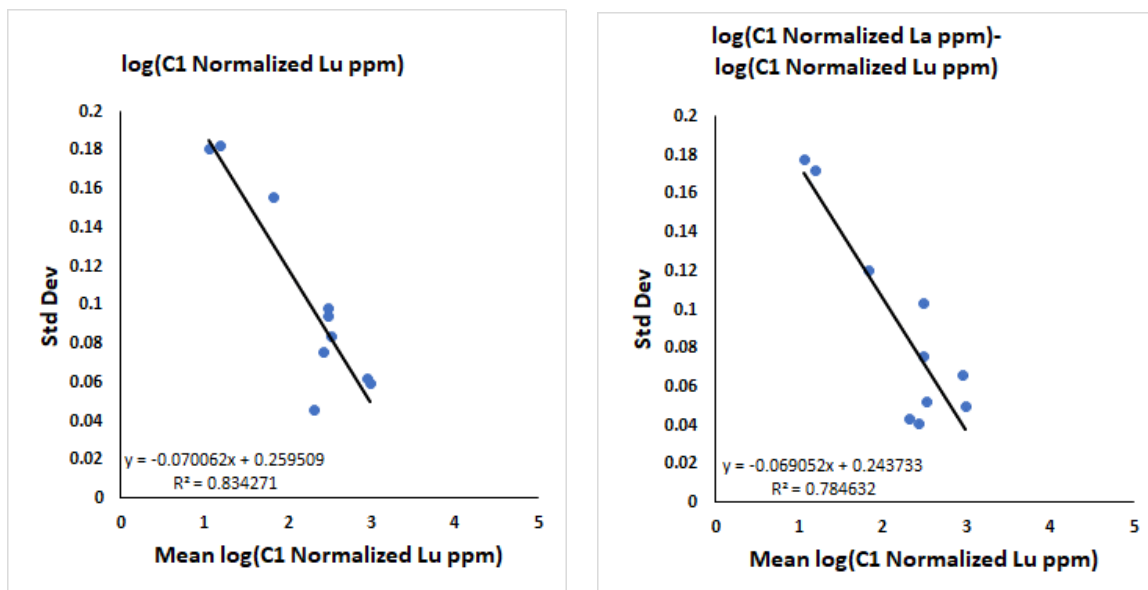


Figure A5o. Calibration of $^{206}\text{Pb}^*/^{238}\text{U}$ Age Std Dev versus Mean $^{206}\text{Pb}^*/^{238}\text{U}$ Age.

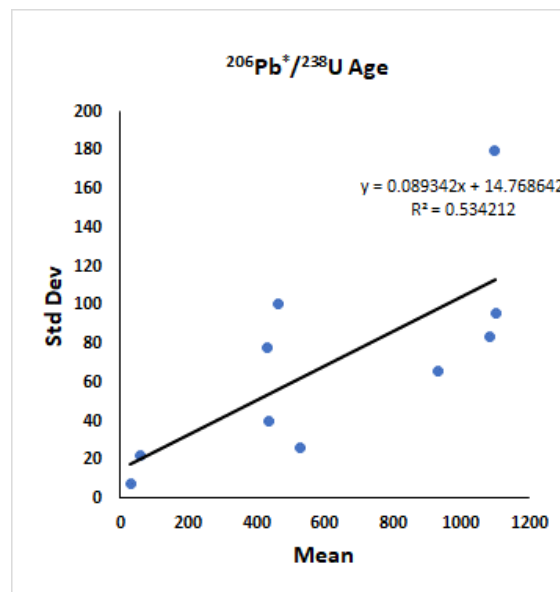


Table A7. Statistical analysis of FT-independent data measured for each standard group data used to calibrate the *Sort by Spot* method used in this study.

log(C1 Normalized La ppm)						log(C1 Normalized Ce ppm)-log(C1 Normalized La ppm)					
Standard Group	Mean ppm value	Std Dev ppm value	Skewness	Kurtosis	Number of Spots	Standard Group	Mean ppm value Difference	Mean ppm value	Std Dev ppm value Difference	Skewness	Kurtosis
	X	Y						X	Y		
AZ	2.201699	0.046244	-0.022268	3.343481	60of 69	AZ	-0.079623	2.201699	0.034519	0.528909	4.692404
B3	3.458924	0.031908	-0.051845	2.776542	65 of 66	B3	0.128476	3.458924	0.034206	2.444999	15.009003
DR+DRG	4.202885	0.013145	-0.570919	5.725927	230 of 232	DR+DRG	-0.266737	4.202885	0.012690	0.034629	5.116578
F5	3.586515	0.087132	0.823378	4.108223	102 of 104	F5	-0.005023	3.586515	0.019385	0.466411	3.925589
FC	3.536592	0.092991	0.250832	5.389727	61 of 66	FC	0.020886	3.536592	0.022458	1.039587	5.734459
IF	3.998489	0.058491	-0.073521	2.068335	54 of 69	IF	-0.137953	3.998489	0.015347	0.183048	3.029001
MM	3.817985	0.081000	0.203124	2.938161	264 of 278	MM	-0.184827	3.817985	0.038788	-0.093392	3.415949
OL	4.066027	0.047896	-0.783628	2.892377	69 of 70	OL	0.020049	4.066027	0.039035	1.089239	4.212498
RA	2.401441	0.088014	0.756097	3.457485	67 of 68	RA	-0.126580	2.401441	0.048914	-1.399128	8.458202
TI	3.175307	0.043482	0.651496	2.758166	65 of 69	TI	0.131615	3.175307	0.025451	0.336267	2.715640
log(C1 Normalized Ce ppm)						log(C1 Normalized Pr ppm)-log(C1 Normalized Ce ppm)					
Standard Group	Mean ppm value	Std Dev ppm value	Skewness	Kurtosis		Standard Group	Mean ppm value Difference	Mean ppm value	Std Dev ppm value Difference	Skewness	Kurtosis
	X	Y						X	Y		
AZ	2.122076	0.04478	0.479793	2.718506		AZ	-0.134967	2.122076	0.041251	0.129993	2.729191
B3	3.587400	0.028100	0.470046	5.804456		B3	0.034101	3.587400	0.023179	-0.390446	6.580905
DR+DRG	3.936148	0.012027	-0.912453	5.793841		DR+DRG	-0.229698	3.936148	0.012220	-0.340431	4.247922
F5	3.581492	0.093587	0.966811	4.201492		F5	-0.034078	3.581492	0.019157	1.847689	11.013196
FC	3.557477	0.087284	1.047258	5.937585		FC	-0.028477	3.557477	0.020412	0.209345	2.284832
IF	3.860536	0.056954	0.078751	1.948518		IF	-0.178572	3.860536	0.019557	0.125534	3.190674
MM	3.633158	0.085070	0.231555	2.915997		MM	-0.205644	3.633158	0.034251	0.136027	2.941075
OL	4.086076	0.055892	-0.214483	3.298371		OL	-0.093005	4.086076	0.028123	-0.836177	5.591966
RA	2.274861	0.075478	0.408172	3.213564		RA	-0.132253	2.274861	0.035266	0.372476	4.631254
TI	3.306922	0.041018	0.433578	2.943849		TI	0.035495	3.306922	0.023204	-0.236156	3.759432
log(C1 Normalized Pr ppm)						log(C1 Normalized Nd ppm)-log(C1 Normalized Pr ppm)					
Standard Group	Mean ppm value	Std Dev ppm value	Skewness	Kurtosis		Standard Group	Mean ppm value Difference	Mean ppm value	Std Dev ppm value Difference	Skewness	Kurtosis
	X	Y						X	Y		
AZ	1.987109	0.062395	0.045149	2.170480		AZ	-0.161874	1.987109	0.055492	0.005175	2.750997
B3	3.621501	0.022875	0.792644	7.514912		B3	0.011994	3.621501	0.025834	-1.063078	4.471554
DR+DRG	3.706450	0.014439	-0.339256	4.638296		DR+DRG	-0.180694	3.706450	0.011380	-0.252855	4.036803
F5	3.547414	0.094099	1.058282	4.418297		F5	-0.047949	3.547414	0.016014	-0.482327	3.303655
FC	3.529000	0.084222	1.226290	5.513608		FC	-0.039694	3.529000	0.020603	0.418617	3.057997
IF	3.681964	0.056753	0.139783	1.769328		IF	-0.173002	3.681964	0.015647	0.741238	4.701056
MM	3.427514	0.097088	0.266936	3.164835		MM	-0.188397	3.427514	0.028450	0.274173	3.442389
OL	3.993071	0.048901	-0.586401	2.932586		OL	-0.149779	3.993071	0.032436	0.892378	10.138741
RA	2.142607	0.079232	0.517590	2.956901		RA	-0.147207	2.142607	0.043351	-0.461754	3.165562

TI	3.342417	0.037095	0.437552	2.892957		TI	0.001982	3.342417	0.018093	-0.282901	2.822504
log(C1 Normalized Nd ppm)						log(C1 Normalized Sm ppm)-log(C1 Normalized Nd ppm)					
Standard Group	Mean ppm value	Std Dev ppm value	Skewness	Kurtosis		Standard Group	Mean ppm value Difference	Mean ppm value	Std Dev ppm value Difference	Skewness	Kurtosis
	X	Y						X	Y		
AZ	1.825235	0.070831	0.224472	3.582640		AZ	-0.254665	1.825235	0.118726	-0.443001	4.762856
B3	3.633495	0.025620	0.182444	3.446224		B3	-0.026239	3.633495	0.023984	-0.068223	3.156565
DR+DRG	3.525756	0.017991	-0.543245	3.957297		DR+DRG	-0.364687	3.525756	0.017714	-0.486857	4.582223
F5	3.499465	0.095769	1.094837	4.544697		F5	-0.159779	3.499465	0.025373	-0.027572	2.942185
FC	3.489306	0.081899	1.247070	5.085854		FC	-0.155906	3.489306	0.031500	-0.035779	3.188913
IF	3.508962	0.055517	0.012748	1.997784		IF	-0.371866	3.508962	0.026894	0.505484	3.029018
MM	3.239118	0.106764	0.265973	3.015476		MM	-0.445236	3.239118	0.045784	-0.102593	3.088961
OL	3.843293	0.052207	-0.349143	2.488556		OL	-0.374898	3.843293	0.033720	-0.460686	5.301264
RA	1.995400	0.074133	0.454106	3.514883		RA	-0.254118	1.995400	0.101718	-0.208390	3.609066
TI	3.344400	0.037427	0.595754	3.656231		TI	0.069628	3.344400	0.023742	-1.050116	5.487454
log(C1 Normalized Sm ppm)						log(C1 Normalized Eu ppm)-log(C1 Normalized Sm ppm)					
Standard Group	Mean ppm value	Std Dev ppm value	Skewness	Kurtosis		Standard Group	Mean ppm value Difference	Mean ppm value	Std Dev ppm value Difference	Skewness	Kurtosis
	X	Y						X	Y		
AZ	1.570570	0.125534	-0.282204	4.304985		AZ	-0.281043	1.570570	0.192502	0.263942	4.559305
B3	3.607256	0.035526	-0.010442	2.950545		B3	-0.597763	3.607256	0.042836	-0.221475	3.025124
DR+DRG	3.161069	0.024880	-0.855749	6.262916		DR+DRG	-0.635166	3.161069	0.031522	0.283756	4.015454
F5	3.339686	0.094931	1.152548	4.329620		F5	-1.158573	3.339686	0.161358	-0.299162	2.930588
FC	3.333400	0.074279	0.980049	4.198285		FC	-1.262733	3.333400	0.125260	0.279883	3.059927
IF	3.137096	0.059871	0.006172	2.390625		IF	-0.389919	3.137096	0.050322	-1.634226	7.585874
MM	2.793881	0.130507	0.135986	3.125189		MM	0.001906	2.793881	0.096924	-0.210364	2.813050
OL	3.468395	0.052103	-0.406632	2.595706		OL	-0.346296	3.468395	0.041509	0.564634	6.259212
RA	1.741283	0.103915	-0.270439	3.774121		RA	-0.225013	1.741283	0.151877	0.392989	3.759978
TI	3.414028	0.039224	0.262813	3.130264		TI	-1.231274	3.414028	0.080311	-0.261020	7.308839
log(C1 Normalized Eu ppm)						log(C1 Normalized Gd ppm)-log(C1 Normalized Eu ppm)					
Standard Group	Mean ppm value	Std Dev ppm value	Skewness	Kurtosis		Standard Group	Mean ppm value Difference	Mean ppm value	Std Dev ppm value Difference	Skewness	Kurtosis
	X	Y						X	Y		
AZ	1.289527	0.158090	-0.717352	2.912967		AZ	0.113963	1.289527	0.184925	-0.258565	2.750370
B3	3.009493	0.055087	-0.259447	2.312157		B3	0.559117	3.009493	0.043943	0.082708	2.913210
DR+DRG	2.525903	0.028479	-0.261268	3.012110		DR+DRG	0.446259	2.525903	0.032333	0.398806	3.550326
F5	2.181114	0.113798	-0.040270	3.778793		F5	1.035603	2.181114	0.156517	0.260387	3.110038
FC	2.070667	0.098545	0.542931	3.684750		FC	1.144076	2.070667	0.132127	-0.403482	2.958674
IF	2.747177	0.071164	-0.105031	2.581214		IF	0.140785	2.747177	0.053598	1.697645	8.674565
MM	2.795787	0.106354	0.073558	2.682140		MM	-0.288349	2.795787	0.100859	0.286236	2.870302
OL	3.122098	0.055035	-0.701602	3.831840		OL	0.030326	3.122098	0.038088	-0.779213	5.764501
RA	1.516269	0.123034	0.524767	2.782434		RA	0.102146	1.516269	0.146481	0.101887	2.673823
TI	2.182754	0.078289	0.114989	4.372599		TI	1.224221	2.182754	0.083245	-0.070464	4.566405

log(C1 Normalized Gd ppm)						log(C1 Normalized Tb ppm)-log(C1 Normalized Gd ppm)					
Standard Group	Mean ppm value	Std Dev ppm value	Skewness	Kurtosis		Standard Group	Mean ppm value Difference	Mean ppm value	Std Dev ppm value Difference	Skewness	Kurtosis
	X	Y						X	Y		
AZ	1.403490	0.125031	-0.241026	3.423925		AZ	-0.091021	1.403490	0.258775	-3.146225	18.950501
B3	3.568610	0.038707	-0.049184	2.566831		B3	-0.064035	3.568610	0.021804	0.147096	3.227282
DR+DRG	2.972161	0.022526	-0.357690	4.121550		DR+DRG	-0.146768	2.972161	0.022862	-0.256168	3.810125
F5	3.216717	0.093919	1.388502	5.314749		F5	-0.113098	3.216717	0.029422	-0.533082	2.643364
FC	3.214743	0.077143	0.591067	3.869151		FC	-0.109137	3.214743	0.027532	-0.116538	3.525221
IF	2.887962	0.061659	0.038966	2.067069		IF	-0.173667	2.887962	0.035928	0.169383	3.451471
MM	2.507439	0.132046	0.219431	3.177865		MM	-0.216691	2.507439	0.051686	-0.348078	3.501691
OL	3.152424	0.054820	-0.054520	2.323043		OL	-0.178455	3.152424	0.033313	-0.10156	4.388082
RA	1.618415	0.094196	-0.095453	3.226383		RA	-0.083338	1.618415	0.136333	0.437034	5.328563
TI	3.406975	0.041546	-0.094443	2.393169		TI	0.011417	3.406975	0.024157	-0.320351	2.543995
log(C1 Normalized Tb ppm)						log(C1 Normalized Dy ppm)-log(C1 Normalized Tb ppm)					
Standard Group	Mean ppm value	Std Dev ppm value	Skewness	Kurtosis		Standard Group	Mean ppm value Difference	Mean ppm value	Std Dev ppm value Difference	Skewness	Kurtosis
	X	Y						X	Y		
AZ	1.312469	0.218908	-3.815626	24.695964		AZ	-0.046503	1.312469	0.231317	3.720014	24.388341
B3	3.504575	0.041076	-0.342420	2.668212		B3	-0.090343	3.504575	0.0195100	0.649282	4.125593
DR+DRG	2.825393	0.024504	-1.217514	8.862386		DR+DRG	-0.104714	2.825393	0.022355	-0.306039	3.775116
F5	3.103618	0.089810	1.112972	4.610453		F5	-0.112167	3.103618	0.027486	0.137415	2.348547
FC	3.105607	0.074029	0.595077	3.747882		FC	-0.105937	3.105607	0.023337	0.139144	3.307039
IF	2.714295	0.056874	0.143015	2.286232		IF	-0.117390	2.714295	0.029741	-0.216047	2.711791
MM	2.290747	0.138612	0.192569	2.846805		MM	-0.140196	2.290747	0.05484	0.014105	2.837923
OL	2.973969	0.053021	-0.104359	2.568734		OL	-0.138837	2.973969	0.029261	-0.063693	3.491082
RA	1.535077	0.112214	0.047890	3.741380		RA	-0.059548	1.535077	0.137383	-0.596599	4.295193
TI	3.418392	0.040589	0.308978	3.173600		TI	-0.057115	3.418392	0.021646	-0.2108700	4.072596
log(C1 Normalized Dy ppm)						log(C1 Normalized Ho ppm)-log(C1 Normalized Dy ppm)					
Standard Group	Mean ppm value	Std Dev ppm value	Skewness	Kurtosis		Standard Group	Mean ppm value Difference	Mean ppm value	Std Dev ppm value Difference	Skewness	Kurtosis
	X	Y						X	Y		
AZ	1.265966	0.103094	-0.274031	3.200534		AZ	-0.041303	1.265966	0.147938	-0.508023	4.129376
B3	3.414232	0.041840	-0.243339	3.068468		B3	-0.068555	3.414232	0.021882	0.203849	3.232079
DR+DRG	2.720679	0.025401	-1.584397	8.633440		DR+DRG	-0.038226	2.720679	0.023977	0.176840	3.823760
F5	2.991451	0.089078	1.015779	4.407444		F5	-0.064873	2.991451	0.027939	0.114507	2.460153
FC	2.999670	0.072886	0.620719	3.471470		FC	-0.068801	2.999670	0.030127	-0.068047	2.815019
IF	2.596905	0.059646	0.215758	2.319753		IF	-0.037134	2.596905	0.034271	0.180692	2.544695
MM	2.150551	0.139094	0.066002	3.134507		MM	-0.073485	2.150551	0.056236	0.095587	3.497979
OL	2.835132	0.052724	0.185229	2.671042		OL	-0.064513	2.835132	0.032724	-0.438281	4.125768
RA	1.475529	0.108550	-0.818145	6.757860		RA	-0.022778	1.475529	0.128442	0.391251	3.352550
TI	3.361276	0.041547	0.723527	3.587832		TI	-0.049533	3.361276	0.022027	-0.401690	2.769236
log(C1 Normalized Ho ppm)						log(C1 Normalized Er ppm)-log(C1 Normalized Ho ppm)					

Standard Group	Mean ppm value	Std Dev ppm value	Skewness	Kurtosis		Standard Group	Mean ppm value Difference	Mean ppm value	Std Dev ppm value Difference	Skewness	Kurtosis
	X	Y						X	Y		
AZ	1.224663	0.138664	-0.587587	3.809946		AZ	-0.038490	1.224663	0.162274	0.968648	6.164729
B3	3.345678	0.039988	0.037681	3.231239		B3	-0.084675	3.345678	0.023720	0.320315	4.185521
DR+DRG	2.682453	0.021882	-1.079063	7.752156		DR+DRG	-0.050822	2.682453	0.021462	-0.205169	3.257285
F5	2.926578	0.083767	0.870371	4.182361		F5	-0.094690	2.926578	0.032994	-0.155774	3.276571
FC	2.930869	0.069269	0.216383	2.838755		FC	-0.089612	2.930869	0.030537	-0.269426	3.982452
IF	2.559771	0.062749	-0.354235	2.282233		IF	-0.042176	2.559771	0.032900	-0.128688	2.607587
MM	2.077066	0.143473	-0.042210	2.885431		MM	-0.063749	2.077066	0.066035	0.392193	4.065565
OL	2.770619	0.059764	-0.291171	2.366037		OL	-0.048946	2.770619	0.034560	-0.655716	5.316139
RA	1.452751	0.092595	-0.058839	2.466869		RA	-0.043239	1.452751	0.125970	-0.526226	2.607951
TI	3.311744	0.042651	0.454877	3.153271		TI	-0.070163	3.311744	0.019282	-0.718034	3.545054
log(C1 Normalized Er ppm)						log(C1 Normalized Tm ppm)-log(C1 Normalized Er ppm)					
Standard Group	Mean ppm value	Std Dev ppm value	Skewness	Kurtosis		Standard Group	Mean ppm value Difference	Mean ppm value	Std Dev ppm value Difference	Skewness	Kurtosis
	X	Y						X	Y		
AZ	1.186173	0.121382	0.017720	2.903962		AZ	-0.137433	1.186173	0.263163	-1.201998	5.722339
B3	3.261003	0.043580	-0.146581	3.236518		B3	-0.100687	3.261003	0.030611	0.375062	3.865160
DR+DRG	2.631631	0.024739	-0.977908	8.912819		DR+DRG	-0.085472	2.631631	0.032074	-0.806650	5.882681
F5	2.831889	0.079592	0.683513	4.764481		F5	-0.122178	2.831889	0.044857	0.240610	3.536381
FC	2.841257	0.068825	0.594431	3.500222		FC	-0.132043	2.841257	0.038728	0.508831	5.600556
IF	2.517595	0.062209	0.039217	2.234221		IF	-0.065379	2.517595	0.042447	0.881103	4.043246
MM	2.013317	0.140472	-0.164793	2.716814		MM	-0.084654	2.013317	0.097149	-0.396223	4.411128
OL	2.721673	0.056671	-0.119052	2.549243		OL	-0.062214	2.721673	0.042026	0.395948	3.815910
RA	1.409512	0.094261	0.075734	2.611391		RA	-0.068370	1.409512	0.165671	-0.591526	3.978743
TI	3.241581	0.041504	0.474783	2.559871		TI	-0.088572	3.241581	0.030245	-0.083882	3.539651
log(C1 Normalized Tm ppm)						log(C1 Normalized Yb ppm)-log(C1 Normalized Tm ppm)					
Standard Group	Mean ppm value	Std Dev ppm value	Skewness	Kurtosis		Standard Group	Mean ppm value Difference	Mean ppm value	Std Dev ppm value Difference	Skewness	Kurtosis
	X	Y						X	Y		
AZ	1.048740	0.252116	-1.819842	8.135960		AZ	-0.002282	1.048740	0.279954	0.817380	4.252999
B3	3.160316	0.046638	-0.373609	3.284162		B3	-0.082970	3.160316	0.030793	0.135406	2.597889
DR+DRG	2.546159	0.034548	-1.310714	7.255522		DR+DRG	-0.101628	2.546159	0.035352	0.453226	3.388518
F5	2.709711	0.089010	0.566071	4.942674		F5	-0.121839	2.709711	0.044089	-0.130820	2.998602
FC	2.709213	0.077628	0.614479	3.292091		FC	-0.116110	2.709213	0.045320	-0.024726	3.069926
IF	2.452216	0.074028	0.056378	3.342935		IF	-0.029927	2.452216	0.056152	0.321305	3.126822
MM	1.928664	0.158882	-0.500025	3.120559		MM	-0.053688	1.928664	0.101469	0.160726	3.566791
OL	2.659460	0.064961	-0.439708	2.707215		OL	-0.052127	2.659460	0.042482	0.161598	2.588971
RA	1.341143	0.171069	-1.207406	5.242085		RA	-0.055524	1.341143	0.205866	0.347425	4.731613
TI	3.153008	0.051820	0.312654	2.689064		TI	-0.090310	3.153008	0.027672	0.252527	2.648481
log(C1 Normalized Yb ppm)						log(C1 Normalized Lu ppm)-log(C1 Normalized Yb ppm)					
Standard	Mean	Std Dev	Skewness	Kurtosis		Standard	Mean	Mean	Std Dev	Skewness	Kurtosis

Group	ppm value X	ppm value Y				Group	ppm value Difference	ppm value X	ppm value Difference Y		
AZ	1.046458	0.211479	-2.007626	12.239161		AZ	0.015030	1.046458	0.280625	2.920491	18.495256
B3	3.077347	0.050687	-0.726160	4.508901		B3	-0.093608	3.077347	0.038469	0.310334	5.506467
DR+DRG	2.444530	0.030382	-1.108472	7.040707		DR+DRG	-0.123516	2.444530	0.043694	-0.122795	3.585642
F5	2.587871	0.081212	0.098655	3.968271		F5	-0.101333	2.587871	0.052102	-0.384490	3.370479
FC	2.593103	0.080208	-0.102538	2.942924		FC	-0.112896	2.593103	0.053376	-0.668800	3.014233
IF	2.422288	0.070269	0.275071	2.796104		IF	0.001402	2.422288	0.047590	-0.171031	2.393716
MM	1.874976	0.152168	-0.314615	3.041734		MM	-0.038245	1.874976	0.101945	-0.155482	3.410037
OL	2.607332	0.060148	-0.420081	2.983395		OL	-0.087149	2.607332	0.059575	-1.284071	6.095363
RA	1.285618	0.136944	-1.350280	5.251219		RA	-0.095444	1.285618	0.180335	-0.933407	4.424260
TI	3.062698	0.054140	0.286877	2.848689		TI	-0.111143	3.062698	0.030894	-0.273867	2.532939
log(C1 Normalized Lu ppm)						log(C1 Normalized La ppm)-log(C1 Normalized Lu ppm)					
Standard Group	Mean ppm value X	Std Dev ppm value Y	Skewness	Kurtosis		Standard Group	Mean ppm value Difference	Mean ppm value X	Std Dev ppm value Difference Y	Skewness	Kurtosis
AZ	1.061488	0.180756	-0.335604	4.800937		AZ	1.140212	1.061488	0.178011	-0.041518	5.231978
B3	2.983739	0.059048	-0.446941	4.118339		B3	0.475185	2.983739	0.049493	0.035465	4.609405
DR+DRG	2.321014	0.045922	-1.050440	7.164176		DR+DRG	1.881871	2.321014	0.043115	0.625514	5.287978
F5	2.486538	0.094058	0.525878	4.376093		F5	1.099977	2.486538	0.075795	0.051766	2.730228
FC	2.480207	0.097969	-0.128296	2.726698		FC	1.056385	2.480207	0.103132	-0.777608	4.551685
IF	2.423690	0.075200	0.084211	2.577375		IF	1.574799	2.423690	0.040555	-0.056425	2.482326
MM	1.836731	0.155358	-0.220915	3.323592		MM	1.981254	1.836731	0.120377	0.413549	3.771992
OL	2.520183	0.083440	-0.597115	2.768056		OL	1.545844	2.520183	0.052265	0.779917	4.490300
RA	1.190174	0.182342	-1.265120	5.004484		RA	1.211267	1.190174	0.171689	1.392987	5.295107
TI	2.951555	0.061750	0.337456	3.170824		TI	0.223752	2.951555	0.066127	0.417713	4.359916
²⁰⁶Pb/²³⁸U Age											
Standard Group	Mean Age X	Std Dev Age Y	Skewness	Kurtosis							
AZ	436.427150	39.743240	0.153149	5.656543							
B3	1099.752463	179.896369	-3.487869	24.340297							
DR+DRG	31.109140	7.604816	-0.328023	3.148634							
F5	1085.077186	83.950341	0.053134	5.396569							
FC	1101.946642	96.117788	-0.736543	5.680127							
IF	59.452754	22.078649	0.268883	3.395134							
MM	529.294165	25.944793	-1.048896	10.741275							
OL	932.771746	65.823626	-0.121097	11.530524							
RA	432.154900	77.693617	1.815901	8.562734							
TI	464.402623	100.284867	4.893348	35.350585							

Table A8. Summary of pooled fission track age analytical results for each AFT sub-group containing ≥ 2 grain ages. *Sub-groups for which $P(\chi^2_{squared}) < 0.05$ are indicated in italics font.* U-Pb ages for apatite grains from M02, M07, M08, M11, M12, M28 are assumed 150 ± 150 Ma (2sigma).

Sub-Group	Grains	Pooled AFT Age (Ma)	Pooled CI-95% (Ma)	Pooled CI+95% (Ma)	Pooled Ns (track)	Pooled Area (cm ² cm)	Pooled Rho	Pooled 1sigma	Median Pb206*/U 238 Age (Ma)	Median -2sigma (Ma)	Median +2sigma (Ma)	Median [U] (ppm)	Median [Th] (ppm)	Median [Sm] (ppm)	Median Etch Figures	Median Dpar (um)	Median Dper (um)	Median Rmr0
M23	40	7.65	1.46	1.8	92	1.54E-03	1.00E-04	5.80E-07	115.1	-15.9	15.8	9.2	21.6	96.1	1	2.04	0.4	0.8349
<i>M23-001 060</i>	3	7.76	3.41	6.09	12	1.019E-04	1.29E-05	2.20E-07	116.3	-15.6	15.6	18.2	53.6	75.9	2	2.11	0.41	0.8436
M23-002 048	5	21.89	12.95	31.64	5	1.941E-04	1.90E-06	4.92E-08	164.5	-23.7	23.6	2.0	6.6	176.1	1	2.00	0.32	0.7205
M23-004 035	6	5.79	2.72	5.12	10	2.320E-04	1.44E-05	1.86E-07	104.2	-13.9	13.9	15.8	44.1	51.4	1	1.99	0.48	0.8457
M23-005 033	4	8.47	3.98	7.49	10	1.699E-04	9.83E-06	1.64E-07	77.3	-10.5	10.5	10.4	23.2	228.0	1	2.21	0.39	0.6974
M23-010 015	3	15.71	9.94	27.00	4	1.310E-04	2.12E-06	6.12E-08	254.2	-38.6	38.4	3.4	10.3	127.3	1	2.11	0.57	0.8457
M25	32	11.13	2.42	3.09	68	1.25E-03	5.09E-05	4.03E-07	116.3	-15.5	15.5	5.4	15.4	159.1	2	2.32	0.5	0.7256
M25-001 060	7	15.92	4.96	7.20	29	2.524E-04	1.52E-05	1.88E-07	129.7	-15.8	15.7	6.6	15.6	121.7	2	2.52	0.67	0.7476
M25-002 048	8	10.42	4.89	9.21	10	3.150E-04	7.99E-06	9.90E-08	101.0	-14.0	14.0	6.7	17.1	247.0	1	2.42	0.47	0.6948
M25-006 033	2	19.33	13.24	41.94	3	9.707E-05	1.29E-06	4.15E-08	219.8	-29.1	29.0	3.3	5.9	63.6	1	2.35	0.41	0.6872
M25-009 018	2	5.57	5.57	11.13	1	8.251E-05	1.49E-06	4.43E-08	62.1	-8.0	7.9	4.5	11.8	200.8	1	2.25	0.58	0.6868
M211	18	16.8	3.57	4.53	72	3.77E-04	3.56E-05	3.14E-07	98	-13	13	9.2	29.4	113.2	2	2.33	0.41	0.8309
M211-001 060	18	16.8	3.57	4.53	72	3.77E-04	3.56E-05	3.14E-07	98	-13	13	9.2	29.4	113.2	2	2.33	0.41	0.8309
M211-004 035	3	9.34	5.22	11.81	6	6.989E-05	5.35E-06	1.16E-07	77.2	-12.6	12.5	11.8	34.4	84.3	2	2.04	0.39	0.8341
M211-033 004	2	10.99	5.16	9.72	10	5.339E-05	7.57E-06	1.46E-07	91.4	-13.1	13.1	35.2	55.9	174.1	2	1.95	0.43	0.8373
M211-037 003	2	61.85	61.85	121.95	1	1.941E-05	1.34E-07	7.04E-09	516.0	-76.2	75.3	1.7	11.7	142.5	1	2.54	0.43	0.5897
M220	36	29.13	3.12	3.49	345	1.41E-03	9.84E-05	5.62E-07	113.2	-13	12.9	14.7	27.3	119.4	3	2.17	0.42	0.8382
M220-001 060	4	39.97	11.04	15.24	39	1.631E-04	8.10E-06	1.52E-07	131.9	-16.4	16.4	6.5	18.1	144.3	4	2.44	0.62	0.7644
M220-002 048	4	28.38	8.86	12.86	29	1.602E-04	8.49E-06	1.60E-07	113.2	-13.8	13.7	6.3	22.4	190.6	3	2.21	0.52	0.7437
M220-004 035	4	28.3	6.38	8.24	63	1.427E-04	1.85E-05	2.84E-07	92.9	-10.5	10.5	29.6	57.2	73.9	4	2.17	0.44	0.8391
<i>M220-005 033</i>	4	30.27	8.74	12.28	35	1.553E-04	9.61E-06	1.66E-07	103.4	-11.4	11.3	12.7	38.3	289.2	3	2.40	0.52	0.8131
M220-010 015	2	65.00	30.57	57.44	10	9.707E-05	1.28E-06	4.71E-08	206.2	-27.0	26.9	3.3	6.3	112.0	2	2.31	0.44	0.8154
M220-013 011	2	26.63	8.20	11.85	30	5.921E-05	9.37E-06	1.89E-07	131.2	-13.7	13.6	34.3	66.7	46.6	4	2.12	0.41	0.8445
M221	14	13.43	2.74	3.44	79	2.65E-04	4.90E-05	4.10E-07	48.2	-6	6	32.8	47.6	221.6	3	2.04	0.37	0.8397
M221 none	-	-	-	-	-	-	-	-	-	-	-	-	-	-	-	-	-	-
Sub-Group	Grains	Pooled AFT Age (Ma)	Pooled CI-95% (Ma)	Pooled CI+95% (Ma)	Pooled Ns (track)	Pooled Area (cm ² cm)	Pooled [U]*Area	Pooled [U]*Area 1sigma	Median Pb206*/U 238 Age (Ma)	Median -2sigma (Ma)	Median +2sigma (Ma)	Median [U] (ppm)	Median [Th] (ppm)	Median [Sm] (ppm)	Median Etch Figures	Median Dpar (um)	Median Dper (um)	Median Rmr0
M02	10	23.21	7.12	10.26	31	1.20E-04	2.64E-03	1.79E-05	150	-150	150	24.1	55.1	127.7	1	2.5	0.1	0.7402
2004 01-006 033	2	137.36	86.64	230.48	4	2.40E-05	5.70E-05	7.37E-07	150	-150	150	2.4	21.3	83	1	2.46	0.1	0.7473
M07	9	17.92	6.08	9.2	24	1.08E-04	2.65E-03	1.71E-05	150	-150	150	23.8	95.5	139.9	1	2.61	0.1	0.7213
2004 02-001 060	2	53.76	27.31	55.27	8	2.40E-05	2.93E-04	3.74E-06	150	-150	150	12.2	83.5	121	1	2.4	0.1	0.7328
M08	17	26.79	4.33	5.16	156	2.04E-04	1.15E-02	6.13E-05	150	-150	150	54.8	52.7	115	1	2.88	0.1	0.6681
2004 03-004 035	2	99.87	36.26	56.68	20	2.40E-05	3.93E-04	5.01E-06	150	-150	150	16.4	45.6	49.9	1	2.68	0.1	0.7073
M11	23	30.97	6.25	7.82	88	2.76E-04	5.61E-03	3.06E-05	150	-150	150	16.9	26	191.8	1	2.69	0.1	0.7065
2004 04-002 048	6	41.44	15.7	25.23	18	7.19E-05	8.57E-04	7.96E-06	150	-150	150	6.7	18.8	174	1	2.81	0.1	0.6828
2004 04-047 003	3	14.39	6.17	10.79	13	3.60E-05	1.79E-03	2.37E-05	150	-150	150	26.4	105.7	428.8	1	2.55	0.1	0.7319
M12	25	31.95	5.61	6.8	125	3.00E-04	7.73E-03	3.62E-05	150	-150	150	19.7	30.1	89.7	1	2.52	0.1	0.7371
2004 05-002 048	2	58.78	23.85	40.02	15	2.40E-05	5.03E-04	7.33E-06	150	-150	150	21	24.2	155.4	1	2.71	0.1	0.6944
2004 05-006 033	3	50.58	14.63	20.56	36	3.60E-05	1.40E-03	2.14E-05	150	-150	150	13.9	13	70.5	1	3.12	0.1	0.6123
2004 05-009 018	2	18.22	9.27	18.83	8	2.40E-05	8.68E-04	1.12E-05	150	-150	150	36.2	91.7	192.9	1	2.17	0.1	0.79
2004 05-013 011	3	49.96	20.8	35.53	14	3.60E-05	5.53E-04	5.94E-06	150	-150	150	16.4	45	53.8	1	2.31	0.1	0.7705

M28	32	21.61	4.02	4.94	108	3.84E-04	9.88E-03	3.98E-05	150	-150	150	18.6	33.1	80.3	1	2.94	0.1	0.6549
2004 07-001 060	6	30.49	13.05	22.79	13	7.19E-05	8.42E-04	7.85E-06	150	-150	150	8	21.8	128.8	1	2.67	0.1	0.7104
2004 07-004 035	5	13.93	5.97	10.43	13	5.99E-05	1.85E-03	1.58E-05	150	-150	150	38	48	57.5	1	2.91	0.1	0.6616
2004 07-006 033	6	20.5	7.78	12.51	18	7.19E-05	1.74E-03	1.84E-05	150	-150	150	12.6	22.5	80.3	1	3.09	0.1	0.6186
2004 07-019 008	2	8.46	5.01	12.28	5	2.40E-05	1.17E-03	1.55E-05	150	-150	150	48.8	93.1	57	1	2.9	0.1	0.6635
2004 07-078 002	2	51.61	23.46	42.87	11	2.40E-05	4.20E-04	5.35E-06	150	-150	150	17.5	125.1	634.9	1	3.78	0.1	0.3863

Table A8. (continued).

Sub-Group	Zeta	1 sigma	Chi-Squared	P(Chi-Squared)
M23	8.33E-06	1.42E-07	48.5708	0.1401
M23-001 060	8.33E-06	1.42E-07	12.82	0.0016
M23-002 048	8.33E-06	1.42E-07	2.15	0.7081
M23-004 035	8.33E-06	1.42E-07	3.68	0.5964
M23-005 033	8.33E-06	1.42E-07	1.57	0.6659
M23-010 015	8.33E-06	1.42E-07	0.85	0.6541
M25	8.33E-06	1.42E-07	22.33	0.8723
M25-001 060	8.33E-06	1.42E-07	0.97	0.9868
M25-002 048	8.33E-06	1.42E-07	2.97	0.8879
M25-006 033	8.33E-06	1.42E-07	0.53	0.4648
M25-009 018	8.33E-06	1.42E-07	1.13	0.2884
M211	8.33E-06	1.42E-07	16.68	0.4759
M211-001 060	8.33E-06	1.42E-07	0.21	0.6446
M211-004 035	8.33E-06	1.42E-07	0.86	0.6520
M211-033 004	8.33E-06	1.42E-07	0.02	0.8803
M211-037 003	8.33E-06	1.42E-07	0.54	0.4609
M220	8.33E-06	1.42E-07	61.71	0.0035
M220-001 060	8.33E-06	1.42E-07	0.39	0.9424
M220-002 048	8.33E-06	1.42E-07	0.53	0.9126
M220-004 035	8.33E-06	1.42E-07	6.41	0.0933
M220-005 033	8.33E-06	1.42E-07	10.26	0.0165
M220-010 015	8.33E-06	1.42E-07	0.77	0.3798
M220-013 011	8.33E-06	1.42E-07	0.73	0.3916
M221	8.33E-06	1.42E-07	7.32	0.8851
M221 none	-	-	-	-
Sub-Group	Zeta	1 sigma	Chi-Squared	P(Chi-Squared)
M02	1.98E-03	7.27E-05	27.69	0.0011
M02-006 033	1.98E-03	7.27E-05	1.80	0.1792
M07	1.98E-03	7.27E-05	21.53	0.0059
M07-001 060	1.98E-03	7.27E-05	1.79	0.1810
M08	1.98E-03	7.27E-05	69.57	0.0000
M08-004 035	1.98E-03	7.27E-05	2.38	0.1232
M11	1.98E-03	7.27E-05	59.77	0.0000
M11-002 048	1.98E-03	7.27E-05	2.41	0.7894
M11-047 003	1.98E-03	7.27E-05	2.03	0.3625
M12	1.98E-03	7.27E-05	111.12	0.0000
M12-002 048	1.98E-03	7.27E-05	2.68	0.1015

M12-006 033	1.98E-03	7.27E-05	24.50	0.0000
M12-009 018	1.98E-03	7.27E-05	2.84	0.0918
M12-013 011	1.98E-03	7.27E-05	4.42	0.1094
M28	1.98E-03	7.27E-05	164.50	0.0000
M28-001 060	1.98E-03	7.27E-05	25.23	0.0001
M28-004 035	1.98E-03	7.27E-05	4.81	0.3076
M28-006 033	1.98E-03	7.27E-05	22.99	0.0003
M28-019 008	1.98E-03	7.27E-05	1.24	0.2655
M28-078 002	1.98E-03	7.27E-05	2.56	0.1096

Table A9. Summary of fission track length analytical results for each AFT sub-group. LA-ICP-MS was not done on M02, M07, M08, M11, M12, M28 AFT length grains.

Sub-Group	CFTs	Mean Length (um)	1 sigma (um)	Std Dev (um)	Median Pb206*/U 238 Age (Ma)	Median -2sigma (Ma)	Median +2sigma (Ma)	Median [U] (ppm)	Median [Th] (ppm)	Median [Sm] (ppm)	Median Etch Figures	Median Dpar (um)	Median Dper (um)	Median Rmr0
M23	101	13.56	0.21	2.08	88.8	-8.93	8.92	48.41	50.31	141.48	4	2.54	0.51	0.8036
M23-001 060	13	12.93	0.46	1.59	95.9	-9.9	9.8	48.4	85.2	104.4	4	2.80	0.51	0.8418
M23-002 048	1	13.41	0.00	0.00	175.1	-18.4	18.3	13.2	29.2	99.3	4	2.43	0.79	0.8464
M23-004 035	6	14.07	0.54	1.21	94.3	-10.0	10.0	28.7	36.3	37.2	4	2.46	0.51	0.8498
M23-005 033	16	13.37	0.78	3.02	86.2	-8.8	8.7	62.8	39.5	235.9	4	3.07	0.70	0.7598
M23-010 015	-	-	-	-	-	-	-	-	-	-	-	-	-	-
M25	89	13.54	0.21	2	118.05	-12.88	12.85	16.09	23.53	125.98	4	2.56	0.71	0.7808
M25-001 060	22	13.32	0.49	2.23	99.2	-9.0	9.0	97.2	140.3	84.4	4	2.86	0.77	0.7808
M25-002 048	9	13.83	0.40	1.14	123.9	-13.3	13.3	7.7	18.8	145.2	4	2.63	0.72	0.7490
M25-006 033	6	12.62	1.26	2.81	97.9	-10.6	10.6	3.6	6.7	66.7	4	2.81	0.83	0.6944
M25-009 018	-	-	-	-	-	-	-	-	-	-	-	-	-	-
M211	26	13.58	0.38	1.89	95.61	-9.36	9.34	99.76	70.86	110.18	4	2.45	0.48	0.7869
M211-001 060	8	12.38	0.72	1.91	95.6	-9.4	9.3	109.1	183.6	110.2	4	2.88	0.89	0.7840
M211-004 035	-	-	-	-	-	-	-	-	-	-	-	-	-	-
M211-033 004	-	-	-	-	-	-	-	-	-	-	-	-	-	-
M211-037 003	-	-	-	-	-	-	-	-	-	-	-	-	-	-
M220	206	13.37	0.12	1.77	98.71	-9.51	9.5	28.21	43.58	99.82	4	2.5	0.51	0.8259
M220-001 060	45	12.93	0.30	1.99	90.9	-9.1	9.0	35.4	49.5	99.8	4	2.50	0.53	0.8261
M220-002 048	12	12.71	0.31	1.03	140.6	-16.0	15.9	19.3	25.2	167.3	4	2.17	0.57	0.8214
M220-004 035	12	13.26	0.50	1.66	102.5	-10.2	10.2	31.6	59.9	42.8	4	2.48	0.45	0.8405
M220-005 033	28	13.90	0.30	1.58	83.4	-7.8	7.8	28.2	61.6	301.0	4	2.68	0.47	0.7830
M220-010 015	1	13.01	0.00	0.00	152.6	-15.9	15.8	6.6	16.9	96.7	4	2.05	0.57	0.8396
M220-013 011	18	13.30	0.39	1.62	106.8	-9.5	9.4	40.2	66.6	56.3	4	2.73	0.59	0.8388
M221	50	12.82	0.22	1.55	45.02	-4.98	4.97	113.13	138.21	191.03	4	2.29	0.43	0.8376
M221 none	-	-	-	-	-	-	-	-	-	-	-	-	-	-
Sub-Group	CFTs	Mean Length (um)	1 sigma (um)	Std Dev (um)								Median Dpar (um)		Median Rmr0
M02	78	12.8	0.33	2.85	150	-150	150					2.58		0.7266
M07	27	11.56	0.44	2.26	150	-150	150					2.45		0.7487
M08	63	13.59	0.27	2.12	150	-150	150					2.75		0.6949
M11	110	12.25	0.19	1.97	150	-150	150					2.91		0.6616
M12	118	13.1	0.12	1.32	150	-150	150					2.58		0.7258
M28	79	13.07	0.32	2.87	150	-150	150					3.05		0.6295

Table A10. Assumed C1 Chondrite and Durango REE ppm values. Durango (DR+DRG) REE ppm values and McClure Mountain (MM) REE ppm values measured in this study are compared to values reported by Chew et al. (2016).

Oxide	Atomic Number	Assumed C1 Chondrite	Assumed Dur-DonG	Measured DR+DRG	Measured McClure Mountain	Measured MM
	amu	McDonough and Sun, (2016) ppm	Chew et al., (2016) ppm	This Study ppm	Chew et al., (2016) ppm	This Study ppm
La ₂ O ₃	57	0.2370	3786.000	3786.277	1764.000	1534.878
Ce ₂ O ₃	58	0.6130	5306.000	5302.979	2859.000	2566.089
Pr ₂ O ₃	59	0.0928	472.500	472.150	275.200	240.468
Nd ₂ O ₃	60	0.4570	1534.000	1537.293	894.400	762.611
Sm ₂ O ₃	62	0.1480	215.200	215.297	106.700	91.881
Eu ₂ O ₃	63	0.0563	18.900	18.883	41.190	34.038
Gd ₂ O ₃	64	0.1990	18.900	18.883	41.190	34.038
Tb ₂ O ₃	65	0.0361	186.900	187.129	74.320	62.967
Dy ₂ O ₃	66	0.2460	24.250	24.224	8.593	6.928
Ho ₂ O ₃	67	0.0546	129.900	130.184	41.620	34.407
Er ₂ O ₃	68	0.1600	26.350	26.391	7.950	6.434
Tm ₂ O ₃	69	0.0247	68.690	68.761	20.300	16.338
Yb ₂ O ₃	70	0.1610	8.745	8.730	2.717	2.120
Lu ₂ O ₃	71	0.0246	45.100	45.017	15.840	12.072

Table A11. Calibration by linear regression of the standard group data from Table A10.

Calibrated Parameter	m	b	b _u	Y _{min}	Y _{umin}
log(C1 Normalized La ppm)	-0.008992	0.090003	0.124791	0.013145	0.047933
log(C1 Normalized Ce ppm)	-0.003972	0.071502	0.107813	0.012027	0.048338
log(C1 Normalized Pr ppm)	-0.011506	0.097654	0.136523	0.014439	0.053308
log(C1 Normalized Nd ppm)	-0.011779	0.099396	0.144917	0.017991	0.063512
log(C1 Normalized Sm ppm)	-0.037076	0.183698	0.234093	0.024880	0.075275
log(C1 Normalized Eu ppm)	-0.049017	0.203687	0.243395	0.028479	0.068187
log(C1 Normalized Gd ppm)	-0.033897	0.168897	0.217040	0.022526	0.070669
log(C1 Normalized Tb ppm)	-0.064841	0.258636	0.304010	0.024504	0.069878
log(C1 Normalized Dy ppm)	-0.033545	0.159970	0.211234	0.025401	0.076665
log(C1 Normalized Ho ppm)	-0.041690	0.180882	0.230066	0.021882	0.071066
log(C1 Normalized Er ppm)	-0.038271	0.167683	0.217523	0.024739	0.074580
log(C1 Normalized Tm ppm)	-0.090468	0.316556	0.346992	0.034548	0.064984
log(C1 Normalized Yb ppm)	-0.072630	0.259829	0.288347	0.030382	0.058901
log(C1 Normalized Lu ppm)	-0.070062	0.259509	0.284043	0.045922	0.070455
log(C1 Normalized Ce ppm)-log(C1 Normalized La ppm)	-0.009322	0.061189	0.076937	0.012690	0.028439
log(C1 Normalized Pr ppm)-log(C1 Normalized Ce ppm)	-0.009764	0.058806	0.069725	0.012220	0.023138
log(C1 Normalized Nd ppm)-log(C1 Normalized Pr ppm)	-0.016628	0.081569	0.098834	0.011380	0.028645
log(C1 Normalized Sm ppm)-log(C1 Normalized Nd ppm)	-0.049170	0.201789	0.222694	0.017714	0.038618
log(C1 Normalized Eu ppm)-log(C1 Normalized Sm ppm)	-0.054854	0.259627	0.344552	0.031522	0.116447
log(C1 Normalized Gd ppm)-log(C1 Normalized Eu ppm)	-0.076924	0.277528	0.324298	0.032333	0.079103
log(C1 Normalized Tb ppm)-log(C1 Normalized Gd ppm)	-0.093990	0.326874	0.390690	0.021804	0.085620
log(C1 Normalized Dy ppm)-log(C1 Normalized Tb ppm)	-0.085043	0.287468	0.342933	0.019510	0.074974
log(C1 Normalized Ho ppm)-log(C1 Normalized Dy ppm)	-0.059390	0.205850	0.224652	0.021882	0.040685
log(C1 Normalized Er ppm)-log(C1 Normalized Ho ppm)	-0.064084	0.216993	0.240756	0.019282	0.043046
log(C1 Normalized Tm ppm)-log(C1 Normalized Er ppm)	-0.100483	0.326445	0.382353	0.030245	0.086153
log(C1 Normalized Yb ppm)-log(C1 Normalized Tm ppm)	-0.115005	0.359576	0.400565	0.027672	0.068661
log(C1 Normalized Lu ppm)-log(C1 Normalized Yb ppm)	-0.108690	0.338872	0.394365	0.030894	0.086386
log(C1 Normalized La ppm)-log(C1 Normalized Lu ppm)	-0.069052	0.243733	0.274395	0.040555	0.071216
²⁰⁶ Pb/ ²³⁸ U Age	0.089342	14.768642	81.642617	7.604816	74.478791
Eu anomaly (only <0 or >=0)	-	-	-	-	-

Notes:

$$\text{Eu anomaly} = \log(\text{C1 Normalized Eu ppm}) - [\log(\text{C1 Normalized Sm ppm}) + \log(\text{C1 Normalized Gd ppm})]/2$$

Table A12. Thermal history implications of the AFT data.

Samp le	Oldest Ma AFT median(2σ)	Peak Ma median(2σ)	Peak °C median(2σ)	EasyRo median(2σ)	BasinRo median(2σ)	EasyDL median(2σ)	°C at 1 Ma median(2σ)	°C at 5 Ma median(2σ)	°C at 10 Ma median(2σ)	°C at 15 Ma median(2σ)	°C at 20 Ma median(2σ)	°C at 30 Ma median(2σ)	°C at 50 Ma median(2σ)
M23	15.00(10.27)	14.50(9.95)	≥167.79(26.33)	≥1.32(0.36)	≥1.04(0.33)	≥1.33(0.45)	22.49(16.98)	66.44(34.09)	120.13(75.20)	≥165.68(44.47)			
M25	18.00(11.53)	18.00(11.47)	≥176.82(20.63)	≥1.46(0.30)	≥1.23(0.32)	≥1.56(0.45)	22.49(18.32)	57.09(29.39)	86.39(62.04)	≥147.56(74.69)			
M211	22.00(16.82)	22.00(13.97)	≥131.19(19.76)	≥0.79(0.13)	≥0.65(0.08)	≥0.65(0.11)	18.16(10.65)	31.70(28.08)	56.02(47.57)	87.59(71.55)	≥115.28(70.52)		
M220	34.00(8.43)	34.00(7.54)	≥164.88(20.19)	≥1.25(0.30)	≥0.92(0.25)	≥1.26(0.41)	19.49(11.54)	40.72(21.75)	59.23(10.89)	64.25(6.90)	68.77(9.09)	≥132.27(70.02)	
M221	14.00(5.43)	13.50(5.24)	≥125.28(23.08)	≥0.73(0.15)	≥0.62(0.09)	≥0.59(0.11)	28.14(23.24)	66.40(18.39)	85.28(37.67)	≥134.11(57.14)			
M02	23.00(13.85)	23.00(13.95)	≥163.42(12.08)	≥1.22(0.18)	≥0.89(0.16)	≥1.20(0.28)	19.02(12.94)	39.50(34.54)	77.25(59.14)	115.95(70.37)	≥146.61(56.98)		
M07	15.00(12.66)	14.00(10.67)	≥170.76(28.24)	≥1.38(0.38)	≥1.12(0.36)	≥1.38(0.49)	27.10(34.07)	103.76(57.30)	131.44(59.66)	≥156.71(59.80)			
M08	8.00(3.67)	3.00(1.87)	71.03(23.55)	0.40(0.10)	0.41(0.09)	0.37(0.09)	38.19(36.33)	48.02(36.69)	20.57(15.68)	35.26(29.95)	51.19(48.34)	90.49(60.06)	≥167.18(28.02)
M11	41.00(2.52)	23.00(16.87)	≥108.75(15.42)	≥0.66(0.12)	≥0.57(0.09)	≥0.54(0.14)	18.93(17.02)	35.47(44.33)	62.96(48.47)	89.11(40.25)	≥94.86(31.48)		
M12	20.00(4.32)	9.00(8.19)	73.23(19.01)	0.42(0.08)	0.43(0.07)	0.39(0.07)	19.98(28.52)	54.76(37.54)	59.87(32.49)	39.38(39.20)	18.16(12.81)	25.04(26.46)	54.03(60.60)
M28	19.50(14.24)	19.00(14.14)	≥177.03(14.90)	≥1.45(0.24)	≥1.23(0.29)	≥1.56(0.40)	23.23(22.86)	61.20(54.99)	100.93(85.41)	134.83(72.82)	≥162.23(62.07)		

Notes:

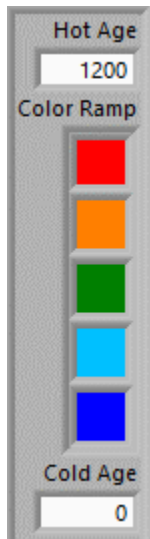
EasyRo from Burnham and Sweeney (1989). BasinRo from Nielsen et al. (2017). EasyDL from Schenk et al. (2017).

Table A13. Time-temperature constraints used for AFT modeling.

Sample	Provenance Start	Deposition	Peak Burial	Present-Day	tT Segment Points
M23	100.0-100.0 Ma 200.0-199.0°C	48.4-44.4 Ma 20.0-10.0°C	43.4-1.0 Ma 200.0-10.0°C	0.0-0.0 Ma 20.0-10.0°C	9, 5, 33
M25	100.0-100.0 Ma 200.0-199.0°C	56.4-42.8 Ma 20.0-10.0°C	41.8-1.0 Ma 200.0-10.0°C	0.0-0.0 Ma 20.0-10.0°C	9, 5, 33
M211	100.0-100.0 Ma 200.0-199.0°C	46.0-40.8 Ma 20.0-10.0°C	39.8-1.0 Ma 200.0-10.0°C	0.0-0.0 Ma 20.0-10.0°C	9, 5, 33
M220	100.0-100.0 Ma 200.0-199.0°C	46.5-43.3 Ma 20.0-10.0°C	42.3-1.0 Ma 200.0-10.0°C	0.0-0.0 Ma 20.0-10.0°C	9, 5, 33
M221	100.0-100.0 Ma 200.0-199.0°C	24.6-22.2 Ma 20.0-10.0°C	21.2-1.0 Ma 200.0-10.0°C	0.0-0.0 Ma 20.0-10.0°C	9, 5, 33
M02	150.0-150.0 Ma 200.0-199.0°C	46.6-42.1 Ma 20.0-10.0°C	41.1-1.0 Ma 200.0-10.0°C	0.0-0.0 Ma 20.0-10.0°C	9, 5, 33
M07	150.0-150.0 Ma 200.0-199.0°C	32.6-29.0 Ma 20.0-10.0°C	28.0-1.0 Ma 200.0-10.0°C	0.0-0.0 Ma 20.0-10.0°C	9, 5, 33
M08	150.0-150.0 Ma 200.0-199.0°C	11.6-5.3 Ma 20.0-10.0°C	4.3-1.0 Ma 200.0-10.0°C	0.0-0.0 Ma 20.0-10.0°C	9, 5, 33
M11	150.0-150.0 Ma 200.0-199.0°C	43.2-39.2 Ma 20.0-10.0°C	38.2-1.0 Ma 200.0-10.0°C	0.0-0.0 Ma 20.0-10.0°C	9, 5, 33
M12	150.0-150.0 Ma 200.0-199.0°C	23.0-16.0 Ma 20.0-10.0°C	15.0-1.0 Ma 200.0-10.0°C	0.0-0.0 Ma 20.0-10.0°C	9, 5, 33
M28	150.0-150.0 Ma 200.0-199.0°C	46.0-40.0 Ma 20.0-10.0°C	39.0-1.0 Ma 200.0-10.0°C	0.0-0.0 Ma 20.0-10.0°C	9, 5, 33

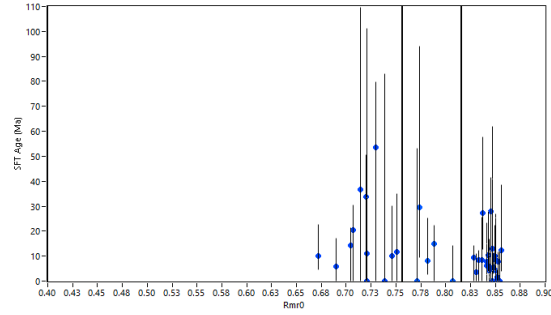
Part III: FT^3 Model Results

AFT age and length data were modeled using parameter $rmr0$ from Ketcham et al. (1999). For samples M23, M25, M211, M220, M221, $rmr0$ was calculated using the full suite of chemical composition analyses obtained by LA-ICP-MS. For samples M02, M07, M08, M11, M12, M28 $rmr0$ was calculated from parameter $Dpar$. Data not modeled are shown in black symbols. Some individual points were deleted to force $P(\chi^2) \geq 0.05$. Plots here are color coded using this color ramp based on median U-Pb age.

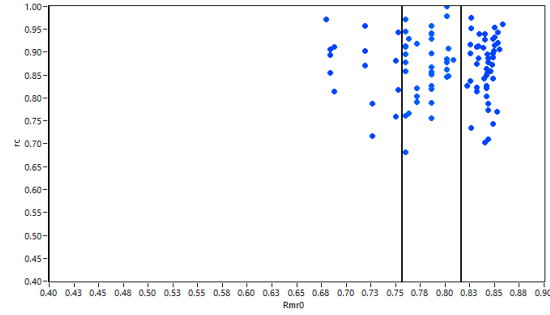


M23

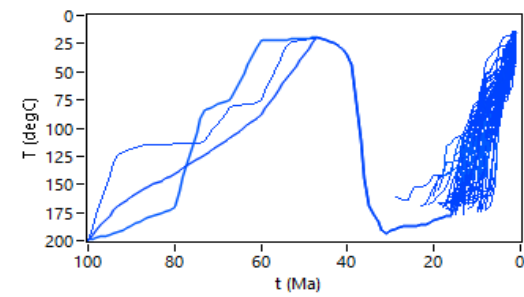
SFT Age Data: P1325_001_Sub Group_000_0_



CFT Data: P1325_001_Sub Group_000_0_



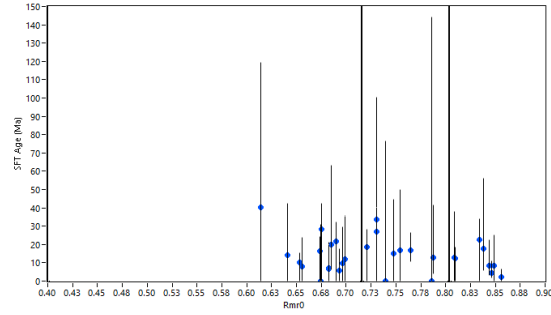
Model tT Population: P1325_001_



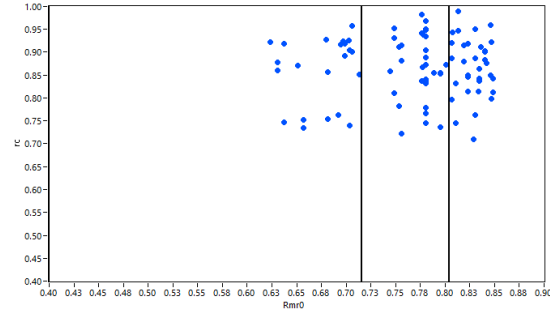
Sample		Best Fit Model												Measured								
Sub-Group	Pop.	Oldest AFT (Ma)	SFT GOF	CFT GOF	Strat. Age (Ma)	Peak t (Ma)	Peak T (°C)	Easy-Ro (%)	Basin-Ro (%)	Easy-DL (%)	AFT Age (Ma)	lc/lc0	Isig	AFT Age (Ma)	CI -95% (Ma)	CI +95% (Ma)	lc/lc0	Isig	Spots	CFTs	UPb Age (Ma)	Rmr0
MM23-000	Pop-1	10	0.6773	0.9578	10	10	108	0.62	0.55	0.51	7.2	0.8470	0.0796	6.5	1.4	1.8	0.8710	0.0711	23	49	104	0.8437
MM23-000	Pop-2	13	0.9925	0.9931	13	13	148	0.90	0.69	0.78	8.8	0.8350	0.1117	8.8	4.5	9.0	0.8712	0.0709	5	36	138	0.7843
MM23-000	Pop-3	19	0.5751	0.9324	19	18	168	1.36	1.09	1.37	9.8	0.7871	0.1549	12.4	4.6	7.2	0.8788	0.0878	12	16	103	0.7197

M25

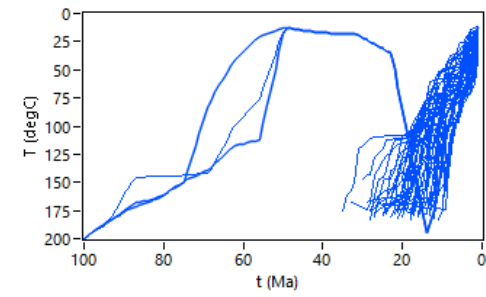
SFT Age Data: P1325_002_Sub Group_000_0_



CFT Data: P1325_002_Sub Group_000_0_

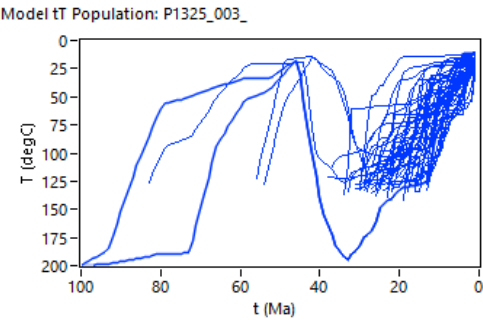
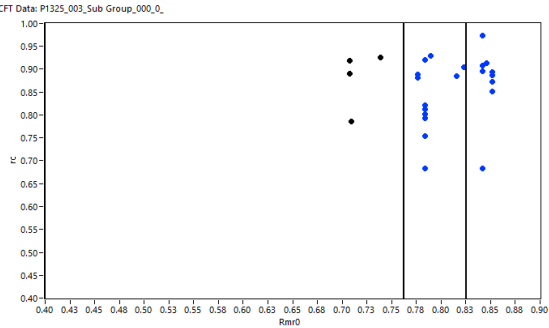
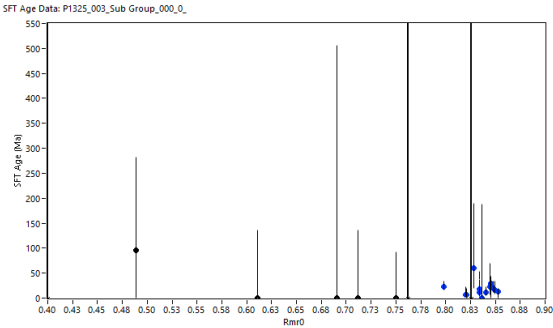


Model tT Population: P1325_002_



Sample		Best Fit Model												Measured									
Sub-Group	Pop.	Oldest AFT (Ma)	SFT GOF	CFT GOF	Strat. Age (Ma)	Peak t (Ma)	Peak T (°C)	Easy-Ro (%)	Basin-Ro (%)	Easy-DL (%)	AFT Age (Ma)	lc/lc0	1sig	AFT Age (Ma)	CI -95% (Ma)	CI +95% (Ma)	lc/lc0	1sig	Spots	CFTs	UPb Age (Ma)	Rmr0	
MM25-000	Pop-1	13	0.4409	0.8547	13	13	99	0.56	0.52	0.48	9.9	0.8572	0.0729	6.8	2.5	4.0	0.8686	0.0639	8	34	120	0.8359	
MM25-000	Pop-2	14	0.3266	0.7937	14	14	132	0.75	0.63	0.62	11.0	0.8732	0.0674	15.8	4.9	7.1	0.8678	0.0708	9	32	122	0.7642	
MM25-000	Pop-3	16	0.9854	0.7561	16	16	180	1.45	1.23	1.60	11.5	0.8577	0.1083	11.4	4.1	6.4	0.8683	0.0837	15	23	129	0.7000	

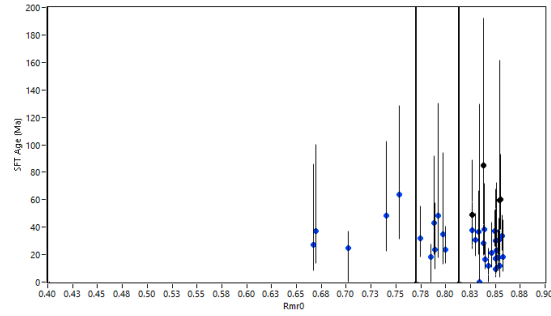
M211



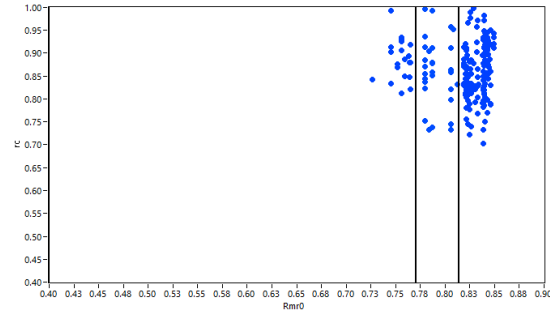
Sample		Best Fit Model												Measured									
Sub-Group	Pop.	Oldest AFT (Ma)	SFT GOF	CFT GOF	Strat. Age (Ma)	Peak t (Ma)	Peak T (°C)	Easy-Ro (%)	Basin-Ro (%)	Easy-DL (%)	AFT Age (Ma)	Ic/Ic0	1sig	AFT Age (Ma)	CI -95% (Ma)	CI +95% (Ma)	Ic/Ic0	1sig	Spots	CFTs	UPb Age (Ma)	Rmr0	
MM211-000	Pop-1	22	0.9889	0.9365	22	22	110	0.64	0.56	0.52	15.8	0.8580	0.0982	15.9	4.2	5.8	0.8752	0.0791	10	9	86	0.8441	
MM211-000	Pop-2	26	0.8215	0.9759	26	26	140	0.85	0.68	0.69	18.5	0.8541	0.1019	16.8	5.2	7.6	0.8567	0.0942	3	13	89	0.8022	

M220

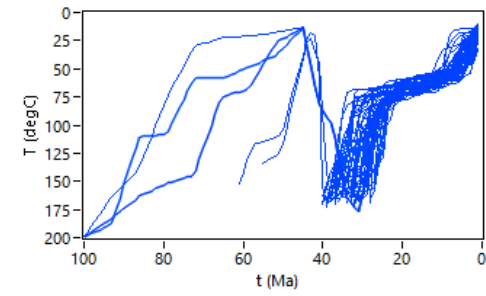
SFT Age Data: P1325_004_Sub Group_000_0_



CFT Data: P1325_004_Sub Group_000_0_

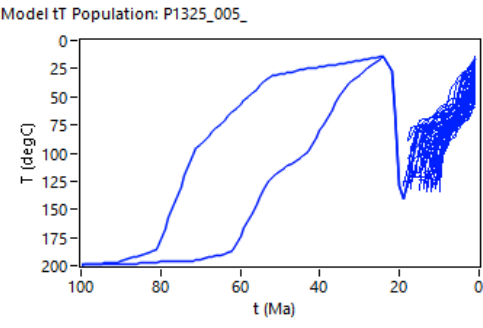
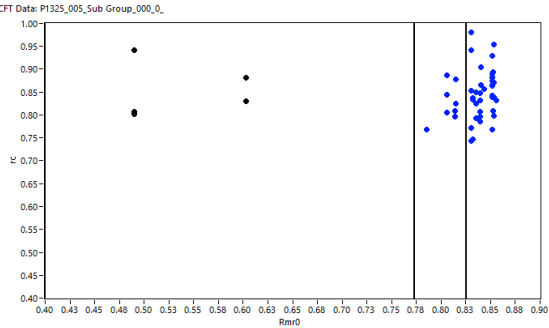
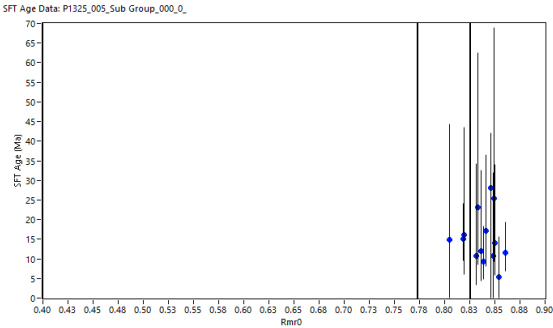


Model tT Population: P1325_004_



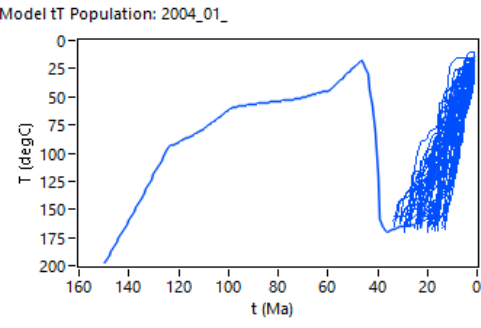
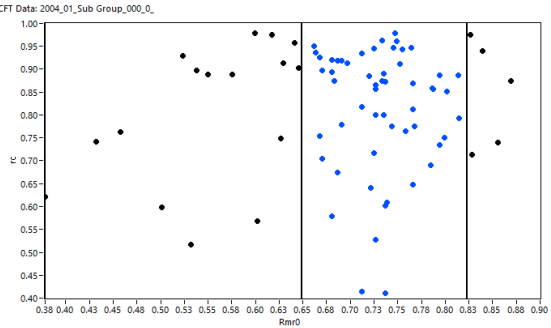
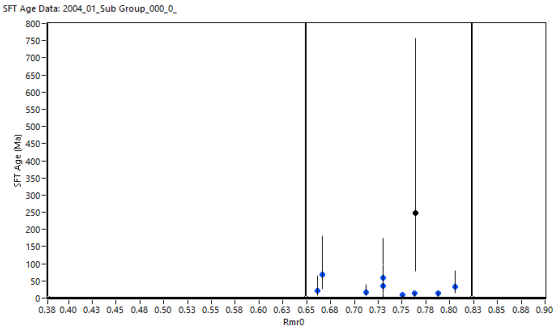
Sample		Best Fit Model												Measured									
Sub-Group	Pop.	Oldest AFT (Ma)	SFT GOF	CFT GOF	Strat. Age (Ma)	Peak t (Ma)	Peak T (°C)	Easy-Ro (%)	Basin-Ro (%)	Easy-DL (%)	AFT Age (Ma)	lc/lc0	Isig	AFT Age (Ma)	CI -95% (Ma)	CI +95% (Ma)	lc/lc0	Isig	Spots	CFTs	UPb Age (Ma)	Rmr0	
MM220-000	Pop-1	34	0.9266	0.6693	34	34	107	0.62	0.55	0.51	25.2	0.8486	0.0702	24.9	3.1	3.5	0.8586	0.0581	20	152	98	0.8427	
MM220-000	Pop-2	36	0.9542	0.9354	36	36	140	0.85	0.68	0.69	27.7	0.8650	0.0708	28.1	7.1	9.4	0.8601	0.0712	7	31	117	0.7880	
MM220-000	Pop-3	37	0.3999	0.9996	37	37	151	0.96	0.70	0.87	29.0	0.8741	0.0663	40.4	13.5	20.4	0.9026	0.0658	5	23	102	0.7291	

M221



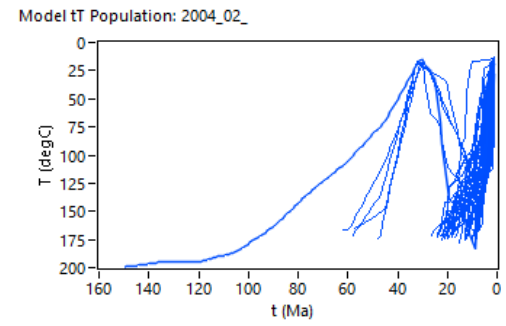
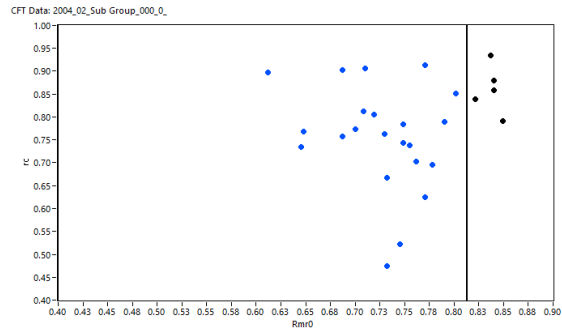
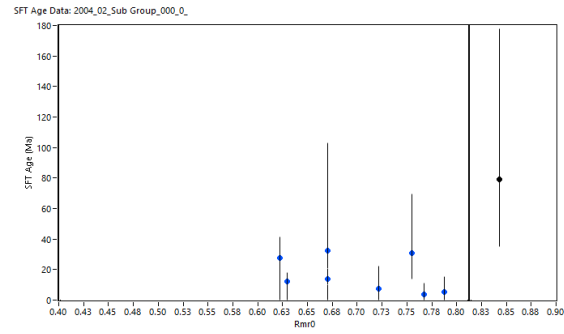
Sample		Best Fit Model												Measured									
Sub-Group	Pop.	Oldest AFT (Ma)	SFT GOF	CFT GOF	Strat. Age (Ma)	Peak t (Ma)	Peak T (°C)	Easy-Ro (%)	Basin-Ro (%)	Easy-DL (%)	AFT Age (Ma)	lc/lc0	1sig	AFT Age (Ma)	CI -95% (Ma)	CI +95% (Ma)	lc/lc0	1sig	Spots	CFTs	UPb Age (Ma)	Rmr0	
MM221-000	Pop-1	18	0.8967	0.5747	18	18	104	0.60	0.54	0.51	12.7	0.8238	0.0578	12.2	2.9	3.8	0.8470	0.0542	11	37	54	0.8430	
MM221-000	Pop-2	18	0.8304	0.8718	18	18	104	0.60	0.54	0.51	13.7	0.8456	0.0464	14.7	4.9	7.4	0.8264	0.0410	3	8	35	0.8144	

M02



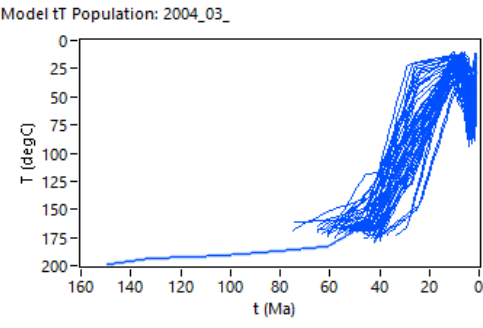
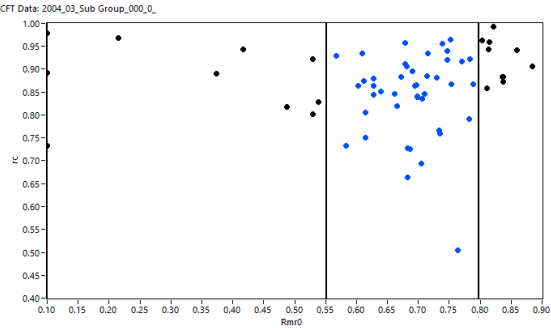
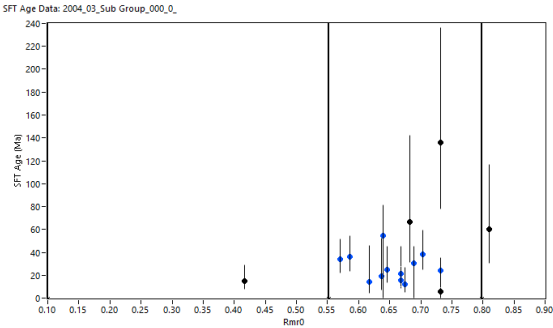
Sample		Best Fit Model												Measured									
Sub-Group	Pop.	Oldest AFT (Ma)	SFT GOF	CFT GOF	Strat. Age (Ma)	Peak t (Ma)	Peak T (°C)	Easy-Ro (%)	Basin-Ro (%)	Easy-DL (%)	AFT Age (Ma)	lc/lc0	Isig	AFT Age (Ma)	CI -95% (Ma)	CI +95% (Ma)	lc/lc0	Isig	Spots	CFTs	UPb Age (Ma)	Rmr0	
MM02-000	Pop-2	34	0.8550	0.9242	34	34	165	1.22	0.89	1.23	23.0	0.8368	0.1094	21.2	6.8	9.9	0.8215	0.1408	9	57	125	0.7328	

M07



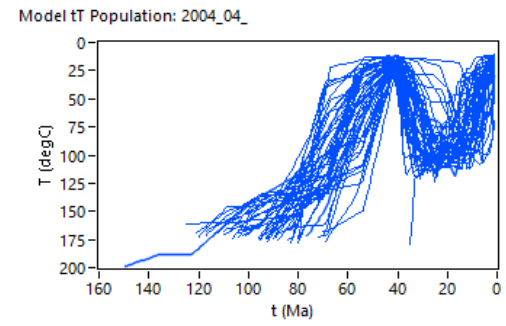
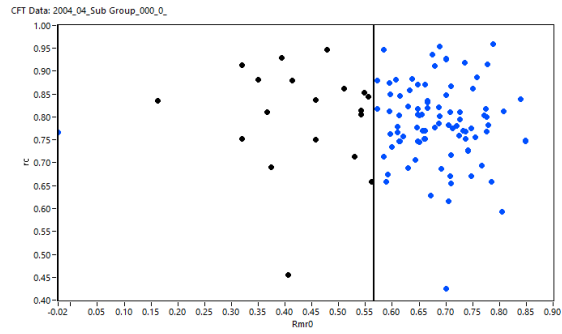
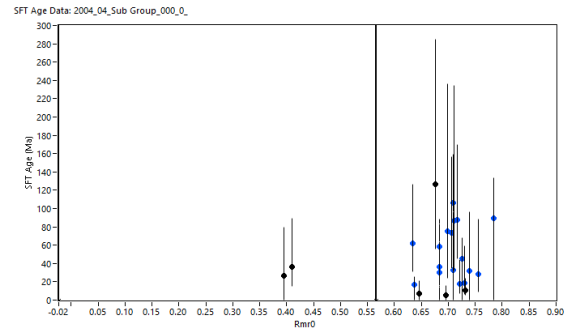
Sample		Best Fit Model												Measured								
Sub-Group	Pop.	Oldest AFT (Ma)	SFT GOF	CFT GOF	Strat. Age (Ma)	Peak t (Ma)	Peak T (°C)	Easy-Ro (%)	Basin-Ro (%)	Easy-DL (%)	AFT Age (Ma)	lc/lc0	Isig	AFT Age (Ma)	CI -95% (Ma)	CI +95% (Ma)	lc/lc0	Isig	Spots	CFTs	UPb Age (Ma)	Rmr0
MM07-000	Pop-2	24	0.9334	0.8381	24	24	173	1.38	1.12	1.35	14.9	0.8013	0.1036	14.2	5.4	8.7	0.7560	0.1139	8	22	125	0.7138

M08



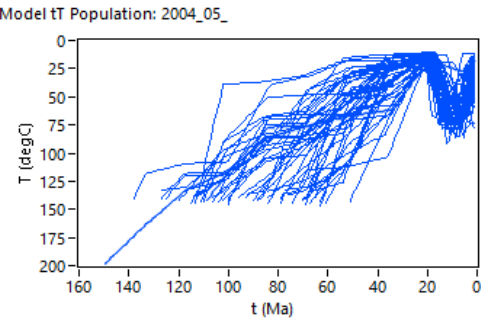
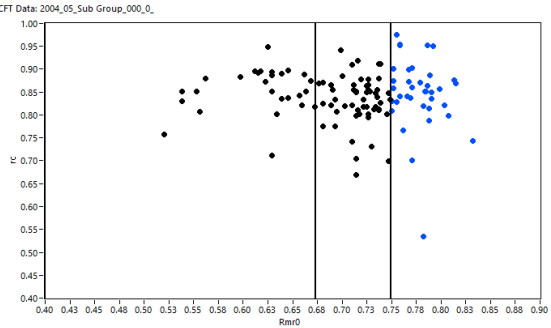
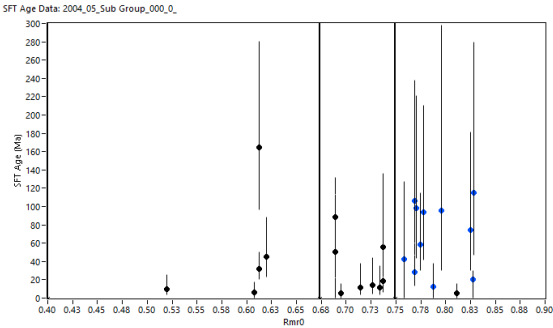
Sample		Best Fit Model												Measured									
Sub-Group	Pop.	Oldest AFT (Ma)	SFT GOF	CFT GOF	Strat. Age (Ma)	Peak t (Ma)	Peak T (°C)	Easy-Ro (%)	Basin-Ro (%)	Easy-DL (%)	AFT Age (Ma)	lc/lc0	1sig	AFT Age (Ma)	CI - 95% (Ma)	CI +95% (Ma)	lc/lc0	1sig	Spots	CFTs	UPb Age (Ma)	Rmr0	
MM08-000	Pop-2	40	0.9545	0.9471	7	3	67	0.39	0.40	0.35	25.3	0.8209	0.1125	25.6	4.6	5.7	0.8449	0.0911	12	43	125	0.7000	

M11



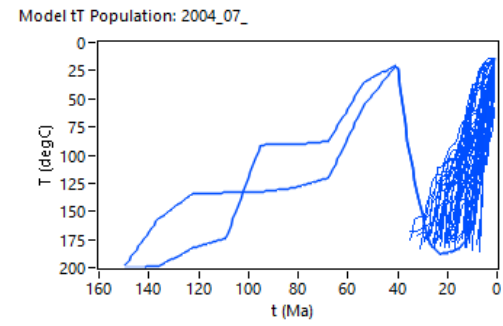
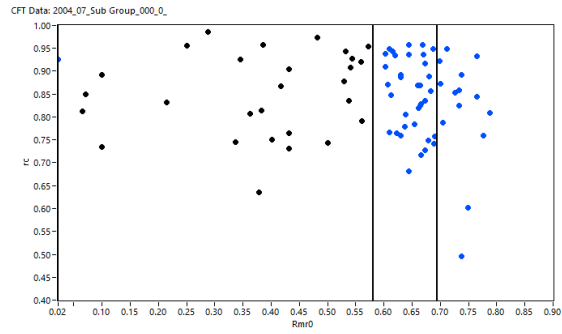
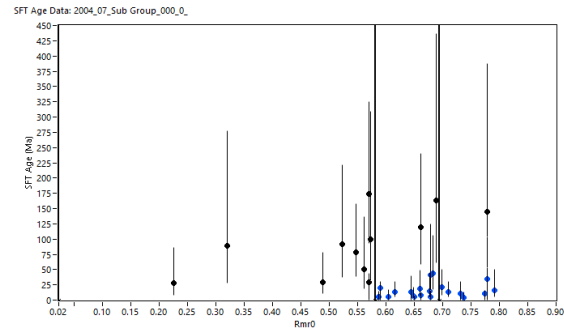
Sample		Best Fit Model												Measured									
Sub-Group	Pop.	Oldest AFT (Ma)	SFT GOF	CFT GOF	Strat. Age (Ma)	Peak t (Ma)	Peak T (°C)	Easy-Ro (%)	Basin-Ro (%)	Easy-DL (%)	AFT Age (Ma)	lc/lc0	Isig	AFT Age (Ma)	CI -95% (Ma)	CI +95% (Ma)	lc/lc0	Isig	Spots	CFTs	UPb Age (Ma)	Rmr0	
MM11-000	Pop-1	83	0.7917	0.4896	39	11	111	0.66	0.57	0.54	43.6	0.7546	0.1120	40.5	9.1	11.7	0.7865	0.0873	17	91	125	0.7000	

M12



Sample		Best Fit Model												Measured									
Sub-Group	Pop.	Oldest AFT (Ma)	SFT GOF	CFT GOF	Strat. Age (Ma)	Peak t (Ma)	Peak T (°C)	Easy-Ro (%)	Basin-Ro (%)	Easy-DL (%)	AFT Age (Ma)	lc/lc0	Isig	AFT Age (Ma)	CI -95% (Ma)	CI +95% (Ma)	lc/lc0	Isig	Spots	CFTs	UPb Age (Ma)	Rmr0	
MM12-000	Pop-1	78	0.9659	0.9999	22	12	78	0.44	0.44	0.40	55.8	0.8384	0.0765	55.0	13.8	18.4	0.8470	0.0785	11	37	125	0.7785	

M28



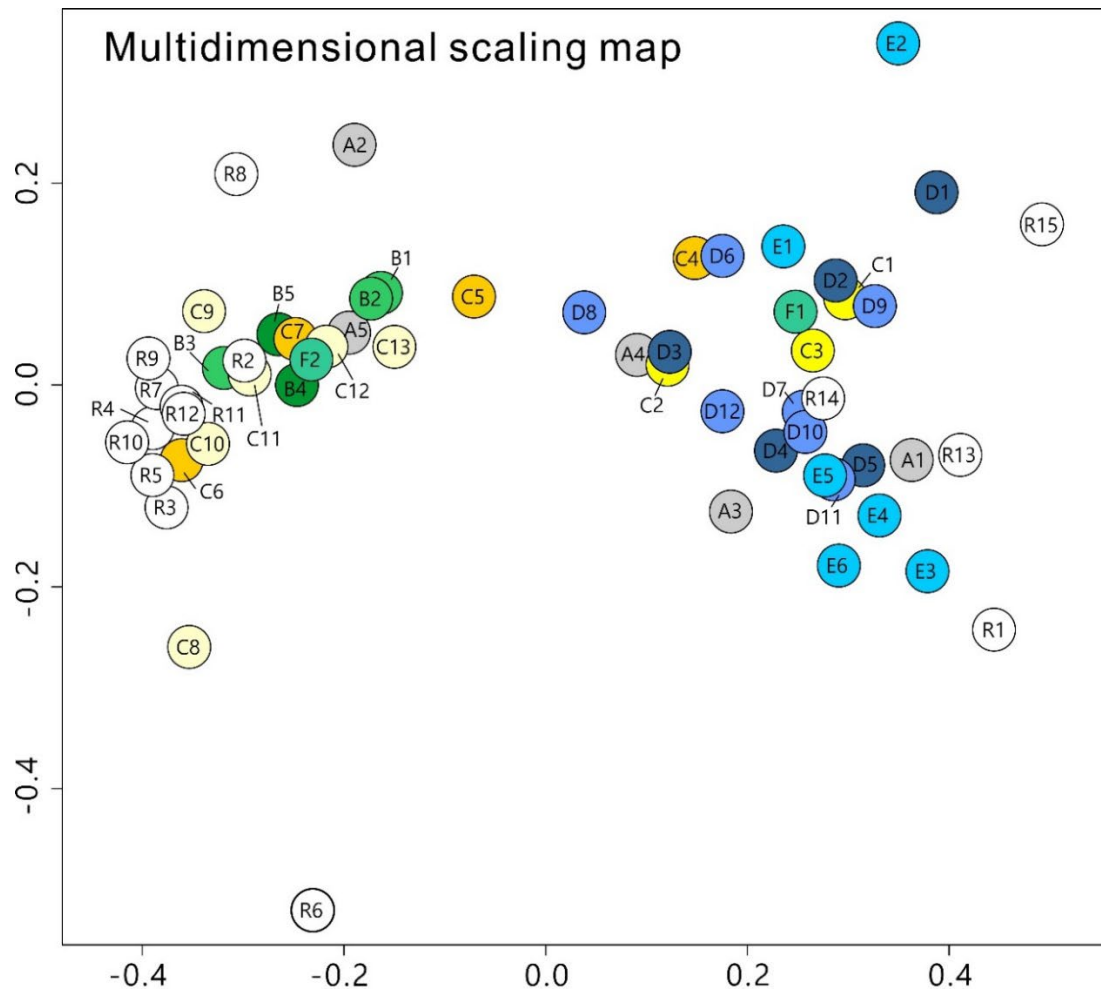
Sample		Best Fit Model												Measured									
Sub-Group	Pop.	Oldest AFT (Ma)	SFT GOF	CFT GOF	Strat. Age (Ma)	Peak t (Ma)	Peak T (°C)	Easy-Ro (%)	Basin-Ro (%)	Easy-DL (%)	AFT Age (Ma)	lc/lc0	1sig	AFT Age (Ma)	CI -95% (Ma)	CI +95% (Ma)	lc/lc0	1sig	Spots	CFTs	UPb Age (Ma)	Rmr0	
MM28-000	Pop-1	19	0.9365	0.9998	19	19	166	1.19	0.86	1.22	12.8	0.8334	0.1102	13.2	5.0	8.0	0.8351	0.1323	7	16	125	0.7358	
MM28-000	Pop-2	20	0.6639	0.8598	20	20	172	1.37	1.11	1.36	13.4	0.8334	0.1102	11.3	3.4	4.9	0.8469	0.0810	13	35	125	0.7000	

Supplemental Material C. Full Results

The results are shown in our Excel tables (Table S1, Table S2, and Table S3).

Supplemental Material D. Compiled Detrital Zircon U-Pb Data

Figure S4. Extensive detrital zircon U-Pb data summary with MDS plot.



Modern Rivers	Himalayan forland and deepwater fans	Indo-Burman Ranges	Forearc Subbasins	Backarc Subbasin	Potential Sources
A1 Irrawaddy River	B1 Neogene, Himalayan Foreland	C1 Eocene southern IBR	D1 Paleocene Paunggyi Fm., Chindwin	E1 Paleocene, Shwebo-Minwun	R1 Gangdese arc
A2 Salween trunk river	B2 Neogene, Bengal Basin	C2 Oligocene southern IBR	D2 Lower-Middle Eocene Laungshay-Pondaung Fms., Chindwin	E2 Lower Eocene Maie Fm., Shwebo-Minwun	R2 Paleozoic Lhasa
A3 Yarlung Tsong trunk river	B3 Paleogene, Bengal Basin	C3 Miocene southern IBR	D3 Upper Eocene Yaw Fm., Chindwin	E3 Middle Eocene Pondaung Fm., Shwebo-Minwun	R3 India and Shilong plateau
A4 Siang River	B4 Bengal Fan	C4 Eocene central IBR	D4 Upper Oligocene Tonhe Fm., Chindwin	E4 Middle-Upper Oligocene Padaung-Okhmintaung Fms., Shwebo-Minwun	R4 Tethyan Himalaya
A5 Bramaputra River	B5 Nicobar Fan	C5 Oligocene central IBR	D5 Miocene Letkat-Natma Fms., Chindwin	E5 Lower Miocene Shwetaung-Moza Fm., Shwebo-Minwun	R5 Greater Himalaya
	F1 Oligocene-Miocene Andaman flysch GOLI7	C6 Lower Miocene central IBR	D6 Paleocene Paunggyi Fm., Minbu	E6 Upper Miocene-Pliocene Irrawaddy Fm., Shwebo-Minwun	R6 Lesser Himalaya
	F2 Andaman Flysch (after screening GOLI7)	C7 Mid-Miocene-Pliocene central IBR	D7 Lower-Middle Eocene Laungshay-Pondaung Fms., Minbu		R7 Naga Metamorphic rocks, IBR
		C8 Lower Eocene Sylhet Fm., northern IBR	D8 Upper Eocene Yaw Fm., Minbu		R8 Triassic budites, IBR
		C9 Mid-Upper Eocene Phokphur Fm., northern IBR	D9 Lower Oligocene Shwezetaung Fm., Minbu		R9 Burma Terrane, Katha
		C10 Mid-Upper Eocene Kopli Fm., northern IBR	D10 Upper Oligocene Okhmintaung Fm., Minbu		R10 Mogok Metamorphic rocks
		C11 Oligocene Jenam Fm., northern IBR	D11 Lower-Middle Miocene Pyawbwe-Obogon Fm., Minbu		R11 Sibumasu Terrane
		C12 Lower Miocene Bhuban Fm., northern IBR	D12 Upper Miocene-Pliocene Irrawaddy Fm., Minbu		R12 Tengchong Terrane
		C13 Upper Mio-Pliocene Bokabil Fm., northern IBR			R13 Dianxi-Burma
					R14 Eocene West Sumatra
					R15 Rivers flowing Western Myanmar Arc

Table S4.

Summarized detrital zircon U-Pb ages from western Myanmar and adjacent regions. The results are shown in our Excel table.